Increasing the Brightness of Light Sources

Ling Fu

Increasing the Brightness of Light Sources

Dissertation
zur
Erlangung des Doktorgrades
der Naturwissenschaften
(Dr. rer. nat.)

dem
Fachbereich Physik
der Philipps-Universität Marburg

vorgelegt von
Ling Fu
aus der V.R. China

Marburg 2006

Vom Fachbereich Physik der Philipps-Universität Marburg
als Dissertation angenommen am: .....

Erstgutachter:	**Prof. Dr. H. Ries**
Zweitgutachter:	**Prof. Dr. H. Jänsch**

Tag der mündlichen Prüfung: **16.11.2006**

Zusammenfassung

Das Ziel dieser Arbeit ist es, die *Erhöhung der spektralen Strahldichte von Lichtquellen* mittels Licht-Recycling zu untersuchen und eine Abschätzung des Potentials dieser Methode zu erarbeiten. Dazu wurde ein physikalisches Modell der Lichterzeugung in thermischen und lumineszenten Quellen erstellt und an verschiedenen Typen von Lichtquellen sowie einem Prototyp der Carambola, einer von uns entwickelten und hier vorgestellten Optik für deterministisches Licht-Recycling verifiziert.

Für moderne Beleuchtungssysteme sind kompakte Größe und hohe Helligkeit (Strahldichte) wichtige Eigenschaften. Licht-Recycling kann die Strahldichte des von einer Lichtquelle ausgesendeten Lichts um den Preis des Verringerns der insgesamt in den Phasenraum abgestrahlten Energie erhöhen. Licht-Recycling bedeutet die Reflexion eines Teils des ausgestrahlten Lichts zur Quelle. Ein Teil dieses reflektierten Lichts entgeht der Absorption in der Quelle und steht weiter zur Verfügung. Infolgedessen kann die Strahldichte eines verkleinerten Phasenraums im Vergleich zur Helligkeit der ursprünglichen Quelle erhöht werden. In dieser Arbeit wird diese Grundregel des Licht-Recycling auf verschiedene künstliche Lichtquellen angewendet, um eine Erhöhung der Helligkeit zu erreichen.

Zumächst werden die Möglichkeiten zur Erhöhung der Helligkeit von Lichtquellen mittels Licht-Recycling theoretisch überprüft, auf der Grundlage der Gesetze der Thermodynamik, insbesondere des Kirchhoffschen Strahlungsgesetzes, des Planckschen Gesetzes, des Lambert-Beerschen Gesetzes, der Etendueerhaltung und des Helligkeitstheorems.

Aus experimenteller Sicht werden die Strahlungseigenschaften der drei unterschiedlichen Lichtquellen Kurzbogenlampen, Glühlampen und Leuchtdioden (LEDs) im Hinblick auf ihre Eignung für das Licht-Recycling untersucht. Exemplare dieser Lichtquellen werden in Experimenten zum Licht-Recycling eingesetzt, um

- Effekte intrinsischen Licht-Recyclings zu erkennen, beispielsweise das durch die Wicklung des Drahtes entstehende Licht-Recycling in Glühlampen.
- die zur Erstellung von physikalischen Modellen benötigten Parameter, wie Emissivität und Absorptivität der Kurzbogenlampen oder die Reflektivität und den Quantenwirkungsgrad von LEDs zu messen.

- die Grundlage für die Entwicklung von Optiken für das Licht-Recycling auf der Basis der gemessenen Parameter zu schaffen. Die Carambola ist eine von uns für deterministisches Licht-Recycling entwickelte Optik.

Zwei physikalische Modelle zur Simulation der Strahlungsverteilung von Lichtquellen, eins für Glühlampen, das andere für lumineszente Quellen (LEDs) werden erstellt. Beide sind mit Messungen hoher Auflösung validiert. Die physikalischen Modelle sind in der Lage, die Strahlungsverteilung mit einigen erforderlichen Parametern (Geometrie, Materialeigenschaften und Betriebsbedingungen der Lichtquelle) analytisch zu modellieren. Sie sind auf andere Quellen mit ähnlichen Eigenschaften anwendbar. Die Vorteile der Prägnanz, der hohen Genauigkeit und der breiten Anwendbarkeit kombinierend, können die physikalischen Modelle in Strahlverfolgungssoftware integriert werden.

Zur experimentellen Untersuchung des Effekts des Licht-Recycling ist eine optische Vorrichtung, die Carambola, mit deterministischem (im Gegensatz zu stochastischem) und mehrfachem Licht-Recycling bestimmt. Um die mögliche maximale Erhöhung der Strahldichte, die mit der Carambola erreichbar ist, zu simulieren, werden einige Kombinationen von Quellen und Carambola mit Strahlverfolgung modelliert. Dieses wird auf Quellen mit unterschiedlicher Emissivität und unterschiedlichen Strahlungseigenschaften (optische Dicke) und auf Carambola mit unterschiedlichen Geometrien und optischen Eigenschaften angewendet. Daraus kann man schließen, dass Xenon Hochdrucklampen aufgrund ihrer geringen optischen Dicke, ihrer gleichmässigen spektralen Absorptivität für das Licht-Recycling besonders geeignet sind. In der Strahlverfolgung wird diese Eignung der Xenonlampe und der für das Licht-Recycling bestätigt. Im Laufe dieser Arbeit wurde ein Prototyp einer fünf-rippigen reflektierenden Carambola aus Aluminium hergestellt.

Die experimentellen Resultate mit der Carambola liegen unterhalb der theoretischen Erwartungen, die Diskrepanzen können erklärt werden. Eine Carambola muß ein hohes Reflexionsvermögen und eine genaue Form haben, wenn ein deutlicher Effekt des Licht-Recycling gezeigt werden soll. Die Carambola kann verbessert werden durch das Polieren und Versilbern der Reflektoren, durch Verwendung von Quellen kleiner optischer Dicke und kompakter Größe, hohem tatsächlichem Reflexionsvermögen und externem Quantenwirkungsgrad (LED).

Theoretische Untersuchung und experimentelle Messungen des Licht-Recycling zeigen, daß dieser Effekt entweder eine tatsächliche Eigenschaft der Quelle ist, oder durch eine besonders entworfene Optik verursacht werden kann. Durch das Wiederverwerten des Lichtes kann die spektrale Strahldichte eines Phasenraums erhöht werden.

Sowohl die theoretische Untersuchungen als auch die experimentellen Messungen des Licht-Recyclings demonstrierten eine signifikante Erhöhung der Strahldichte optisch dünner Quellen.

Contents

List of Figures

List of Tables

1. Introduction

1.1. Motivation

For artificial light sources of any size the quantity of the produced light is the most important feature. The quality of the produced light is of prime importance in illumination. The quality of light can be measured as the ratio of the radiant energy to the phase space (étendue or throughput, see Sec. 2.1) of the radiation. This density is termed *spectral radiance* in radiometry, *luminance* or *brightness* in photometry. Radiance is radiant flux per unit area and projected solid angle, indicated as

$$L_\lambda = \frac{\Phi_\mathrm{e}}{N^2 A_\mathrm{s}\,\Omega_\mathrm{p}}\ , \tag{1.1}$$

where Φ_e is the radiant flux, N is the refractive index of the medium, A_s is the light-emitting area and Ω_p is the projected solid angle.

The higher the radiance, the higher the quality of the radiation. This can be illustrated with the following example: assume a novel lamp producing the same quantity of light as a standard lamp used for comparison. Both lamps have an identical far-field distribution but the novel lamp emits power in a reduced phase space, i. e. with a higher radiance. The lamp shall be part of an illumination system. Then we could scale down the subsequent optics, e. g. the condenser and objective of a direct video projector by a factor corresponding to the ratio of standard phase space to the reduced phase space, for the standard lamp and the novel lamp, respectively. A smaller light-emitting body appears much brighter than a larger one at a constant power per solid angle. In many cases compact size is an economic advantage. For this reason many designers would go as far as sacrificing a certain quantity of the light only to reach higher radiance (higher quality) for the remaining light.

The size and the radiance of a source are restricted by material properties including thermal conductivity, resistivity etc. Consider a thermal source, e. g. a tungsten filament lamp, operated at a constant current. The radiance drops with the thickness of the wire governed by $L_\lambda \propto 1/d^3$, where L_λ is the spectral radiance and d is the thickness of the filament wire. Assuming that the tungsten filament can be approximated as a black body, Stefan-Boltzmann's law yields $T^4 \propto 1\,/d^3$, where T is the absolute temperature of the filament in Kelvin. Decreasing the thickness of the wire in order to increase the radiance of the source will lead to higher temperature.

On reaching the melting point of the material, the filament will melt at its thinnest point.

Driving lamps at a voltage higher than the rated value in order to produce an enhanced radiance is not recommendable. The lifetime of an incandescent source will be shortened due to the increased temperature. Empirically, the lifetime of a tungsten filament lamp is approximately proportional to $1/V^{16}$ [29], where V is the operating voltage, e. g. for a 20 W tungsten halogen lamp, a voltage increase of 5% (from 12 V to 12.6 V) leads to an electrical power consumption increase of 8% and an efficacy increase of 6% (from 16 lm/W to 17 lm/W), but a decrease of lifetime by 50% (from 2000 to 1000 hours). Likewise, a voltage dimmed by 5% will double the lifetime at the expense of reducing the lamp's efficacy by 7%, and its light output by 5%. This may be an acceptable tradeoff for a source either with a high cost or in a location difficult to access.

Thus the operating temperature and the spectral radiance of tungsten filament lamps are limited by the material properties. The halogen cycle allows to increase the operating temperature and with it the spectral radiance and the efficacy without reducing the lifetime of the lamp. Light recycling, as will be shown, is an independent method which may be used in addition.

An example for solid state devices is the light-emitting diode (LED) which in an approximation emits light from a two-dimensional surface area. The incandescent lamp with a straight or coiled wire is a three-dimensional surface source, where the surface area is the outer surface of a cylindric wire. Three-dimensional volume sources include gas discharge lamps. Because of the properties of their materials, the efficiencies of light sources are far below unity. A tungsten incandescent lamp operated at 2500 K has an efficiency of around 7% for the visible spectrum.

Looking at Eq. (1.1) mathematically, it is possible to increase the radiance of light sources either by increasing the radiant flux, or by decreasing the emitting area, or the solid angle. The above discussion proves that it is not effective to enhance the radiance by merely increasing the input power of the source or decreasing the emitting area. Generating and collecting as much light as possible and compressing the light into a reduced phase space via light recycling is an approach to increase the radiance of the source. Light recycling involves recirculating part of the emitted light through the source repeatedly and extracting the reflected or transmitted light in the same space phase as the originally emitted light, resulting in a brightness enhancement at a reduced solid angle compared with systems without light recycling. The physical meaning of light recycling will be explained in detail in Chap. 2.

1.2. Brightness enhancement of light sources: brief history

In some special illumination systems such as high brightness video projectors and car headlamps, the principle of light recycling has been widely used. One of the applications is interpreted as back-reflection. Assume that radiation can be reflected back to light sources and fractions of it will be reflected, absorbed and transmitted. The reflected part will escape the source eventually as loss. The absorbed fraction increases the luminous efficacy by heating, which will affect the heat management. The transmitted light (the back-reflected radiation) will be superimposed onto the direct radiation of the source in the same phase space and thereby the brightness is increased at the specific phase space compared with the case in the absence of back-reflection.

140 years ago, Sibbald [60] used reflectors to enhance the illumination for his magic lantern, a slide projector for opaque pictures . In 1926 Reeb et al. [51] reported an application of additional mirrors for cinema projection with incandescent lamps and reflectors. Both works illustrate that reflecting light back to the system facilitates the illumination. However, the mechanism of the back-reflection in the magic lantern shown in Fig. 1.1 is not light recycling, since the reflected light is not superposed onto the direct radiation in the same phase space. In turn the brightness of the source is not enhanced.

In modern lamps, one of the successful applications of the back-reflection principle is an Ultra High Pressure (UHP) lamp for projection, shown in Fig. 1.2 [55]. In this work one-half cavity of the UHP lamp is coated with a dichroic coating. Due to the unique reflective and transmissive properties of the coating for different wavelengths, the forward radiation in the range of visible light is reflected back towards the source itself, but most part in the infrared (IR) and ultraviolet (UV) is transmitted out of the lamp. The reflected light is superposed onto the direct radiation, i. e. not recirculated fraction of light, in the same phase space. The combined light is redirected by a parabolic reflector towards the exit of the system. The light collection is reportedly improved by 20−30%, in turn the radiance of the source is increased due to the reduction of étendue. The world's most compact projection systems of today are based on these lamps.

Another application of light recycling is a projection engine of Li et al. [37], shown in Fig. 1.3. The system consists of a dual-paraboloid reflector with a lensed tapered light pipe and a light pipe based polarization recovery system as the illumination section. The dual-paraboloid reflector system is a 1:1 imaging coaxial system and symmetric with respect to the bisector of the optical axis. The first reflector collects half of the light (towards the left-hand side) emitted by the lamp placed at its focus and images it into infinity. The second paraboloid reflector is an upward flip of the first one and it focuses the light onto the target. The collimated beam entering the

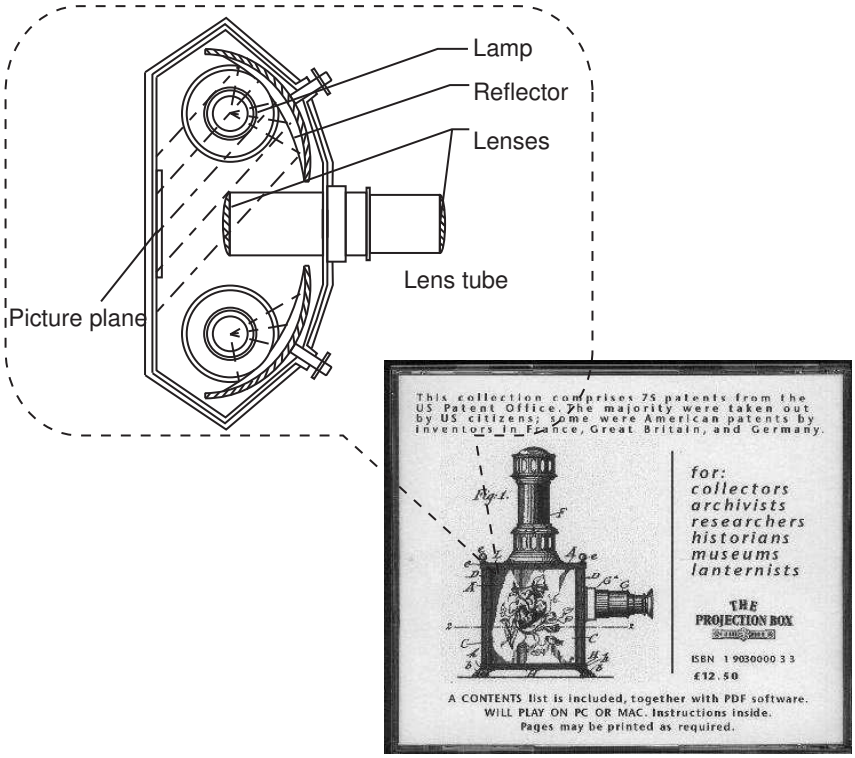

Figure 1.1.: A slide projector for opaque pictures−the magic lantern of G. Sibbald [60]. Two or more reflectors are constructed in the interior of the lantern opposite to the picture plane symmetrically with respect to the optical axis of the lens tube. The light emitted towards the reflectors is reflected to the picture plane. In this manner, the brightness of the source is not increased because there is no reduction of the phase space of the source.

second parabolic reflector will concentrate at its focus and is guided into the light pipe. The spherical retro-reflector images the lamp onto itself. By collecting the other half of the light (towards the right-hand side) and reflecting it back into the system via the retro-reflector, the brightness of the system is increased.

More than the above-mentioned applications of sources like incandescent lamps or discharge lamps, solid-state lighting sources like LEDs are widely used as indicators, in displays and in illumination etc. Their advantages include small size, high reliability, high brightness, high efficiency and long lifespan. A comparison of luminous efficacies of traditional sources and those of LEDs is shown in Table 1.1. In order to replace the commonly used incandescent lamps and fluorescent lamps with LEDs, high luminous efficacy and high brightness are desirable [22, 27, 42, 46]. For this purpose, efforts are made in the field of material science, mechanism and optical design.

In 1999 and 2000, Guo et al. [22, 23] reported their work on a white-light emit-

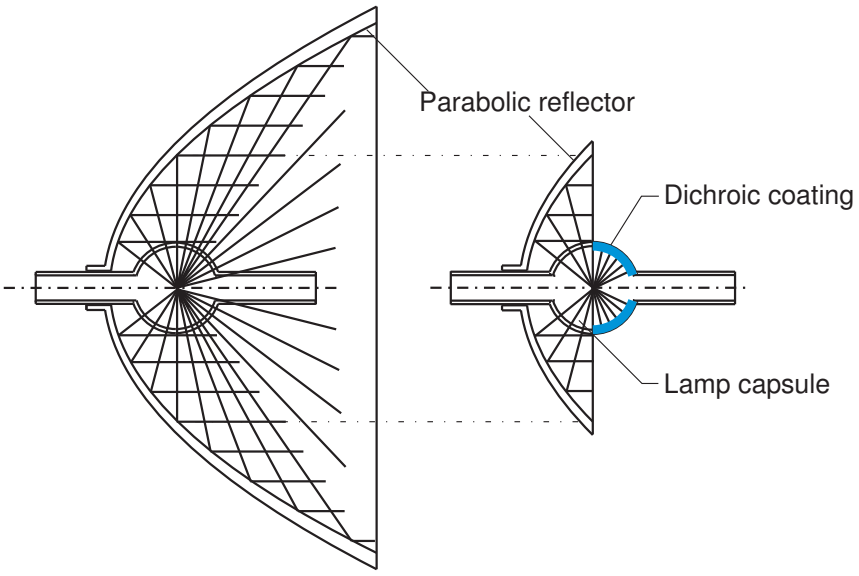

Figure 1.2.: Comparison of identical short-arc lamps without coating (left-hand side) and with a dichroic coating on the right hemisphere of the lamp capsule (right-hand side), as proposed by researchers from Philips [55]. The dichroic coating is reflective in the range of visible light, but transmissive in the range of the undesired UV and IR radiation. The capsule is spherical. The light emitted towards the coating is reflected back to the source, passing the source a second time, and is superimposed onto the direct radiation. The total light is reflected by a paraboloidal reflector with a smaller aperture compared with the system on the left-hand side. Therefore the brightness is increased due to a reduced étendue.

Table 1.1.: Comparison of luminous efficacies of different light sources.

Light sources	Luminous efficacy [lm/W]
100 W tungsten incandescent	17[a]
20 W tungsten-halogen lamp	16[a]
Compact fluorescent	60[b]
100 W mercury discharge lamp	45[a]
High power white LED (2004)	40−60[b]
White LED prototypes (2005)	80−100[b]
White LED of industry target (2012)	150−200[b]

[a] Source: measurements
[b] Source: [29].

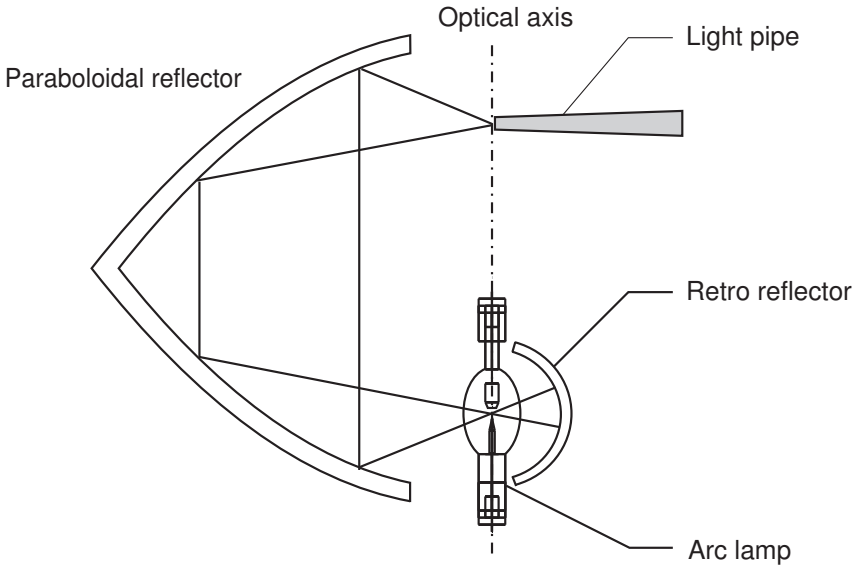

Figure 1.3.: A dual-paraboloid reflector system for projection display. The illumination section includes a dual-paraboloid reflector with a tapered light pipe. The dual-paraboloid reflector is a 1:1 imaging coaxial system and symmetric with respect to the bisector of the optical axis. The first reflector collects the half of the light (towards the left-hand side) emitted by the lamp placed at its focus and images into infinity. The second paraboloid reflector is an upward flip of the first one and it focuses the light onto the target. The collimated beam entering the second parabolic reflector will concentrate at its focus and is guided into the light pipe. The spherical retro-reflector collects the other half of the light (towards the right-hand side) and reflects it back into the system as recycled light, leading to a brightness increase of the system, except for a small reduction of the total radiant power due to the absorption of the source [37].

ting photon-recycling semiconductor LED (PRS-LED). The device consists of a GaInN/GaN LED emitting in the blue spectral range and an AlGaInP photon recycling semiconductor emitting at the complementary color. The PRS-LED has two emission lines, one in the blue and one in the amber wavelength range. The expected maximum luminous efficacy of the PRS-LED exceeds 300 lm/W, higher than the efficacy of phosphor-based white LEDs (70 lm/W). Note that the mentioned photon recycling is different from the light recycling that we investigate.

In 2005, Narendran et al. [46] reported on improving the efficacy of white LED by means of scattered photon extraction (SPE). Phosphors commonly used in white LEDs backscatter more than half of the down-converted light, of which a significant fraction is lost within the package, leading to a reduction of the overall efficacy. An experimental study shows that the backscattered photons can be extracted and the

efficacy can be increased to over 80−100 lm/W by placing the phosphor away from the semiconductor dye. As an additional benefit, the lifetime of sources is extended. Another work in this field is presented by Luo et al. [42]. In order to increase the phosphor efficiency in white LEDs, an optimized packaging configuration which employs a diffuse reflector cup, a large separation between the primary emitter (the LED chip) and the wavelength converter (the phosphor) and a hemispherical encapsulate cap is presented. The simulation results show that the phosphor efficiency can be enhanced by up to 50% over conventional phosphor-in-specular-cup configuration with a flat encapsulation.

In most recent publications of Beeson et al. [2, 3, 70], an inspiring design on an LED-based light sources for projection displays utilizing novel light-recycling cavities with small output étendue is reported. The LED-based projection systems have several advantages over commonly used systems based on UHP arc lamps, including a long lifetime, a large color gamut, modifiable wavelength etc. Optical projection display systems are constrained by the system étendue. In order to maximize the utilization of the source light flux, the étendue of the source cannot be greater than the étendue of the rest of the projection system. Due to the restriction, it is very difficult to achieve a high brightness in the projection display using a planar array of LEDs as source. However, on the basis of light recycling the inherent reflectivity of LEDs is utilized in the designed optics to enhance the average brightness of LED light sources and the brightness of the cavity output. The brightness enhancement factors (defined in detail in Chap. 2) of 1.3−2.0 are achieved experimentally.

This work focuses on increasing the brightness of light sources, including thermal sources and non-thermal sources, particularly solid-state sources LEDs by developing and improving their optics via light recycling. For this purpose, the mechanism of light recycling is investigated in theory and in experiment. The principle of light recycling is elaborated on as the core, based on fundamental laws in thermodynamics including Kirchhoff's law on radiation, Planck's law, Lambert-Beer's law and the brightness theorem. In experiments, the radiation properties of three different types of light sources are investigated, which are characterized by their light-generating processes, i. e. a short-arc lamp by direct emission from atoms and molecules in gas discharges; a filament lamp by incandescence−the glow from solids; and LEDs by electroluminescence−the conversion of electrical energy into light. Chap. 2 involves the measurements of light radiation from short-arc lamps. Meanwhile, the absorption and emission properties are investigated, which are the important parameters for evaluating light recycling in light sources.

In Chap. 3 a physical model for simulating the radiance distribution of filament light sources is described, based on thermodynamics, geometry, material and electrical properties of filament source. In this model, emission, absorption and light recycling properties are taken into consideration based on the measurements of light radiation of the light sources. The model is validated with high resolution absolute radiation measurements.

A physical model for the generation of the radiance distribution of luminescent sources (LEDs) is presented in Chap. 4 based on the generalization of Kirchhoff's law and Planck's law. Thereby luminescent sources can be treated thermally as well in terms of the spectral radiation. The required parameters in the model, e. g. absoptivity, reflectivity, external quantum efficiency, I−V characteristics of LEDs are derived from measurements. In an LED-based light recycling experiment aiming at an investigation of the light recycling effect in semiconductors, brightness enhancement of LEDs is achieved via light recycling.

In order to increase the brightness of light sources an optical device, the *Carambola* is described in Chap. 5. The design principle and the theoretical brightness enhancement are explained. The experimental results of brightness increase are analyzed. In conclusion, the methods of improving the Carambola for seeking a higher brightness enhancement are discussed. The need for applications of the Carambola is anticipated.

2. Theory of light recycling

2.1. Concepts

Radiometry and Photometry

In light measurement, two concepts, i. e. radiometry and photometry should be distinguished. Radiometry is the measurement of electromagnetic radiation in the wavelength range of $10-10^6$ nm, including the ultraviolet, the visible light and the infrared. The radiant flux Φ_e is used for defining the radiant energy per unit time, in Watt [W].

In contrast, photometry is the measurement of visible light as perceived by human vision, in the wavelength range of $360-830$ nm. The luminous flux Φ_v is used to define the total light emission per unit time detected by the human eye, in lumen [lm], corresponding to a radiant flux of $1/683$ W at 555 nm (the most sensitive wavelength for human vision). The main difference between radiometry and photometry is that they deal with the light in different spectral bands.

The luminous flux Φ_v is linked to the radiant flux Φ_e by the spectral luminous efficacy K_λ, indicated as

$$K_\lambda = \frac{\Phi_v(\lambda)}{\Phi_e(\lambda)} \,, \tag{2.1}$$

in units of lm/W. According to the definition of the lumen, K_λ has the value $K_{max} = 683$ lm/W at a wavelength of 555 nm, which is the wavelength of maximum sensitivity for photopic (day) vision. In contrast, for scotopic or dark-adapted vision the maximum sensitivity occurs at 505 nm.

At other wavelengths, K_λ is given by

$$K_\lambda = K_{max} V_\lambda = 683\, V_\lambda \,, \tag{2.2}$$

where V_λ is the relative sensitivity of the human eye, termed the luminosity function or spectral luminous efficiency (not efficacy) [14, 43]. It is a dimensionless quantity. As a normalized function, the maximum relative sensitivity, i. e. unity occurs at the wavelength of 555 nm.

Summarizing Eqs. (2.1) and (2.2) yields the luminous flux as

$$\Phi_v = 683\, V_\lambda\, \Phi_e \,. \tag{2.3}$$

For a light source with a total electrical input power P, a radiant flux Φ_e and a luminous flux Φ_v, its power efficiency (or radiant efficiency) is defined as

$$\eta_e = \frac{\Phi_e}{P} , \tag{2.4}$$

a dimensionless quantity. And the luminous efficacy η_v is expressed as

$$\eta_v = \frac{\Phi_v}{P} , \tag{2.5}$$

in units of lm/W like K_λ. However, $\eta_v < K_\lambda$, because the energy loss is inevitable in the course of energy conversion from electrical input into light output.

In illumination system design, according to different applications, preferential consideration is given to the radiance, the luminous efficacy, the power efficiency and the color.

Etendue

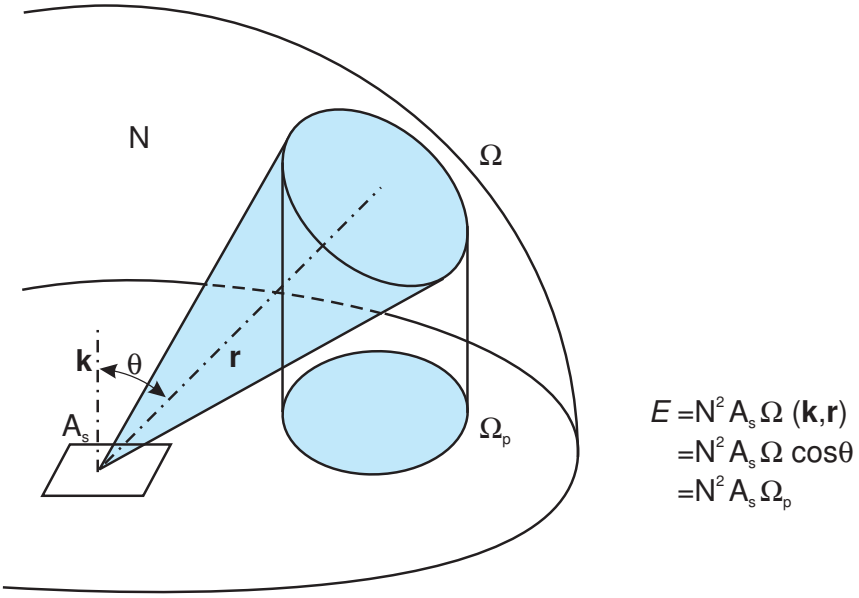

Figure 2.1.: The étendue is defined for example at a source plane (or an image plane) as the product of the area of the source (or the image) A_s, the projected solid angle Ω_p subtended by the light and the square of the refractive index of the medium N according to Eq. (2.6). Ω is the solid angle subtended by light on a sphere. θ is the angle between the surface normal $\mathbf{k}$ and the specified light propagation direction $\mathbf{r}$.

In the definition of the radiance in Eq. (1.1), the denominator is termed étendue. The étendue is defined for example at a source plane (or image plane) as

$$E = N^2 A_s \Omega_p , \tag{2.6}$$

in units of $m^2\,sr$, where N is the refractive index of the medium, A_s is the area of the source (or of the image), Ω_p is the projected solid angle subtended by the light, shown in Fig. 2.1. The étendue is a geometrical quantity and is a measure of the power-gathering ability of the system in which the total flux is given by the product of this quantity with the radiance of the source (Eq. (1.1)). The étendue can never decrease when passing subsequent optical elements (either stays constant or increases). It is conserved in a lossless system (assuming without reflection, absorption or scattering) as light passes through the optical system, in the limit of geometrical optics.

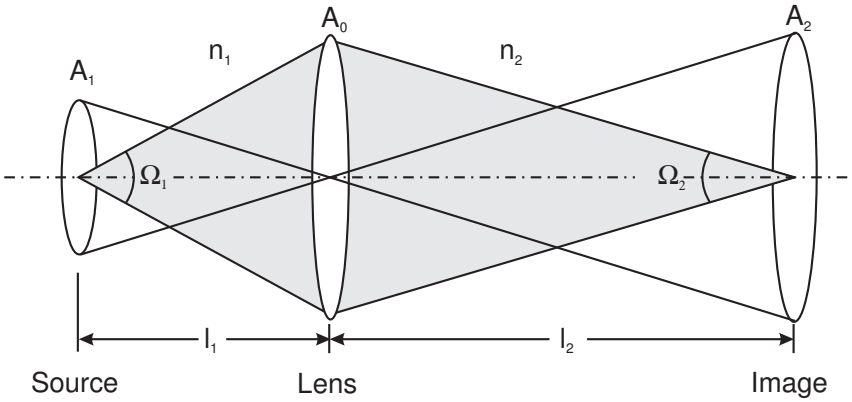

Figure 2.2.: An optical system used to visualize the conservation of étendue and the conservation of radiance. In a lossless system (without reflection, absorption or scattering), the total radiant flux is transferred from the source plane to the image plane. The definition of the étendue in Eq. (2.6) and the geometrical object-image relation yield the conservation of étendue.

The lossless optical system in Fig. 2.2 is used to visualize the conservation of étendue and the conservation of radiance. In the system the lens, the source and the image are designated with subscripts 0, 1, 2 respectively. For simplicity, assume that all the three elements are of circular shape and coaxial. A_0, A_1, A_2 are the respective areas of the elements, Ω_1 and Ω_2 are the respective projected solid angles, N_1 and N_2 are the refractive indices in the source space and in the image space, l_1 and l_2 are the object distance and the image distance. According to the definition of the étendue in Eq. (2.6), the respective quantities at the source plane and the image plane are given by

$$\begin{aligned} E_1 &= N_1^2\, A_1\, \Omega_1 \;=\; N_1^2\, A_1\, A_0 / l_1^2\,, \\ E_2 &= N_2^2\, A_2\, \Omega_2 \;=\; N_2^2\, A_2\, A_0 / l_2^2\,. \end{aligned} \tag{2.7}$$

The geometrical object-image relation in Fig. 2.2 yields the lateral magnification

Γ as

$$\Gamma = \left(\frac{A_2}{A_1}\right)^{\frac{1}{2}} = \frac{N_1\, l_2}{N_2\, l_1} \,. \tag{2.8}$$

Summarizing Eqs. (2.7), (2.8) yields the conservation of étendue as

$$E_1 = E_2 \,. \tag{2.9}$$

Note that the étendue conservation is independent of the power conservation. According to the definition of radiance in Eq. (1.1), the total radiant flux Φ_e transferred from the source plane to the image plane in the lossless system is given by

$$\Phi_\mathrm{e} = L_1\, E_1 = L_2\, E_2 \,. \tag{2.10}$$

As a result of the energy conservation and the étendue conservation, the relationship between the source radiance L_1 and the image radiance L_2 is derived as

$$L_1 = L_2 \,. \tag{2.11}$$

This conclusion is termed the radiance theorem or brightness theorem, interpreted as to the fact that in a passive system, no image can be brighter than the source itself. This is a result of the second law of thermodynamics. Based on the conservation of étendue and the radiance theorem, we note that

- in order to maximize the utilization of the source radiant flux, the étendue of the source must be less than or equal to the étendue of the optical system, otherwise the remaining flux would spill out of the system as loss.
- for Lambertian or approximate Lambertian sources (i. e. emitters or scatters) whose radiance is independent of the viewing angle by definition [7, 63], the radiance is of significance to any illumination system. The radiance is often chosen as one of the important parameters in the optical design of imaging and non-imaging systems.

The radiance theorem states that it is impossible to increase the radiance of light by means of passive optical devices. This seems intuitively right because the spectral radiance is connected to temperature. Any increase of the radiance would imply an increase in temperature and therefore violate the second law of thermodynamics. However, consider a special case of a Lambertian source that has a reflective emitting surface, an optical system can be designed to recycle a portion of the emitted light back to the source and redirect the remainder of the light to an exit via light recycling. The area of the output exit may be smaller than the intrinsic light-emitting area of the source, namely the effective light-emitting area may decrease, while the projected solid angle may not increase. Is the resulting output étendue reduced for this case? Is it possible to increase the brightness of the source higher than the intrinsic brightness via light recycling?

The answer is yes! This does not contradict the second law of thermodynamics, because light recycling reduces the irreversible entropy production inherent to the radiation process. It is equivalent to increasing the optical thickness of sources for the price of reducing the total étendue of emitted radiation by the same factor. Kirchhoff's law on radiation will give a good explanation.

2.2. Kirchhoff's law on radiation and light recycling

Kirchhoff's law and Planck's law on thermal radiation

Any object with a temperature above absolute zero radiates electromagnetic energy, whose spectral and directional properties can be described with the radiance. As an ideal radiator, a black body is an object which absorbs all electromagnetic radiation that falls onto it. In thermal equilibrium, the spectral radiance of a black body depends only on its temperature, independent of shape or material of the body, expressed with Planck's radiation law [49]

$$L_\lambda^{\mathrm{Pl}}(T) = \frac{2hc^2}{\lambda^5} \frac{1}{\exp\left(\frac{h\,c}{\lambda\,k_\mathrm{B}\,T}\right) - 1} \,, \tag{2.12}$$

where $L_\lambda^{\mathrm{Pl}}(T)$ is the spectral radiance of a black body in thermal equilibrium, h is Planck's constant ($6.626 \cdot 10^{-34}\,\mathrm{J\,s}$), k_B is Boltzmann's constant ($1.381 \cdot 10^{-23}\,\mathrm{J/K}$), T is the absolute equilibrium temperature, c is the velocity of light, λ is the wavelength of the emitted light, c and λ are measured in the medium where the radiance is evaluated.

The total power radiated per unit area by a black body is given by Stefan-Boltzmann's law [5]

$$E = \sigma T^4 \,, \quad \text{with} \quad \sigma = \frac{2\pi^5 k_\mathrm{B}^4}{15\,h^3\,c^2} \,, \tag{2.13}$$

where σ is Stefan-Boltzmann's constant.

In reality, no object behaves like an ideal black body, instead the emitted radiation at a given wavelength and a given temperature is a fraction of what the ideal emission at the same temperature would be, expressed as

$$L_\lambda(T) = \varepsilon(\lambda, T)\, L_\lambda^{\mathrm{Pl}}(T) \,, \tag{2.14}$$

where $\varepsilon(\lambda, T)$ is the emissivity of the material. It specifies how well a real body radiates energy as compared with a black body of the same size, shape and temperature. The maximum possible value of $\varepsilon(\lambda, T)$ is unity, in the case of black bodies. The emissivity depends on factors including temperature, emission angle, and wavelength (involving selective radiators, illustrated with the spectral radiation of short-arc lamps in Fig. 2.3). For simplicity, the emissivity of most materials within

a limited spectral band is assumed to be wavelength-independent, i. e. the emissivity stays constant. This is known as the grey body assumption. Compared with the unity emissivity of a black body, the emissivity of a grey body is smaller than one, i. e. no object can emit more energy than a black body at the same temperature. Fig. 2.3 illustrates the spectral radiance of a grey body at 6500 K with a constant spectral emissivity of 0.5. As comparison the spectral radiance of a black body at the same temperature is shown in the same graph.

Another intrinsic material property closely connected with the emissivity is the absorptivity α, defined as the fraction of incident light that is absorbed by the material. Under the condition of the same temperature and the same wavelength, the absorptivity and the emissivity are related by Kirchhoff's law on thermal radiation [33]

$$\alpha(\lambda, T, ...) = \varepsilon(\lambda, T, ...) \ , \tag{2.15}$$

which implies that

- a good absorber at a specific wavelength is also a good emitter at the same wavelength, and vice versa;
- a good absorber is a poor reflector. Light incident on a material is either reflected, absorbed or transmitted (without considering scattering). Energy conservation requires for the same spectral interval, $\alpha + r + t = 1$, where α, r and t are the fractional absorbed (absorptivity), reflected (reflectivity) and transmitted flux (transmissivity). For a special case of an opaque object which is sufficiently thick $t = 0$, in turn $\alpha + r = 1$. Strong absorption results in a weak reflection, and vice versa.

If this were not true, a colder body with a higher emissivity than absorptivity would warm up a warmer body with a higher absorptivity than emissivity, so that heat would flow from the lower temperature to the higher temperature level. This would contradict the second law of thermodynamics, stating that a passive system cannot produce a positive heat flow from a colder body to a warmer body [11].

The principle of light recycling

Kirchhoff's law is the foundation of light recycling. The principle of light recycling is interpreted as following. A light source emits light. Assume that part of the emitted light is reflected back to the source itself, where it is either reflected, absorbed or transmitted. Being a non-black body the spectral emissivity of the source is less than unity and so is the absorptivity. Thus the fraction of the light escaping absorption can be redirected to pass the source exit as illustrated in Fig. 2.4. The virtue of light recycling is that the recycled light is superposed onto the original direct radiation in the same phase space. The collected power is increased without

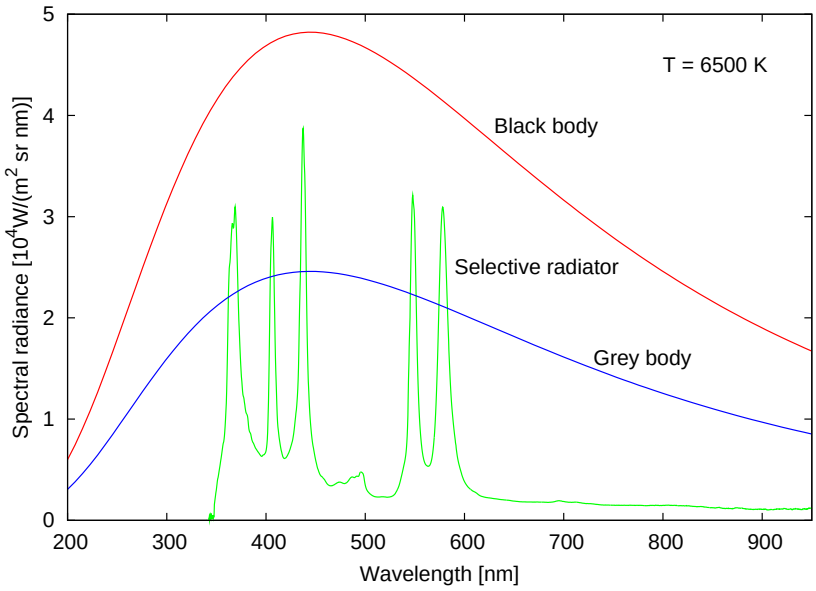

Figure 2.3.: Comparison of spectral radiance of three different thermal radiators at 6500 K: a black body (with unity emissivity), a grey body with a constant emissivity of 0.5, and a selective radiator with a wavelength-dependent emissivity (a short-arc lamp). The radiance quantity is the product of the black body's radiation at the same temperature with the respective spectral emissivity, following Eq. (2.14).

increasing the étendue, thus the output radiance is increased. The total power emitted is reduced by the amount of absorption of the recycled light. Some of the total power is sacrificed for the advantage of extracting the remaining light for increasing the brightness. Quality of light is increased while the quantity of light is reduced by the amount of absorption.

The concept of *brightness enhancement* η is introduced in order to describe the quality of light due to light recycling, defined as the ratio of the resulting radiance consisting of the direct and the recycled radiation to the direct radiation emitted by the naked source in the absence of light recycling. The lower limit $\eta = 1$ is the case in which no brightness increase is achieved.

Increasing the radiance by light recycling increases the temperature of the radiation since the temperature is related to the spectral radiance. Clausius theorem defines that the change in entropy $\mathrm{d}S$ of a thermodynamics system

$$\mathrm{d}S = \delta Q/T \,, \tag{2.16}$$

in units of J/K, δQ is the heat transferred, T is the absolute temperature. The temperature increase amounts to reducing the entropy, this seems to contradict the second law of thermodynamics which states the total entropy of any thermodynam-

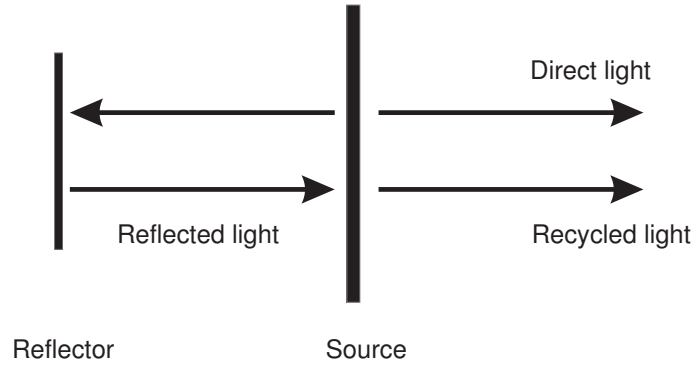

Figure 2.4.: Principle of light recycling. A source (non-black body) emits light in all directions. Assume that part of the light is reflected back to the source with an absorptivity less than unity. Part of the returned light escapes absorption and re-emerges from the source and is superimposed into the same phase space as radiation directly emitted by the source, leading to an increased brightness in this phase space. As a downside of this principle, the total luminous flux is reduced by the amount absorbed.

ically isolated system can only increase over time, approaching a maximum value,

$$\mathrm{d}S/\mathrm{d}t \geq 0 \,, \tag{2.17}$$

where S is the entropy and t is the time.

The equality sign holds only when the entropy is at its maximum (equilibrium) value. The process is achieved without dumping heat at some lower temperature reservoir in order to carry the excess entropy. In fact the emission of light is an irreversible process in which entropy is produced [53]. Light recycling reduces the entropy production rate of the emission process inside the lamp and thereby achieves a lower entropy content of the emitted radiation.

In order to investigate the limits of this principle we need to consider absorption and emission within an infinitesimal slab of material as indicated in Fig. 2.5. In passing through the slab, the radiance of the incident light decreases due to absorption by an amount proportional to the local radiance $-\tau(z)\, L_\lambda(z)\, \mathrm{d}z$, where $L_\lambda(z)$ is the local radiance, $\mathrm{d}z$ is an infinitesimal path element within the material, $\tau(z)$ is the absorption coefficient, connected to the absorptivity $\alpha(z)$ by Lambert-Beer's law

$$\alpha(z) = 1 - \exp\left(-\tau(z)\, z\right) \,. \tag{2.18}$$

The radiance of the light can also increase by emission from the material contained within the slab in local thermodynamic equilibrium at a local temperature. The net change of radiance is the sum of the two contributions, expressed as

$$\frac{\mathrm{d}L_\lambda(z)}{\mathrm{d}z} = \tau(z) \left(L_\lambda^{\mathrm{Pl}}(z) - L_\lambda(z)\right) \,. \tag{2.19}$$

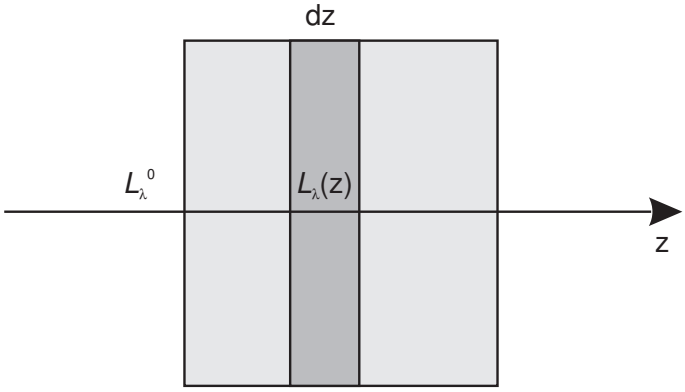

Figure 2.5.: In a volume source absorption and emission happen simultaneously and is distributed over the entire light path. In an infinitesimal path element dz, absorption is proportional to the local radiance whereas emission is a function of emissivity and thermodynamic parameters, resulting in a net change of radiance given by Eq. (2.19). For the case of light recycling, the initial radiation L_λ^0 is the recycled light, and may not be zero.

Solving the differential transfer equation in closed form for a homogeneous system, where τ and L_λ^{Pl} are independent of location, yields [7, 54]

$$L_\lambda(z) = L_\lambda^{\mathrm{Pl}} - \exp\left(-\tau z\right)\left(L_\lambda^{\mathrm{Pl}} - L_\lambda^0\right) \ , \tag{2.20}$$

where the initial radiation L_λ^0 is the recycled light, and may not be zero.

By definition the brightness enhancement factor is the ratio of the radiance with the recycled light to the radiance in the absence of recycled light, expressed as

$$\begin{aligned} \eta &= \frac{L_\lambda(z)}{L_\lambda(z)|_{L_\lambda^0=0}} \\ &= \frac{L_\lambda(z)}{\left(1-\exp(-\tau z)\right)\, L_\lambda^{\mathrm{Pl}}} \ . \end{aligned} \tag{2.21}$$

The solution in Eq. (2.20) yields the limits of light recycling

- in the limit of an optically thick source, i. e. the optical thickness (the product of the absorption coefficient τ and the geometrical path length z) $\tau z \gg 1$, the absorptivity approaches unity and the radiance approaches the equilibrium radiance as given by Planck's law in Eq. (2.12). Therefore a thick source is optically black. In this case the light enhancement factor is one, i. e. light recycling shows no benefit for black bodies or approximate black bodies, as all recycled light will be absorbed, and none will be transmitted or reflected.

- in the opposite limit of an optically thin source, i. e. the optical thickness $\tau z \ll 1$, the absorptivity is far below unity and the radiance of the originally

emitted light may be far from the equilibrium radiance. The radiance depends linearly on the optical thickness τz. In this case the initial radiance L_λ^0 amounts to that emitted by the naked source in the absence of light recycling, given by

$$L_\lambda^0 = (1 - \exp(-\tau z))\, L_\lambda^{\mathrm{Pl}} \,. \tag{2.22}$$

Combining Eqs. (2.20)−(2.22) yields the brightness enhancement factor η

$$\eta = \frac{(1 - \exp(-2\tau z))\, L_\lambda^{\mathrm{Pl}}}{(1 - \exp(-\tau z))\, L_\lambda^{\mathrm{Pl}}} = 1 + \exp(-\tau z) \,. \tag{2.23}$$

Both limits of light recycling can be explained with Eq. (2.23). From a thermodynamic point of view, light recycling in an optically thin source amounts to optically multiplying the optical thickness of the source by a factor of two (in terms of one transit through the source). This principle can be applied recursively more than once, leading to the resulting radiance after the n-th transit as

$$L_\lambda^{\mathrm{n}}(z) = (1 - \exp(-n\tau z))\, L_\lambda^{\mathrm{Pl}} \,. \tag{2.24}$$

Consequently, the light enhancement factor is given by

$$\eta = \frac{1 - \exp(-n\tau z)}{1 - \exp(-\tau z)} = \sum_{i=1}^{n} \exp\left(-(i-1)\,\tau z\right) \,. \tag{2.25}$$

The result reveals that a low absorptivity has a high potential for light recycling.

2.3. Light recycling with short-arc lamps

2.3.1. Experimental method and setup

The spectral radiation of a high-pressure short-arc lamp with light recycling is measured to investigate its absorption and emission characteristics, in turn to investigate the light recycling effect in the source. The experimental setup is shown in Fig. 2.6. The measured source is a high-pressure short-arc discharge lamp, whose luminous zone is shown in Fig. 2.7 (a). The lamp is a thermal radiator, which is usually spectrally selective and radiates mainly in specific spectral lines, i. e. a selective radiator. It is chosen as the investigated source for having the advantage of a transparent plasma zone inside the capsule of the lamp, so that light can transit the source multiplely despite the existing absorption. The lamp contains a small amount of mercury and either argon or xenon which acts as starting gas, as the mercury vaporizes in the startup phase of the lamp. When the lamp is cold, the gas pressure inside is lower than atmospheric pressure and small droplets of mercury can be seen. When the lamp is in operation, the mercury vaporizes and reaches a pressure of up to ten

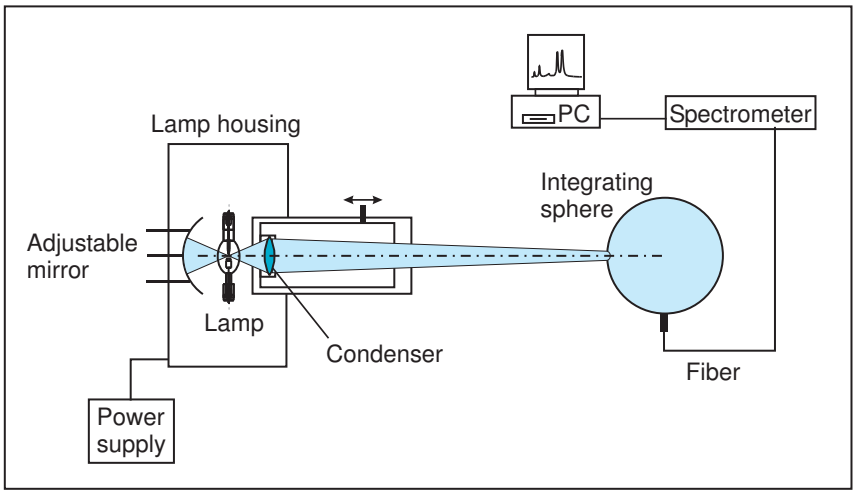

Figure 2.6.: Experimental setup for light recycling. A high-pressure short-arc lamp is powered with a DC power supply. It is situated in a housing for the purposes of safety and cooling. An adjustable spherical reflector is mounted on the left-hand side of the lamp to reflect the light back towards the lamp, and a short focal-length condenser is placed on the right-hand side for concentrating the beam. The integrating sphere scatters the incident light repeatedly, so that a uniform radiation distribution is obtained. Spectroscopic measurements are taken with a spectrometer with an operating band ranging from 360 nm to 1000 nm and a PC.

bars. With the increase of the pressure, the elastic collisions between electrons and gas atoms cause an energy transfer from electrons to the gas atoms, so that the gas is heated. At a pressure of around 1 bar, the gas temperature is nearly the same as the electron temperature, which is typically in the range of $4000-6000\,\mathrm{K}$, whereas the lamp wall temperature is about $1000\,\mathrm{K}$. From the center of the lamp to the outer region near its wall exists a plasma temperature gradient, resulting in a radial particle density distribution.

High temperature favors excitation and ionization. As the arc center is hot, most of the current flow occurs there, and most of the radiation is produced in the center, therefore the center looks much brighter than the outer zone. The center region (between the anode and the cathode) is named the hot zone, whereas the outer region (surrounding the center) is named the cold zone. The cold zone serves as radiation absorber and stabilizes the arc. The luminance area in the center is very small, about $0.25\times0.35\,\mathrm{mm}^2$.

Light produced near the center will traverse the hot zone and the cold zone on the way out (Fig. 2.7 (a)), leading to absorption and energy loss. After being collimated by the condenser (Fig. 2.6), the light is imaged onto the entrance of the integrating

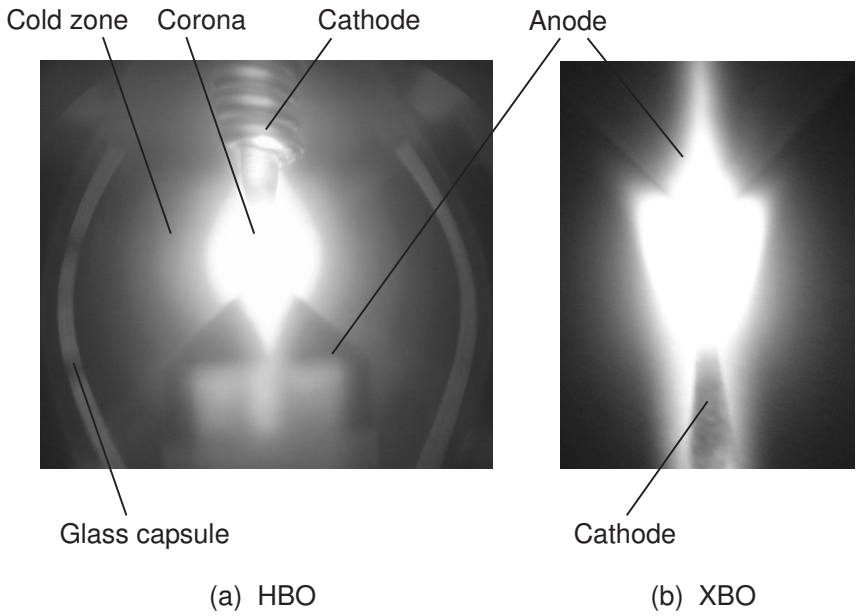

Figure 2.7.: (a) An image of the high-pressure short-arc lamp HBO, (b) an image of the high-pressure short-arc lamp XBO on the entrance of the integrating sphere in the setup in Fig. 2.6. From the center to the glass wall of the lamp exists a plasma temperature gradient, leading to a radial particle density distribution and a brightness gradient.

sphere. We call this the direct radiation (DR) in Fig. 2.8. Light emitted in the back direction is reflected back to the source by a spherical mirror, then passes through the source. After passing through the objective, a reflected radiation (RR) is imaged onto the same entrance of the integrating sphere. By adjusting the mirror, DR and RR can be either placed side by side, or onto the same area, resulting in a superimposed radiation (SR), following the principle of light recycling. With the spectrometer and the PC, on-line spectral radiation measurements are taken.

The intensity of the measured spectral radiation is always smaller than the black-body radiation at the same temperature. The difference results from the absorption in the plasma. In the various parts of a high-pressure short-arc lamp, the plasma is in, or close to the state of local thermodynamic equilibrium (LTE) [52], although there are temperature gradients and radiation escapes. LTE means that at one location all energy levels of electrons are populated according to Boltzmann distribution at a definite temperature. It is a condition under which a material emits radiation based on its intrinsic properties and its temperature, uninfluenced by the magnitude of any incident radiation. It is important to note that the LTE applies only to massive particles. In a radiating gas, the photons being emitted and absorbed by the gas need not to be in thermodynamic equilibrium with each other or with the massive particles of the gas in order for LTE to exist. The thermodynamic laws which relate plasma properties to the local temperature still hold, while analyzing

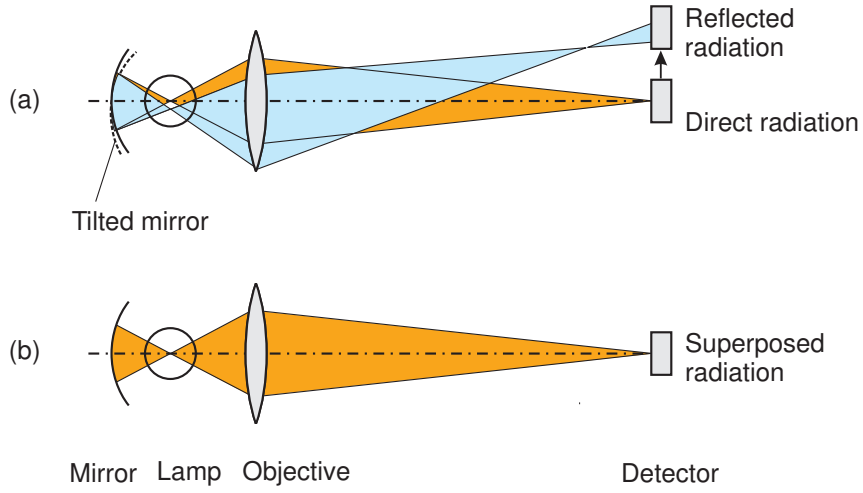

Figure 2.8.: Operating mechanism of the HBO lamp and the principle of light recycling. The objective images the direct radiation (DR) onto the entrance of the detector. The light emitted to the opposite side is reflected to the lamp by a spherical reflector, and passes through the objective. A reflected radiation (RR) is imaged onto the entrance of the detector. (a) shows DR and RR side-by-side, due to the off-axial reflector, (b) shows a superposed radiation (SR) of DR and RR due to the on-axial reflector.

the spectral radiation.

2.3.2. Results and discussion

High-pressure mercury short-arc lamp (HBO)

The three measured quantities consisting of the direct radiation, the reflected radiation and the superposed radiation are illustrated in Fig. 2.9. The results reveal that the curves are not in a linear relation to each other because of the spectral absorption property of the lamp (a selective radiator). The source shows a stronger emission at several spectral lines than at the neighboring wavelengths due to the transition of mercury atoms between specific energy levels, shown in Fig. 2.10 (a).

With the measured radiation, the absorptivities in the cold zone and hot zone are calculated. The absorptivity in the cold zone can be derived by comparing DR and RR. For DR, light passes through the hot zone and the cold zone once successively before escaping the lamp; while for the side-by-side RR, before leaving the source eventually, light traverses the entire cold zone again after being reflected back towards the source. With Lambert-Beer's law there are

$$L_{\mathrm{RR}}(\lambda) \;=\; L_{\mathrm{DR}}(\lambda)\,\exp\left(-\Delta_{\mathrm{c}}\right)\;, \tag{2.26}$$

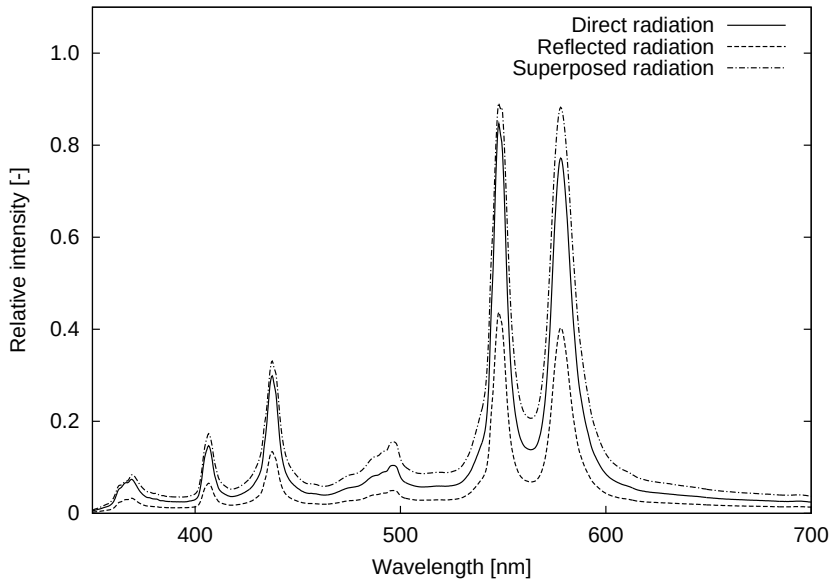

Figure 2.9.: Spectral radiation of the direct radiation (DR), reflected radiation (RR) and superposed radiation (SR) of DR and RR of an HBO lamp.

$$\alpha_{\mathrm{c}}(\lambda, T) \;=\; 1 - \exp\left(-\Delta_{\mathrm{c}}\right) \;=\; 1 - \frac{L_{\mathrm{RR}}(\lambda)}{L_{\mathrm{DR}}(\lambda)}\,, \tag{2.27}$$

where $L_{\mathrm{DR}}(\lambda)$, $L_{\mathrm{RR}}(\lambda)$ are the respective spectral intensities of DR and RR, obtained from measurement. Δ_{c} is the optical thickness of the cold zone, $\alpha_{\mathrm{c}}(\lambda, T)$ is the absorptivity of the cold zone.

Figure 2.11 shows a continuous absorptivity in the cold zone. The temperature in this region is relatively lower than that in the center, giving rise to a higher density of particles. The combination of the high density and the large geometrical dimension in the cold zone yields a stronger absorption in the cold zone than in the hot zone except at the characteristic spectral lines.

By adjusting the mirror in Fig. 2.8, the reflected radiation is superimposed onto the direct radiation. A comparison of the optical paths reveals that the reflected radiation differs from the previous RR by light passing through not only the entire cold zone but also through the hot zone, yielding the spectral intensity of the superposed radiation as

$$L_{\mathrm{SR}}(\lambda) = L_{\mathrm{DR}}(\lambda) + L_{\mathrm{DR}}(\lambda)\, \exp\left(-\Delta_{\mathrm{c}} - \Delta_{\mathrm{h}}\right)\,, \tag{2.28}$$

where Δ_{h} is the optical thickness of the hot zone. With Eqs. (2.26) and (2.28) the absorptivity in the hot zone $a_{\mathrm{h}}(\lambda, T)$ is expressed as

$$\alpha_{\mathrm{h}}(\lambda, T) = 1 - \exp\left(-\Delta_{\mathrm{h}}\right) = 1 - \frac{L_{\mathrm{SR}}(\lambda) - L_{\mathrm{DR}}(\lambda)}{L_{\mathrm{RR}}(\lambda)}\,. \tag{2.29}$$

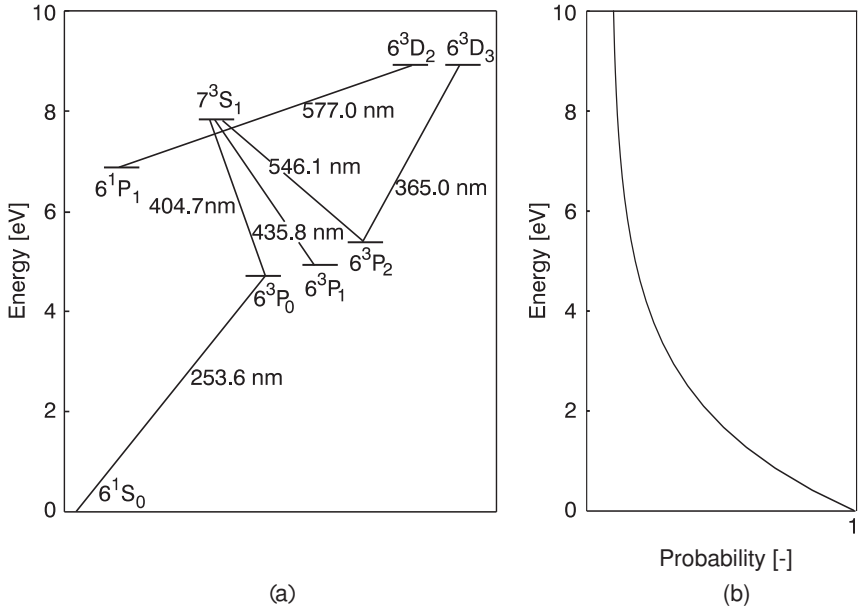

Figure 2.10.: (a) Energy levels of mercury atoms. The transitions of mercury atoms between different energy levels contribute to the radiation transfer. The spectral lines of emitted light are determined by the energy differences between certain energy levels; (b) schematically shows that the probability of energy level of an arbitrary atom is populated according to Boltzmann distribution, it is an exponentially decreasing function of the energy, given by Eq. (2.30).

The curve of the absorptivity in the hot zone in Fig. 2.11 shows a relatively weak absorption at all wavelengthes. At several spectral lines, the absorption is much stronger than at neighboring wavelengths. A comparison of the absorptivity in the hot zone and that in the cold zone reveals that absorption (or emission) in the hot zone is wavelength-dependent and temperature-dependent. The absorption in the plasma of the short-arc lamp increases with the temperature. The fact that strong absorption happens at the same wavelength as strong emission happens, proves Kirchhoff's law that a good absorber is also a good emitter at the same wavelength.

The measured results of the radiation and the calculated absorptivities reveal that

- the wavelengths of the spectral lines are specified by the energy difference between certain energy levels. The energy level diagram of mercury in Fig. 2.10 (a) illustrates the transition process [25, 30];
- the changes in absorptivity (or emissivity) depend on temperature and wavelength, due to the different occupation and transition of atoms between specific energy levels. Boltzmann distribution gives an explanation.

At absolute zero temperature, all atoms populate in the ground level. The popu-

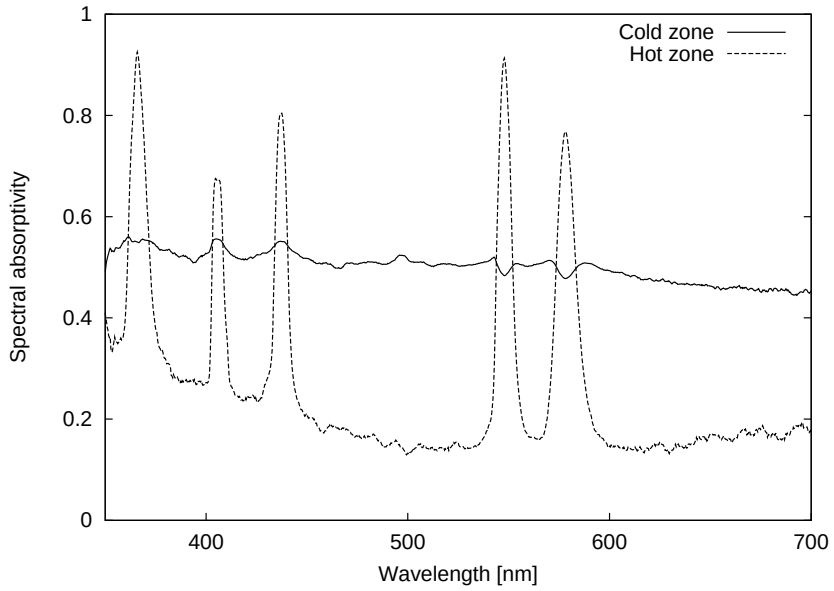

Figure 2.11.: Spectral absorptivities in the cold zone and in the hot zone in the HBO lamp.

lations of higher energy levels increase with the temperature. The probability of an arbitrary atom in any energy level E_i is given by Boltzmann distribution

$$p(E_\mathrm{i}) \propto \exp\left(-\frac{E_\mathrm{i}}{k_\mathrm{B}\,T}\right) , \qquad i = 1, 2, ..., \tag{2.30}$$

schematically shown in Fig. 2.10 (b). It reveals that the population probability increases exponentially with the temperature but decreases exponentially with the energy. The higher the temperature, the more densely the energy level is populated. The higher the energy level, the more sparsely the energy level is populated. However, this does not necessarily hold under non-equilibrium conditions, e. g. the population inversion for laser.

Light is emitted when atoms transit from higher energy levels to lower levels, a high population probability of atoms in higher energy levels favors light emission. The relation of atoms occupying the higher energy level E_H and the lower level E_L with respective concentrations C_H and C_L is given by Boltzmann distribution

$$\frac{C_\mathrm{H}}{C_\mathrm{L}} = \exp\left(-\frac{E_\mathrm{H} - E_\mathrm{L}}{k_\mathrm{B}\,T}\right) . \tag{2.31}$$

The population ratio is an exponentially increasing function of the temperature T. In the case of the investigated HBO lamp, when the temperature of the arc increases ($> 4000\,\mathrm{K}$), the higher energy levels are densely populated, more light can be emitted from the center, consequently radiation varies more dramatically than T^4 (Stefan-Boltzmann's law), leading to the increase of the emissivity as well as the

absorptivity. If the temperature is high enough, the source can radiate as well as a black body at the main spectral lines. On the contrary, at a low temperature of the arc, e. g. if $T < 1000\,\mathrm{K}$, all energy levels are barely occupied except the ground level, leading to almost no radiation from the source.

Light is emitted with several characteristic spectral lines (in Fig.2.9), due to the discontinuous energy levels and the nonproportional number of atoms occupying energy levels. Light at each energy interval is emitted with different contribution to the total radiation. All these reasons give rise to the wavelength-dependent and temperature-dependent emissivity.

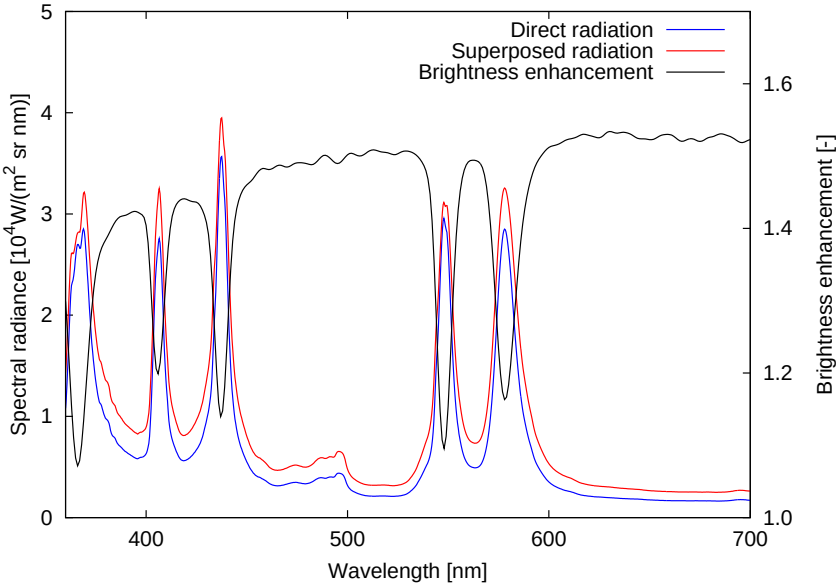

Figure 2.12.: Light recycling effect in the HBO lamp. The brightness enhancement is the ratio of the superposed radiation to the direct radiation, the average value amounts to 1.45 over the entire spectral band. The curves reveal a weak brightness increase at the spectral lines where strong emission happens, resulting from the strong absorption. The brightness enhancement is also wavelength-dependent, i. e. red light increases more than green light, due to a weaker absorption of the red light.

A comparison of the direct radiation and the superposed radiation yields the brightness enhancement factor $\eta = L_{\mathrm{SR}}(\lambda)/L_{\mathrm{DR}}(\lambda)$, shown in Fig. 2.12. It reveals the light recycling effect in the investigated lamp. In the same phase space as the original direct radiation, the average brightness enhancement factor approaches 1.45 due to light recycling. Superposing the reflected radiation onto the direct radiation in the same phase space is equivalent to increasing the optical thickness of the source. As a consequence, the total luminous flux decreases slightly due to the absorption in the plasma, whereas the collected luminous flux in this phase space may increase

via light recycling, leading to an increased brightness. Fig. 2.12 shows a wavelength-dependent brightness enhancement, i. e. red light increases more than green light, due to a weaker absorption of the red light.

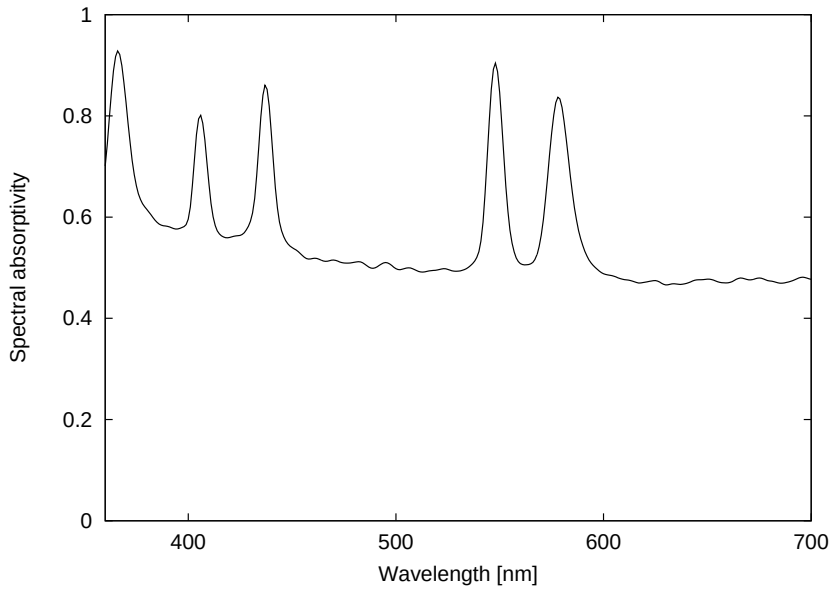

Figure 2.13.: The total absorptivity of the plasma in the HBO lamp. Both the absorption in the cold zone and in the hot zone play roles in the resulting absorption. The total absorptivity is calculated with Eq. (2.32), connected with the absorptivity of the cold zone and that of the hot zone by Eq. (2.33).

In reality, both the absorption in the cold zone and in the hot zone contribute to the absorption of the plasma in the HBO lamp. With Eq. (2.28) the total absorptivity $\alpha_{\mathrm{tot}}(\lambda, T)$ is expressed as

$$\alpha_{\mathrm{tot}}(\lambda, T) = 1 - \exp\left(-\Delta_{\mathrm{c}} - \Delta_{\mathrm{h}}\right) = 2 - \frac{L_{\mathrm{SR}}(\lambda)}{L_{\mathrm{DR}}(\lambda)} \,, \tag{2.32}$$

illustrated in Fig. 2.13. The total absorptivity $\alpha_{\mathrm{tot}}(\lambda, T)$ is higher than either that of the cold zone $\alpha_{\mathrm{c}}(\lambda, T)$ or that of the hot zone $\alpha_{\mathrm{h}}(\lambda, T)$. The relation between the three quantities is derived as

$$\alpha_{\mathrm{tot}}(\lambda, T) = \alpha_{\mathrm{c}}(\lambda, T) + \alpha_{\mathrm{h}}(\lambda, T) - \alpha_{\mathrm{c}}(\lambda, T)\, \alpha_{\mathrm{h}}(\lambda, T) \,. \tag{2.33}$$

By means of an investigation of the light path of the radiation, the light emerging from the center of the bright corona, named initial radiation $L_0(\lambda)$ is related to $L_{\mathrm{DR}}(\lambda)$ by

$$L_{\mathrm{DR}}\left(\lambda\right) = L_0(\lambda)\, \exp\left(-\frac{\Delta_{\mathrm{c}} + \Delta_{\mathrm{h}}}{2}\right) \,. \tag{2.34}$$

Summarizing Eqs. (2.32) and (2.34) yields

$$L_0(\lambda) = \sqrt{\frac{L_{\mathrm{DR}}^3}{L_{\mathrm{SR}} - L_{\mathrm{DR}}}} \,. \tag{2.35}$$

The calculated result is illustrated in Fig. 2.14. The initial radiation is equivalent to the blackbody radiation at a certain temperature T, given by Planck's law in Eq. (2.12)

$$T = \frac{hc/\lambda}{k_{\mathrm{B}} \ln\left(\frac{2hc^2}{\lambda^5 L_\lambda^{\mathrm{Pl}}} + 1\right)} \,, \qquad \text{with} \quad L_\lambda^{\mathrm{Pl}} = L_0. \tag{2.36}$$

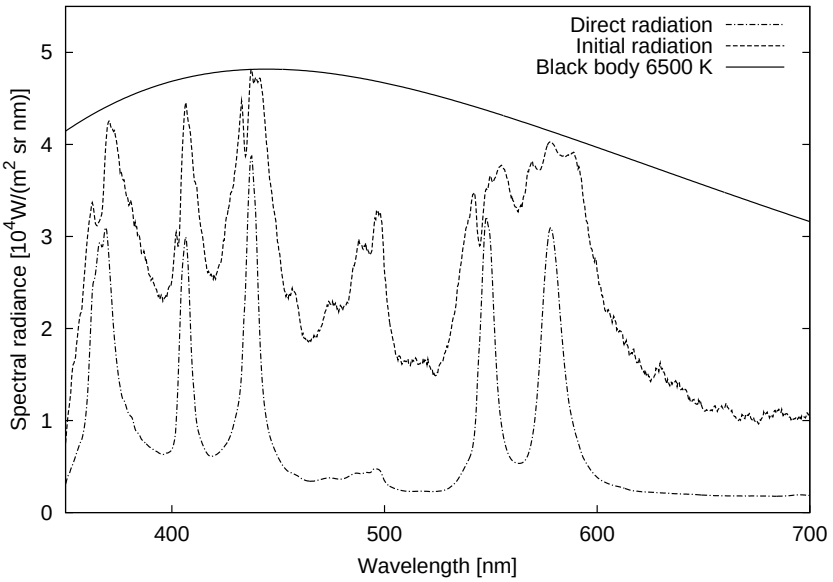

Figure 2.14.: Spectral distribution of the HBO lamp, i. e. the direct radiation, the initial radiation of light emerging from the center before traversing the plasma region, and the spectral radiation of a black body at 6500 K according to Planck's law, which is closest to the initial intensity plotted as envelope.

The initial intensity approaches blackbody radiation. However, for the HBO lamp, the derived initial intensity is wavelength-dependent, i. e. it is not a smooth continuous curve. To ensure that the intensity over all wavelengths is below the blackbody radiation at the same temperature, the maximum temperature of 6500 K calculated from the measured data is chosen as the black body's temperature, following Planck's law which describes the thermodynamic limit: no object can emit more than a black body at the same temperature.

The LTE and Boltzmann distribution offer the possibility to calculate the pressure inside the lamp.

Under the LTE, a form of Kirchhoff's law for a hot body at a temperature T applies [24],

$$\epsilon_\lambda(T) = \tau_{\mathrm{tot}}(\lambda, T)\, L_\lambda^{\mathrm{Pl}}(T)\ , \tag{2.37}$$

where $\epsilon_\lambda(T)$ is the emission coefficient expressed in $\mathrm{W/(m^3\,sr\,nm)}$. Note that this quantity is the emissivity $\varepsilon(\lambda, T)$. The power emitted per unit volume is $4\pi\,\epsilon_\lambda(T)$. $\tau_{\mathrm{tot}}(\lambda, T)$ is an averaged absorption coefficient of the plasma, related to the total absorptivity $\alpha_{\mathrm{tot}}(\lambda, T)$ and the size of the source d by Lambert-Beer's law

$$\tau_{\mathrm{tot}}(\lambda, T) = -\frac{\ln\left(1 - \alpha_{\mathrm{tot}}(\lambda, T)\right)}{d}\ . \tag{2.38}$$

Equation (2.20) is valid only if the absorption coefficient $\tau(z)$ is independent of position. This implies that the temperature T is also independent of position z because the absorption coefficient depends on T, as revealed in Fig. 2.11. Therefore Eq. (2.38) is based on the simplified assumption that there are only two temperatures: a high temperature in the hot zone and a low temperature in the cold zone.

The emission coefficient of characteristic spectral lines at a certain temperature T is given by [12, 13]

$$\begin{aligned} \epsilon_\lambda(T) &= \frac{1}{4\,\pi}\frac{hc}{\lambda}\,A_{\mathrm{HL}}C_{\mathrm{H}} \\ &= \frac{1}{4\,\pi}\,\frac{hc}{\lambda}\,g_{\mathrm{H}}\,A_{\mathrm{HL}}\,\frac{p}{k_{\mathrm{B}}\,T}\,\exp\left(-\frac{E_{\mathrm{H}}}{k_{\mathrm{B}}\,T}\right)\ , \end{aligned} \tag{2.39}$$

where hc/λ is the photon energy, A_{HL} is the transition probability, specified as the average number of atom transitions per second, C_{H} is the concentration of atoms at the higher level, in units of $\mathrm{m^{-3}}$, g_{H} is the statistical weight of the higher level, E_{H} is the excitation energy and p is the vapor pressure. In Eq. (2.39) the ideal gas equation is applied. Here, we choose four mercury lines, 365.0 nm, 404.7 nm, 435.8 nm and 546.1 nm. Using the transition probabilities of empirical results [25], the pressure is approximated and listed in Table 2.1.

The pressure values (in Table 2.1) of the four spectral lines are very close, they are in the same order of magnitude as common mercury arc lamps. The possible reasons of the errors are:

- measurement error: geometry, radiometry;
- calculation error: the approximation of the geometrical dimension of the source, the used data of the empirical transition probabilities from literature.

The results show that using the spectroscopic method to analyze the temperature and the pressure is feasible.

Table 2.1.: Spectroscopic data of analyzed mercury lines. Transition: atoms transfer from the initial level to the final level, A_{HL} is the transition probability, g_{H} is the statistical weight of the higher level, $\epsilon_\lambda(T)$ is the emission coefficient, p is the vapor pressure inside the lamp.

λ	Transition[a]	$g_{\mathrm{H}}A_{\mathrm{HL}}$[a]	$\epsilon_\lambda(T)$[b]	p
[nm]	[$10^8\,\mathrm{s}^{-1}$]		[$10^7\,\mathrm{W/(m^3\,sr\,nm)}$]	[bar]
365.0	$6^3D_3 - 6^3P_2$	13.7	7.24	9.3
404.7	$7^3S_1 - 6^3P_0$	0.95	3.91	11.2
435.8	$7^3S_1 - 6^3P_1$	1.71	5.27	9.1
546.1	$7^3S_1 - 6^3P_2$	1.82	5.44	11.0

[a] Source: [20, 25]
[b] Source: [12].

High-pressure short-arc xenon lamp (XBO)

With the same setup (Fig. 2.6), a 75 W XBO lamp (Fig. 2.7 (b)) is measured. Filled mostly with xenon gas, the XBO lamp shows a spectral distribution different from the HBO lamp. It is a combination of thermal radiation of the plasma with Xe-lines. The emission (Fig. 2.15) approximates a continuum in the UV and visible light, but shows the strong spectral Xe-lines at the wavelength longer than 760 nm.

The light recycling effect of the XBO lamp is shown in Fig. 2.12. The experimental results are listed in Table 2.2. Compared with the brightness enhancement factor of 1.45 of the HBO lamp, the XBO lamp achieves an average factor of 1.70 in the spectral range $360 - 830$ nm. It offers a good potential for increasing the radiance of the XBO lamp by means of light recycling.

Table 2.2.: Comparison of HBO (100 W) and XBO (75 W) lamps.

Item	HBO	XBO
Materials	Hg, Ar/Xe	Xe
Efficacy [lm/W]	47	13
Average absorptivity	0.55	0.30
Average transmittance	0.45	0.70
Center temperature [K]	6500	5500

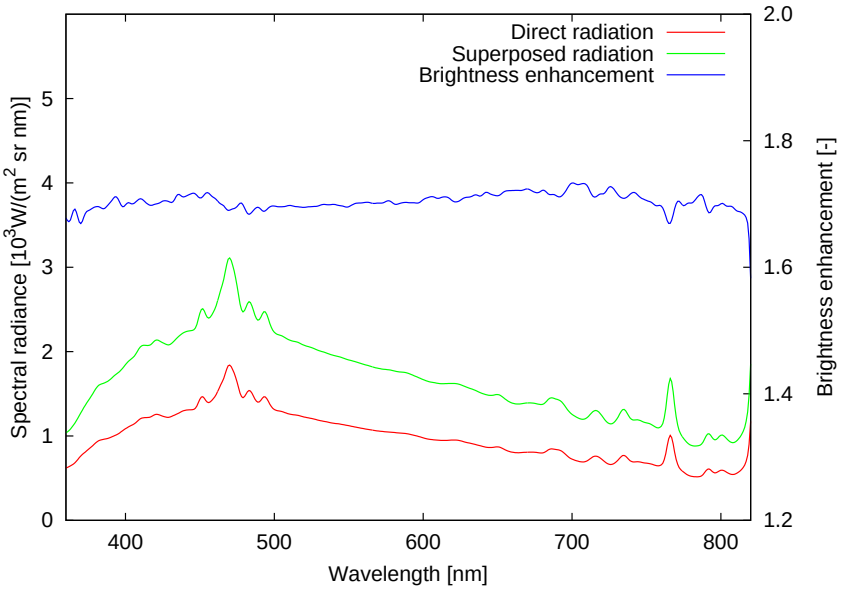

Figure 2.15.: Light recycling effect in the XBO lamp. The brightness enhancement factor averages 1.70 over the spectral range 360 to 830 nm.

2.4. Summary

Kirchhoff's law and Planck's law are the theoretical foundations of increasing the brightness of light sources via light recycling.

Back-reflection, a kind of light recycling using a spherical reflector for HBO and XBO, is successfully applied to short-arc lamps. Most of the radiant light is redirected to the exit of the system, so that the brightness is increased by 45% for the HBO lamp, 70% for the XBO lamp within a reduced phase space.

In addition, with the spectroscopic measurement the absorptivity/emissivity of two kinds of discharge lamps are derived. The results reveal that the XBO lamp is preferable for brightness increase via light recycling than the HBO lamp, due to its spectral continuum radiation and lower spectral absorptivity. The lower the absorptivity of the source, the greater potential to achieve brightness enhancement via light recycling. This conclusion will be verified again in the physical model of tungsten filament lamps in the next chapter.

3. Thermal light sources

Filament lamps emit light directly by incandescence, i. e. the glow from solids, especially metals, different from the light-emitting mechanism of short-arc lamps discussed in Sec. 2.2. In addition, light recycling is an intrinsic property of filament lamps because of its coiled (or coiled-coil) structure.

In this chapter a thermal source, a 20 W tungsten filament lamp is investigated, for the purpose of setting up a physical model for simulating the radiance distribution of filament sources with respect to location, direction and wavelength based on physical laws. The physical model applies to any kind of filament lamp, it is the basis of source modelling in ray-tracing. In addition to basic physical laws the model needs a few parameters to describe the geometry, the material of the filament. The values of these parameters can be determined from independent measurements. In this work the needed parameters are identified via a global optimization process [16, 18].

The filament of the tungsten halogen lamp is sealed into a small quartz envelope filled with halogen gas such as iodine or bromine. Quartz, or fused silica, has a higher heat resistance and a better transmissivity in the UV than glass. At a high operating temperature, the halogen gas combines with tungsten atoms as they evaporate and redeposit on the filament, but not on the envelope wall. This halogen cycle prevents a blackening of the bulb wall through life. Blackening of the bulbs happens to conventional incandescent lamps because of the bulky size, the lower operating temperature and pressure and in absence of halogen, compared with tungsten halogen lamps. The gas filling inside the tube is of a higher pressure than that of normal incandescent lamps, about 7-8 bars. This slows down the tungsten diffusion and evaporation, hence extending the lifetime of the halogen lamp.

Based on the spectroscopic measurement of radiation, microscopic measurement of geometry (Fig. 3.1) and ray-tracing simulation of light recycling, the physical model of the spectral radiance distribution of the filament lamp is established. The interdependence of the submodules used in the model is shown in Fig. 3.2. The model consists of modules of the geometry of the filament, and its material properties. These two submodules are integrated with the thermal model, and yield the radiation model. In detail,

- in the geometry model, the coil is parameterized by the location along the filament. The recycling of light emitted by parts of the filament facing other parts of the filament is an important issue in the calculation of the emitted

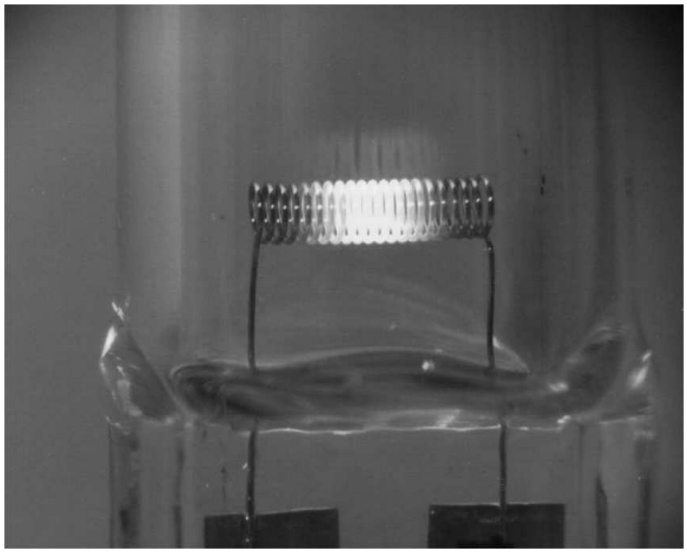

Figure 3.1.: Photograph of the 20 W halogen lamp at a low current (0.5 A) for better visualization. The temperature is highly inhomogeneous in this regime.

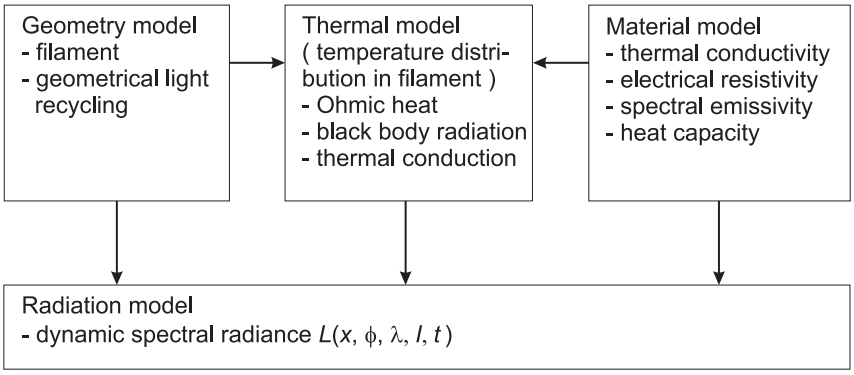

Figure 3.2.: Flow chart of the physical modelling of filament lamp, interdependence of the submodules used.

radiance. Light recycling is described geometrically at this stage. The geometrical module (Sec. 3.1.1) delivers its results to the thermal model and the radiation model;

- the material model deals with the properties of the material including thermal conductivity, the electrical resistivity, the heat capacity, and the spectral emissivity. Tungsten is the material of choice for the filament wire due to the highest melting point of all metals. The results of the material model are used in the thermal model and in the radiation model;

- the thermal model yields the temperature distribution along the filament by solving an instationary heat balance equation, taking into account Ohmic heat

and thermal conduction of the wire. The results of this model (Sec. 3.1.2) are merged in the radiation model.

- in the radiation model the results of the submodules are integrated within Planck's law of spectral radiance. The result is the dynamic spectral radiance $L(x, \phi, \lambda, I, t)$, where x is the location along the filament, ϕ is the revolving angle around the wire, λ is the wavelength, I is the driving current, and t is the time.

3.1. Physical modelling of filament lamps

3.1.1. Geometrical model of the filament

The coil

Two important parameters for the heat balance are length L and radius R_c of the filament. The length as defined here refers to the stretched filament, before being wound up into a coil. Consider a unit length of coil, its cross-section area determines the thermal and electrical resistance, its circumference determines the light-emitting surface. For the circular cross section, the cross-section area and the circumference are expressed as: $A_\mathrm{c} = \pi R_\mathrm{c}^2$ and $C = 2\pi R_\mathrm{c}$. Any other convex cross-section shapes can be described analogously. It is of technical importance to keep the two quantities constant along the filament. This assumption holds in the model. The reason, that the cross-section area and the circumference are essential whereas the exact form of the filament is irrelevant is rooted in the relatively high thermal conductivity. The temperature is essentially constant over a cross section. Consequently the temperature distribution in one-dimensional space is modelled in Sec. 3.1.2.

The secondary form of the filament, the coil, is characterized by another two parameters: the winding radius of the coil R_w and its slope S_w. The geometrical model is described in detail, in order to specify nomenclature and the parametrization. Firstly, a space curve $\mathbf{Z} = \mathbf{Z}(x)$ with $0 \leq x \leq L$ is constructed, where x is the location along the filament. The function traces the center of the filament and is parameterized by the location along the filament

$$\mathbf{Z}(x) = R_\mathrm{w} \left(\frac{\psi}{S_\mathrm{w}}, \cos\psi, \sin\psi \right), \quad \text{with } \psi = \frac{x\, S_\mathrm{w}}{R_\mathrm{w}\sqrt{1 + S_\mathrm{w}^2}}, \tag{3.1}$$

In addition, the local orthogonal system is given

$$\mathbf{T}(x) = \frac{1}{\sqrt{1 + S_\mathrm{w}^2}} \left(1,\ -S_\mathrm{w} \sin\psi,\ S_\mathrm{w} \cos\psi\right),$$

$$\begin{aligned} \mathbf{K}(x) &= (0,\ -\cos\psi,\ -\sin\psi)\ , \\ \mathbf{N}(x) &= \frac{1}{\sqrt{1+S_{\mathrm{w}}^2}}\,(S_{\mathrm{w}},\ \sin\psi,\ -\cos\psi)\ , \end{aligned} \tag{3.2}$$

where $\mathbf{T}(x)$, $\mathbf{K}(x)$ and $\mathbf{N}(x)$ are the tangent vector, curvature and normal vector, respectively. The parametric function of the filament surface is given as $\mathbf{F} = \mathbf{F}(x, \phi)$. ϕ is defined as the revolving angle of a surface element around the filament. With $0 \leq x \leq L$ and $0 \leq \phi \leq 2\pi$, the parametric function is given as

$$\mathbf{F}(x,\phi) = \mathbf{Z}(x) + R_{\mathrm{c}}\cos\phi\,\mathbf{K}(x) + R_{\mathrm{c}}\sin\phi\,\mathbf{N}(x)\ . \tag{3.3}$$

Choosing Eq. (3.3) as a new parametric function of a coiled coil, and applying the vector derivation again, the parametric function of a coiled-coil surface can be derived in a seemingly complicated form due to the multiple coordinate projection.

Geometrical light recycling

The geometry of the coil is partially concave. A fraction of light emitted from a surface element on the inside of the coil will hit the other parts of the coil. This effect is considered, because it has an effect on the far field radiation distribution, and is the source of light recycling in the filament lamp. The geometrical light recycling factor ξ is defined as that fraction of the emitted light from a surface element which returns to the source again. It is the intrinsic property of the source resulting from its geometry. Under the assumption of Lambertian radiation, light recycling is a purely geometrical quantity. The light recycling factor varies for the location on the filament.

It is possible to approximate the recycling factor as a function of location as

$$\xi(\phi) = \frac{R_{\mathrm{c}} S_{\mathrm{w}}(1+\cos\phi)}{2\pi R_{\mathrm{w}}}\ . \tag{3.4}$$

However, we chose to determine the recycling factor by Monte Carlo ray-tracing with LightTools$^{\mathrm{TM}}$ (Fig. 3.3). Consider a surface element on the filament as a Lambertian emitter, the entire filament as the receiver. The emitted light from any surface element will either leave the configuration directly as emitted light, or hit other parts of the filament. The fraction of the emitted light that hits the coil is the recycling factor ξ (the part that is received by the receiver). A continuous recycling factor function of ϕ and x is obtained via interpolation. This method is used in the model.

The results of geometrical recycling factors from the ray-tracing simulation and from the approximation in Eq. (3.4) are shown in Fig. 3.4. The recycling factor

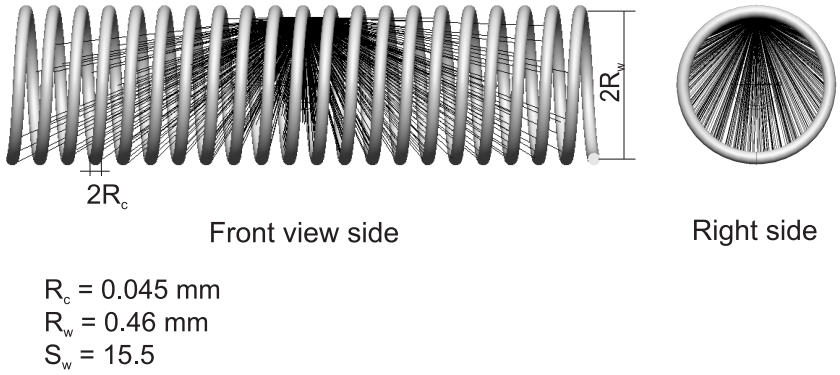

Figure 3.3.: Simulation model for deriving geometrical recycling factors of the filament. A specific surface element situated innermost and in the middle of the configuration is viewed as a Lambertian emitter with unity emitting power. The entire filament is chosen as the receiver. By means of Monte Carlo ray-tracing, the fraction of emitted light from the surface element that hits the receiver is specified as the geometrical recycling factor. $R_\mathrm{c} = 0.045\,\mathrm{mm}$, $R_\mathrm{w} = 0.46\,\mathrm{mm}$, $S_\mathrm{w} = 15.5$, the filament length $4\,\mathrm{mm}$.

is zero on the outside ($\phi = \pi$) and maximal on the inside ($\phi = 0$) of the wire at the center. It decreases towards the ends. Denser coils feature higher geometrical recycling (Fig. 3.4 (b)). At the end of the filament, the recycling is asymmetric (Fig. 3.4 (c)). Note that in the context the data of Configuration 2 (see Fig. 3.4) are used.

Figure 3.5 presents the one-dimensional geometrical recycling factor (averaged over ϕ) along the length of the filament. It is symmetrical with respect to the midpoint of the filament. The factor drops towards the both ends of the filament.

In this manner the geometrical recycling factor of a coiled-coil filament can also be derived.

3.1.2. Thermal model

Current and operation

A lamp is a thermal emitter. For filament lamps, due to the comparatively high thermal conductivity, the temperature is essentially constant over a cross section. Consequently the temperature distribution could be modelled in one-dimensional space only. We opt for an instationary model and include time dependence because otherwise the boundary conditions are numerically difficult to model [50]. As a consequence, the temperature distribution $T(x,t)$ as a function of the location along

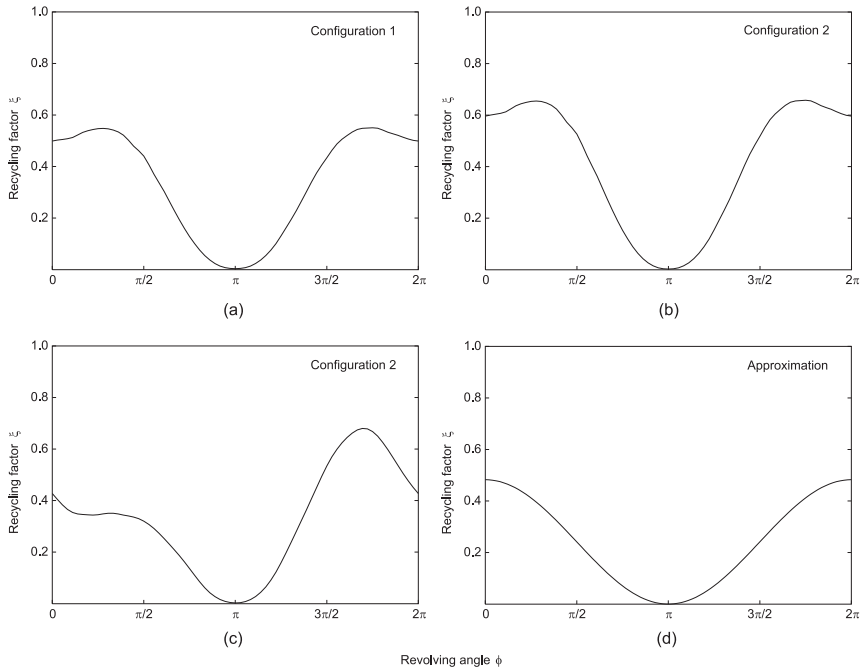

Figure 3.4.: Local recycling factor as a function of the revolving angle around the coil. Four cases are plotted. (a) Configuration 1: $R_c = 0.038\,\mathrm{mm}$, $R_w = 0.46\,\mathrm{mm}$, $S_w = 15.5$, at the center of the filament; (b) Configuration 2: $R_c = 0.045\,\mathrm{mm}$, $R_w = 0.46\,\mathrm{mm}$, $S_w = 15.5$, at the center of the filament; (c) Configuration 2 at the end of the filament; (d) approximation: Eq. (3.4) with the same filament as Configuration 2. Denser coils (Configuration 2) feature higher geometrical recycling. The geometrical recycling factor is zero on the outside ($\phi = \pi$) and maximal on the inside ($\phi = 0$) of the wire at the center. It decreases towards the ends, and is asymmetric at the end.

the filament x and the time t is modelled. As an advantage an AC operation can also be modelled.

Variations of the temperature with the revolving angle ϕ are assumed to be negligible, which is confirmed by spectroscopic measurements.

The temperature distribution is determined by solving an instationary differential equation which balances all heat contributions. Each one is described in turn.

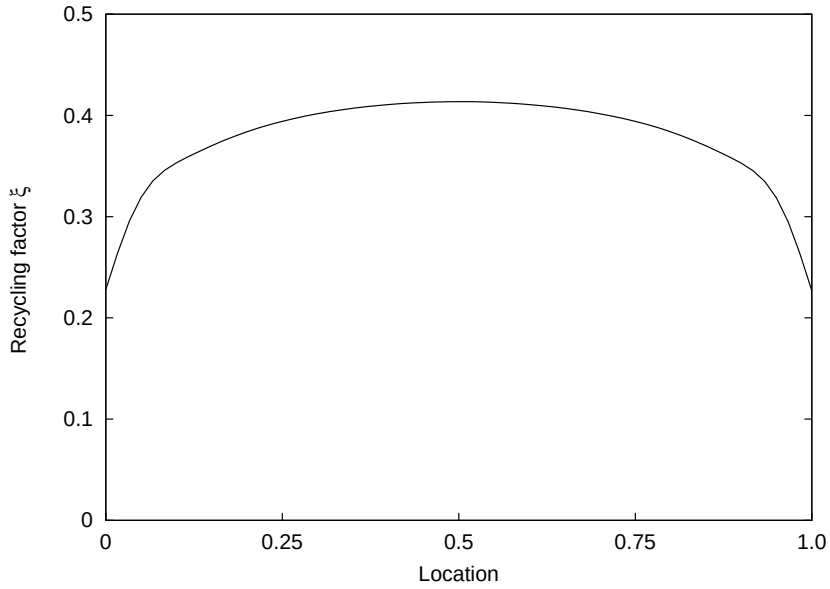

Figure 3.5.: One-dimensional recycling factor calculated by averaging over ϕ as a function of location along the length of the filament (Configuration 2). This is needed for the thermal model. The curve is symmetric with respect to its center.

Ohmic heat

The electrical current I heats up the filament at the heat rate (thermal power) per unit filament length P_Ω, expressed as

$$P_\Omega = \frac{I^2 \rho}{A_\mathrm{c}} \,, \tag{3.5}$$

where A_c is the cross-section area of the wire, defined in Sec. 3.1.1, ρ is the electrical resistivity of the filament material, it is a function of temperature, i. e. $\rho = \rho(T)$. A quadratic fit function of the temperature-dependent resistivity is derived from the experimental measurements

$$\rho = 2.87 \times 10^{-6} - 3.92 \times 10^{-8} \sqrt{5486 - T} \,, \quad \text{with} \quad T < 3200\,\mathrm{K} \,. \tag{3.6}$$

This result is very close to the results from literature [20].

Due to the stable positive differential resistance, filament lamps can be powered with a voltage-control source or a current-control source. In reality lamps are driven with voltage control. For numerical reasons, modelling the radiation in the current-control mode is simpler, as the current is constant along the filament. By integrating the resistivity for known temperature distribution, one can calculate the voltage

$$V = \frac{I}{A_\mathrm{c}} \int_0^L \rho\,(T(x))\,\mathrm{d}x \,. \tag{3.7}$$

Radiation

The filament emits light. The spectral radiation is modelled as a thermal radiation of a greybody radiator by Planck's law. The total radiant flux from any unit length of filament (integrated over all wavelength) is given by Stefan-Boltzmann's law [7]

$$\Phi_\mathrm{e} = C\varepsilon(T)\sigma(T^4 - T_0^4) \; . \tag{3.8}$$

where the ambient temperature $T_0 = 300\,\mathrm{K}$ is a constant, negligible for high filament temperatures, but included for consistency. The spectral emissivity $\varepsilon(T)$ describes the ratio of actually emitted thermal radiance to a blackbody radiation. It generally depends on both color and temperature. However, for the investigated filament lamp, the dependence of the emissivity on the wavelength and the temperature is not as large as that of the short-arc lamp in Chap. 2.3, because of the different emitting materials and emitting mechanism. For the thermal model the one-dimensional emissivity $\varepsilon(T)$ is used.

Thermal conduction

Thermal conduction along the filament is another contribution to the heat balance. The net thermal power W flowing into the observed element is derived with Fick's second law [8]

$$W = A_\mathrm{c}\kappa\frac{\partial^2 T(x,t)}{\partial x^2} \; , \tag{3.9}$$

where κ is the thermal conductivity. For metals, κ is linked to Wiedemann-Franz' law by the electrical resistivity

$$\kappa = \frac{L_\mathrm{w}\,T}{\rho} \; . \tag{3.10}$$

where L_w is the proportionality constant known as Lorenz number $L_\mathrm{w} = 2.45 \cdot 10^{-8}$-$\mathrm{W\,\Omega/K^2}$, independent of material and temperature. Wiedemann-Franz' law can be used to model the thermal conductivity from the electrical resistivity which is easier to measure. However in this work κ is modelled independently from the spectroscopic measurements.

The temperature distribution in the filament is described by means of summarizing Eqs. (3.5) −(3.9) in an instationary balance equation

$$\begin{aligned} c_\mathrm{p}A_\mathrm{c}\frac{\partial T(x,t)}{\partial t} &= P_\Omega + W - \Phi_\mathrm{e} \\ &= \frac{I(t)^2\,\rho(T)}{A_\mathrm{c}} + A_\mathrm{c}\kappa\frac{\partial^2 T(x,t)}{\partial x^2} - C\varepsilon(T)\sigma\left(T(x,t)^4 - T_0^4\right), \end{aligned} \tag{3.11}$$

where c_p is the heat capacity of the material.

This partial differential equation can be solved numerically, with appropriate boundary conditions. Assume that the coil is coupled to the ambient at the both

ends $x = 0$ and $x = L$ with two posts which have a given thermal end-coupling factor k_0. This leads to a mixed condition for the spatial boundary

$$\begin{aligned} \frac{\partial T(0,t)}{\partial x} &= \frac{k_0}{\kappa} \left(T(0,t) - T_0\right) \ , \\ \frac{\partial T(L,t)}{\partial x} &= -\frac{k_0}{\kappa} \left(T(L,t) - T_0)\right) \ . \end{aligned} \tag{3.12}$$

The boundary condition in time is

$$T(x,0) = T_0 \ . \tag{3.13}$$

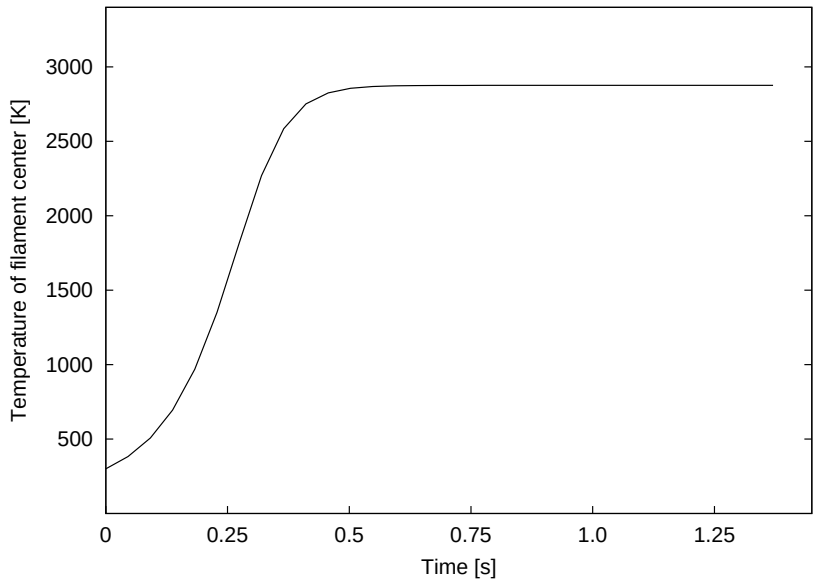

Figure 3.6.: Thermal model of the filament lamp for DC operation: Start-up to thermal equilibrium in the middle of the filament in a DC circuit.

After the current is switched on, the coil approaches the equilibrium temperature, as illustrated in Fig. 3.6 for full operating current at the filament center. The spatial temperature distribution over the entire filament in equilibrium at time 1.3 s at an operating current of 1.67 A, and 2.7 s at an operating current of 1.33 A is shown in Fig. 3.7, for direct current. Fig. 3.8 illustrates the instationary temperature distribution for AC operation. The current was switched off after 0.7 s.

3.1.3. Radiation model

Planck's law

The spectral radiance emitted by the filament is modelled with Planck's law. The spectral radiance emitted by a black body at temperature T and wavelength λ

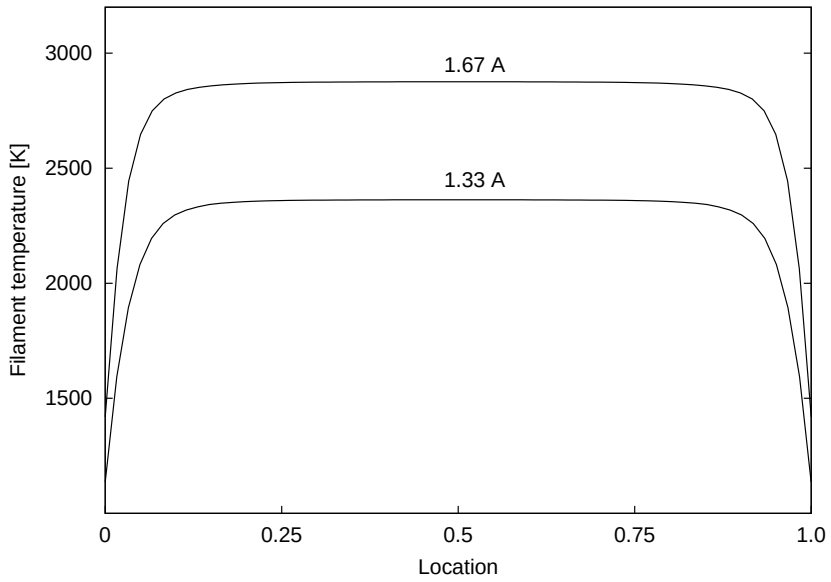

Figure 3.7.: Filament lamp model: Temperature distribution over the entire filament in equilibrium at time 1.3 s (1.67 A), and 2.7 s (1.33 A).

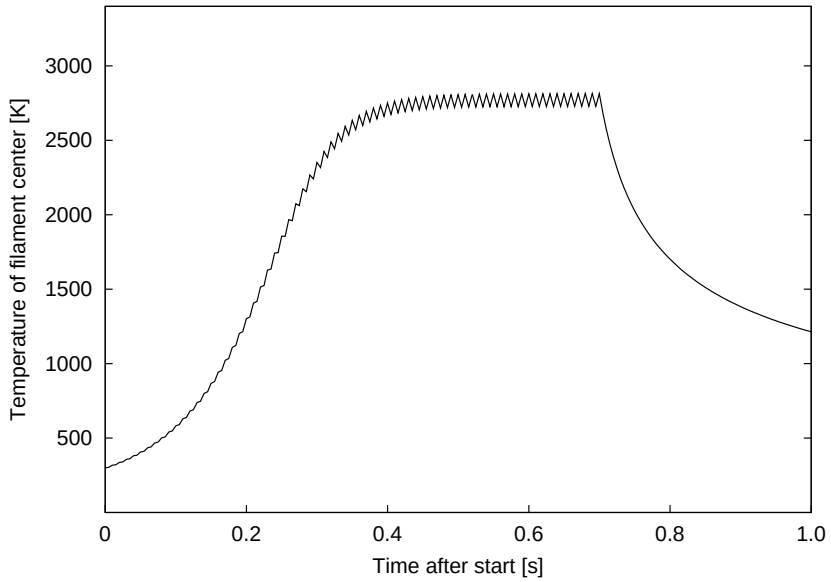

Figure 3.8.: Thermal model of the filament lamp for AC operation: Start-up to thermal equilibrium in an AC circuit, switched off at 0.7 s.

is given in Eq. (2.12). The initial radiation from the filament is modelled with Eq. (2.14). It can be rewritten as

$$L_\lambda(x, \phi, \lambda, t) = \varepsilon(\lambda, T(x,t))\, L_\lambda^{\mathrm{Pl}}(T(x,t)) \; . \tag{3.14}$$

Kirchhoff's law and multiple light recycling

As pointed out in Sec. 3.1.1, for a partially concave emitter part of the emitted radiation falls back onto the emitter. This fraction is defined as recycling factor ξ. If this radiation is not completely absorbed at the emitter, then the rest is reflected and adds to the initially emitted radiation in the same phase space, leading to an increased spectral radiance, which has been proven in the previous work [17, 19]. In fact this process is repeated in a cascade leading to multiple recycling with contributions constituting an infinite geometric series

$$L_\lambda^{\text{eff}} = \varepsilon L_\lambda^{\text{Pl}} \left(1 + \xi(1-\alpha) + \xi^2(1-\alpha)^2 + ...\right) . \tag{3.15}$$

The emissivity ε and the absorptivity α must be equal at equal wavelength as stated by Kirchhoff's law. Therefore multiple recycling enhances the emissivity leading to an effective emissivity

$$\varepsilon_{\text{eff}} = \frac{\varepsilon}{1-\xi(1-\varepsilon)} . \tag{3.16}$$

The effective emissivity calculated according to Eq. (3.16) cannot exceed unity. Fig. 3.9 shows the intrinsic emissivity of tungsten and the effective emissivity at a wavelength of 650 nm. The ratio of the effective emissivity to the material emissivity is the brightness enhancement factor, given by

$$\eta = \frac{\varepsilon_{\text{eff}}}{\varepsilon} = \frac{1}{1-\xi(1-\varepsilon)} . \tag{3.17}$$

The brightness enhancement factor is a function of the geometrical recycling factor ξ and the material emissivity ε, illustrated in Fig. 3.10. This factor increases with the geometrical recycling factor ξ, but decreases with the emissivity/absorptivity of the source. Mathematically, Eq. (3.17) yields two limits,

- $\varepsilon = 1$, unity emissivity of the source yields $\eta = 1$, i. e. no brightness increase. This is in agreement with the first limit in Eq. (2.21) in Sec. 2.2. Light recycling shows no benefit for a black body;
- $\xi = 0$, the geometrical recycling factor of zero yields no brightness increase, i. e. $\eta = 1$. For light sources in totally convex geometries, no intrinsic light recycling exists. However, the brightness can be increased in a specific phase space by using optical devices, e. g. a rear reflector.

In terms of a specific material with a constant spectral emissivity at a certain temperature, the brightness enhancement factor increases with the geometry-based recycling factor ξ, which is adjustable by changing the combination of geometry

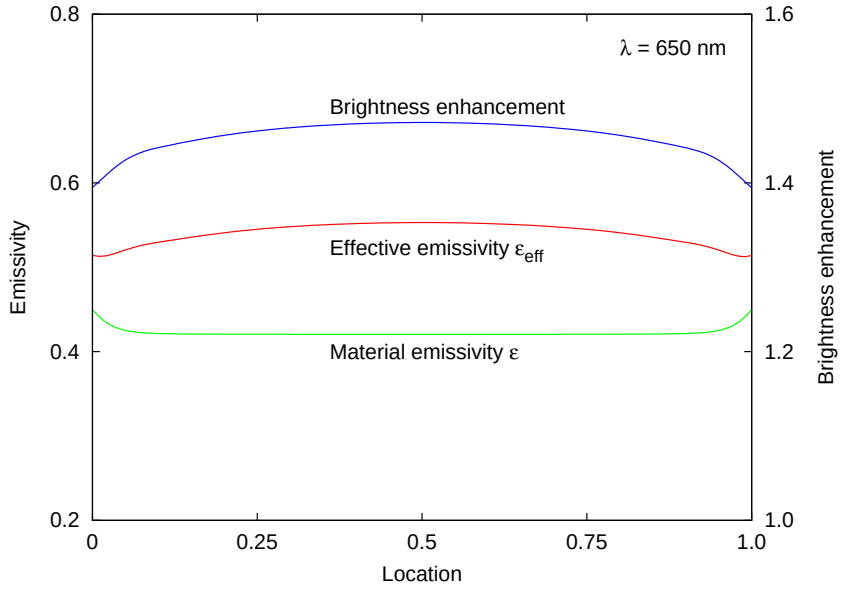

Figure 3.9.: Material emissivity and effective emissivity along the filament according to Eq. (3.16) averaged over ϕ including multiple light recycling and dependence on temperature. Configuration 2.

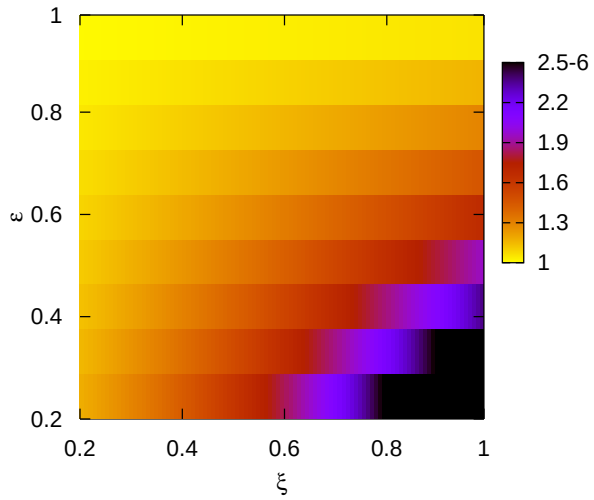

Figure 3.10.: Brightness enhancement increases with the geometrical light recycling factor ξ, but decreases with the material emissivity ε, following Eq. (3.17).

parameters including the wire radius R_c, the winding radius R_w and the winding slope S_w. The results illustrated in Fig. 3.4 reveal that a high ratio of R_c to R_w and

a large S_w feature a high geometrical recycling.

On the other hand, once the parameters of the configuration are chosen, the filament has a fixed geometrical recycling factor. In this case a lower absorptivity is desirable for higher brightness enhancement.

The total power emitted by a surface element P_total is calculated by taking into account the effective emissivity, but on the other hand also a reduction in the projected solid angle into which radiation may leave the emitter without being recycled. It is obtained

$$\begin{aligned} P_\mathrm{total} &= \pi(1-\xi)A_\mathrm{s}\int_0^\infty L_\lambda^\mathrm{eff}\mathrm{d}\lambda \\ &= \varepsilon_\mathrm{eff}(1-\xi)A_\mathrm{s}\sigma(T^4-T_0^4) \\ &= \frac{\varepsilon(1-\xi)}{1-\xi(1-\varepsilon)}A_\mathrm{s}\sigma(T^4-T_0^4)\ , \end{aligned} \tag{3.18}$$

where A_s is the area of a surface element on the filament.

Comparing Eq. (3.18) with Eq. (3.16) shows that the total power emitted per unit area is reduced by multiple recycling compared with the power expected on the grounds of Stefan-Boltzmann's law.

3.2. Measurements and model verification

3.2.1. Experimental setup

In order to verify the physical model of filament lamps, the experimental setup in Fig. 3.11 is used to measure the radiation of a 20 W filament lamp spectroscopically and photographically.

3.2.2. Parameter identification

The physical radiation model outlined in the previous sections includes three submodules: geometrical model, thermal model and radiation model (combined with material model). The parameters included in each submodule are listed in Table 4.1. Some of these parameters, notably the material properties such as the thermal conductivity κ, the electrical resistivity ρ and the spectral emissivity ε are functions of temperature T (and in the case of ε) of wavelength. The values (or the functional relation) may be determined from independent measurements, e. g. from the literature.

In this work we take a different approach, namely to identify the value of the parameters from the measurements of the radiance distribution in order to obtain a best fit between the predictions of the model and the measurements [45]. Three

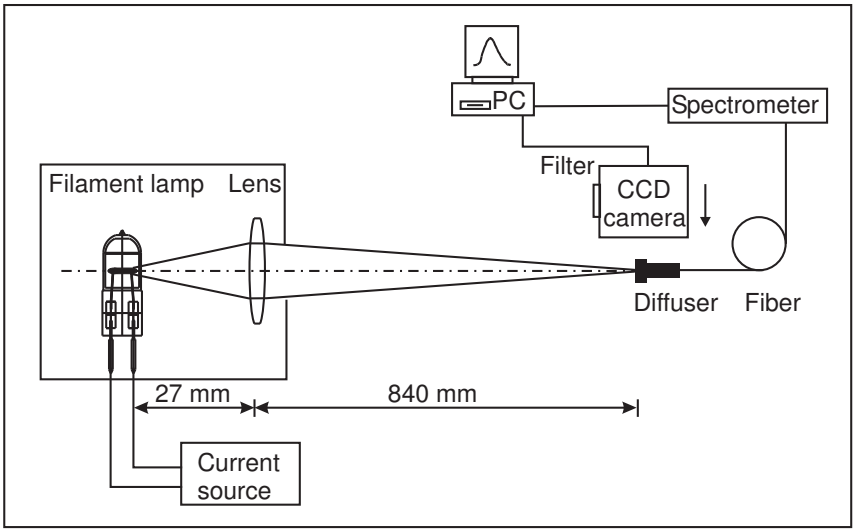

Figure 3.11.: Experimental setup for radiation measurements of a filament lamp. Spectroscopic and photographic measurements are taken with a spectrometer and a high resolution CCD camera.

issues are important in parameter identification: a correct theoretical model, accurate experimental measurements and an objective function. Fig. 3.12 illustrates the flow chart of parameter identification.

For simplicity assume that the functions $\kappa(T)$, $\rho(T)$ and $c_\mathrm{p}(T)$ can be approximated by a linear function in the relevant temperature range of 1500−3200 K. Each function is characterized by the values at two selected temperatures $T_1 = 1500\,\mathrm{K}$ and $T_2 = 3200\,\mathrm{K}$. Thus

$$\begin{bmatrix} \kappa(T) \\ \rho(T) \\ c_p(T) \end{bmatrix} = \frac{1}{\delta T} \begin{bmatrix} \kappa(T_1) & \kappa(T_2) \\ \rho(T_1) & \rho(T_2) \\ c_p(T_1) & c_p(T_2) \end{bmatrix} \begin{bmatrix} T_2 - T \\ T - T_1 \end{bmatrix} , \tag{3.19}$$

where

$$\delta T = T_2 - T_1 ,$$

For $\varepsilon(\lambda, T)$ we use a bilinear interpolation between the values at the selected temperatures and similarly at two selected wavelengths, $\lambda_1 = 360\,\mathrm{nm}$ and $\lambda_2 = 830\,\mathrm{nm}$, $\varepsilon(\lambda, T)$ is expressed as

$$\varepsilon(\lambda, T) = \frac{1}{\delta\lambda\ \delta T} \begin{bmatrix} \lambda_2 - \lambda & \lambda - \lambda_1 \end{bmatrix} \begin{bmatrix} \varepsilon(\lambda_1, T_1) & \varepsilon(\lambda_1, T_2) \\ \varepsilon(\lambda_2, T_1) & \varepsilon(\lambda_2, T_2) \end{bmatrix} \begin{bmatrix} T_2 - T \\ T - T_1 \end{bmatrix} , \tag{3.20}$$

where in analogy,

$$\delta\lambda = \lambda_2 - \lambda_1 .$$

Lamps are used in a rather narrow current (voltage) range limited by a steeply decreasing efficacy at the low end and an unacceptably short lifetime at the high

Table 3.1.: Parameters used in the physical model of filament lamps. The listed data are in the cases of selected conditions, i. e. $T_1 = 1500\,\mathrm{K}$, $T_2 = 3200\,\mathrm{K}$, $\lambda_1 = 360\,\mathrm{nm}$, $\lambda_2 = 830\,\mathrm{nm}$. Any case in between can be derived via a linear (or bilinear) interpolation.

Parameter	Unit	Identified value	Literature
Radius of the filament	mm	$R_\mathrm{c} = 0.045$	
Length of the filament	mm	$L = 61.0$	
Winding radius	mm	$R_\mathrm{w} = 0.46$	
Slope of the coil		$S_\mathrm{w} = 15.5$	
Thermal conductivity	W/(mm K)	$\kappa(T_1) = 0.085$	0.098 @ 2000 K[a]
		$\kappa(T_2) = 0.074$	
Electrical resistivity	Ω mm	$\rho(T_1) = 4.46 \times 10^{-4}$	$4.04{\times}10^{-4}$
		$\rho(T_2) = 10.1 \times 10^{-4}$	$9.95{\times}10^{-4}$
Spectral emissivity	–	$\varepsilon(\lambda_1, T_1) = 0.502$	0.476 @ 467 nm, T_1[a]
		$\varepsilon(\lambda_2, T_1) = 0.420$	0.448 @ 650 nm, T_1[b]
		$\varepsilon(\lambda_1, T_2) = 0.440$	0.452 @ 467 nm, T_2[b]
		$\varepsilon(\lambda_2, T_2) = 0.360$	0.414 @ 650 nm, T_2[b]
Heat capacity	J/(mm^3 K)	$c_\mathrm{p}(T_1) = 3.0 \times 10^{-3}$	3.21×10^{-3} @ T_1[b]
		$c_\mathrm{p}(T_2) = 4.2 \times 10^{-3}$	4.35×10^{-3} @ T_2[b]
Thermal end-coupling	W/(mm^2 K)	$k_0 = 0.038$	

[a] Source: [28]
[b] Source: [20].

end. Consequently, a linear model of the material constants is used, which linearly interpolates between two values of temperature and wavelength.

Equation (3.20) represents a tensor patch. It is possible to use more values and consequently a higher order interpolation instead based on NURBS interpolation [48].

With these approximations the model utilizes a total of 15 numeric parameters listed in Table 4.1. The parameter identification is based on comparing selected measurements with the corresponding model prediction. For this purpose a series of operating conditions with $x = (0.1,\ 0.15,\ 0.2, ...,\ 0.5)$, $\phi = (0,\ \pi)$, $\lambda = (450\,\mathrm{nm},\ 600\,\mathrm{nm},\ 750\,\mathrm{nm})$, $I = (1.33\,\mathrm{A},\ 1.66\,\mathrm{A})$ are chosen, respectively. The spectral radiance is measured with a total of 108 combinations.

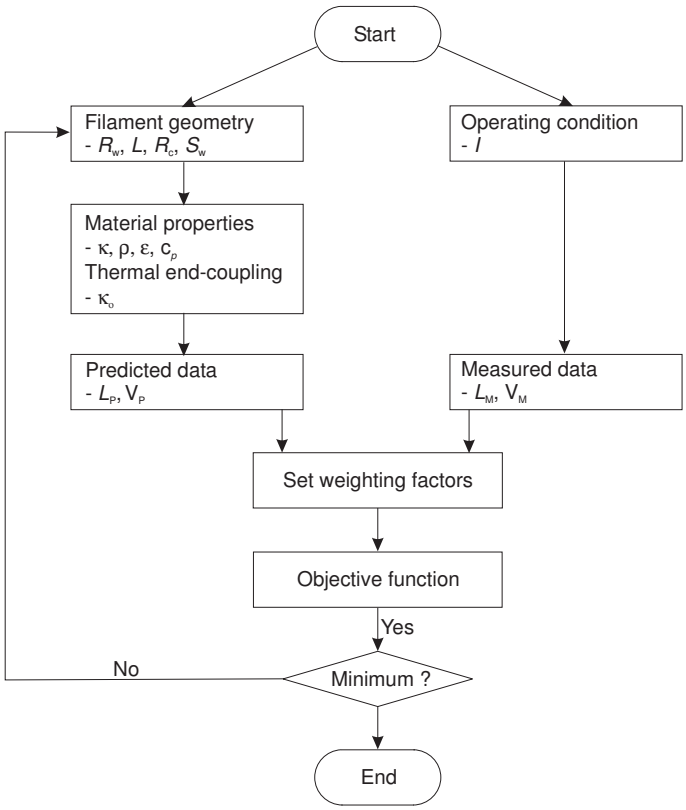

Figure 3.12.: Flow chart of the parameter identification

In addition, for the comparison of radiative data two separate measurements are used for the purpose of parameter identification. From the temperature distribution calculated in an intermediate step the predicted voltage for each operating current is derived and compared with a direct measurement of the actual voltage. The relative error approximates 1.7% on average.

The objective function for seeking minimal variation between the model predictions and the measurements is expressed as

$$\mathrm{obj} = \sum_{i=1}^{M_1} w_1 \left(\frac{L_\mathrm{P} - L_\mathrm{M}}{(L_\mathrm{P} + L_\mathrm{M})/2} \right)_i^2 + \sum_{j=1}^{M_2} w_2 \left(\frac{V_\mathrm{P} - V_\mathrm{M}}{(V_\mathrm{P} + V_\mathrm{M})/2} \right)_j^2 , \tag{3.21}$$

where L_P, V_P are the radiance and voltage data predicted with the model. L_M, V_M are the corresponding quantities derived from the measurements. w_1 and w_2 are the weight factors of the radiance and the voltage, respectively. The number of the radiance data M_1 does not need to equal the number of the voltage data M_2.

The searching process for the minimum is executed by PC automatically. A good starting point and an effective method facilitate the computation. After each iteration, the value of the objective function and the corresponding value of each

variable are returned. The relative error is given by

$$\bar{\sigma} = \sqrt{\frac{\text{obj}}{w_1 M_1 + w_2 M_2}} \,. \tag{3.22}$$

Identified values are listed in Table 4.1. For comparison the values of material properties from literatures are listed in the same table. Applying identified values to the model and comparing with the experimental results, the best fit features a mean square deviation of 9%.

3.2.3. Model verification

Temperature distribution

The radiance of the source is derived via measuring the radiance of the image following the brightness theorem. Bright points (inside the coil in Fig. 3.3) and less bright points (outside the coil) on the cross section of the filament are measured alternately.

The radiance is temperature-dependent. By measuring the radiance and with the emissivity known, the corresponding temperature is given by Eq. (3.14). However, it is not easy to measure the spectral emissivity accurately. Two-wavelength spectral thermometry is a viable approach to this issue if the emissivity is unavailable [61].

Equation (2.14) gives the radiance of a grey body at a certain temperature T. For two close wavelengths λ_1 and λ_2, the relation of the radiance quantities is given by

$$\frac{L_{\lambda_1}(T)}{L_{\lambda_2}(T)} = \frac{\varepsilon\left(\lambda_1, T\right)}{\varepsilon\left(\lambda_2, T\right)} \left(\frac{\lambda_2}{\lambda_1}\right)^5 \frac{\exp\left(hc/\left(\lambda_2 k_\mathrm{B} T\right)\right) - 1}{\exp\left(hc/\left(\lambda_1 k_\mathrm{B} T\right)\right) - 1} \,. \tag{3.23}$$

In the measured spectral range and the temperature range, due to the fact that $\exp\left(hc/\left(\lambda_1 k_\mathrm{B} T\right)\right) \gg 1$ and $\exp\left(hc/\left(\lambda_2 k_\mathrm{B} T\right)\right) \gg 1$, the temperature is derived as

$$T = \frac{\frac{hc}{k_\mathrm{B}}\left(\frac{1}{\lambda_2} - \frac{1}{\lambda_1}\right)}{\ln(L_1/L_2) - \ln(\varepsilon(\lambda_1, T)/\varepsilon(\lambda_2, T)) + 5\ln(\lambda_1/\lambda_2)} \,. \tag{3.24}$$

With a wavelength separation less than 1 nm, we assume $\varepsilon(\lambda_1, T) \approx \varepsilon(\lambda_2, T)$, thus Eq. (3.24) is simplified to

$$T = \frac{\frac{hc}{k_\mathrm{B}}\left(\frac{1}{\lambda_2} - \frac{1}{\lambda_1}\right)}{\ln(L_1/L_2) + 5\ln(\lambda_1/\lambda_2)} \,. \tag{3.25}$$

Equation (3.25) reveals that the temperature of a grey body can be derived via spectroscopic measurement at two close wavelengths without need for the emissivity and absolute intensity measurements.

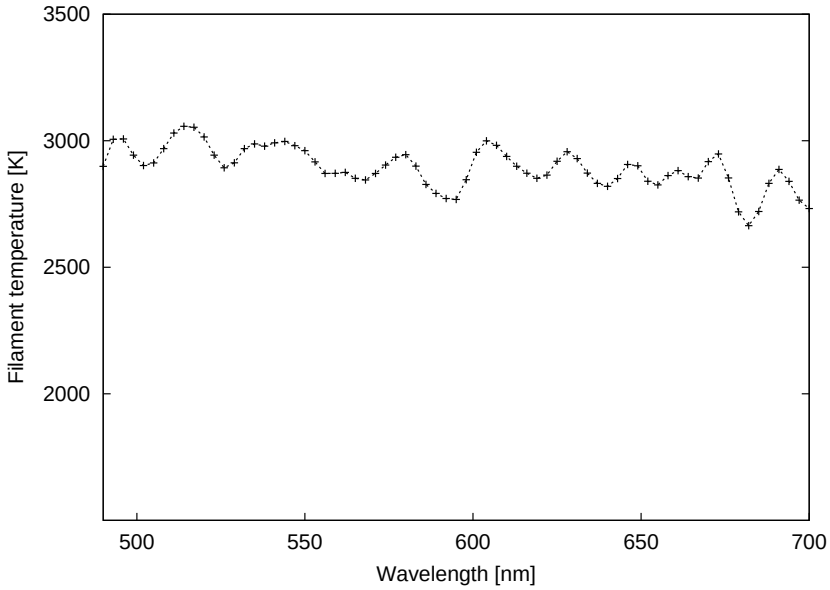

Figure 3.13.: Temperature distribution of the filament center over the wavelengths 490-700 nm. It is calculated with Eq. (3.25) by means of two-wavelength thermometry. The average temperature over the wavelengths approximates 2880 K.

Two-wavelength thermometry is applicable to a source with a continuum spectrum, e. g. the filament lamp used in the physical model, but not to a source with a discrete spectrum (e. g. short-arc discharge lamp HBO), due to the drastic variation in emission. Fig. 3.13 shows the temperature as a function of wavelength and radiance at a sampled point (the center). The averaged temperature over 490-700 nm approximates 2880 K. Fig. 3.14 shows the temperature distribution over the entire length of the filament derived from two-wavelength thermometry.

Light recycling and radiance

Combining Eqs. (3.15) and (3.16) yields the spectral radiance distribution emitted by a surface element

$$L_\lambda(x,\phi,\lambda) = \varepsilon_{\text{eff}}\left(\lambda,\xi(x,\phi)\right)\, L_\lambda^{\text{Pl}}\left(\lambda,T(x)\right)\ , \tag{3.26}$$

where the temperature distribution is calculated previously as the solution of the differential equation Eq. (3.11), $\xi(x)$ is the result of ray-tracing simulation in Sec. 3.1.1. This equation specifies the brightness of a given surface element as it appears to an external observer.

Figure 3.15 (a) shows the visualized prediction of the detail model (Eq. (3.26)) in a photo-realistic rendering of the light as it would appear at a wavelength of 650 nm.

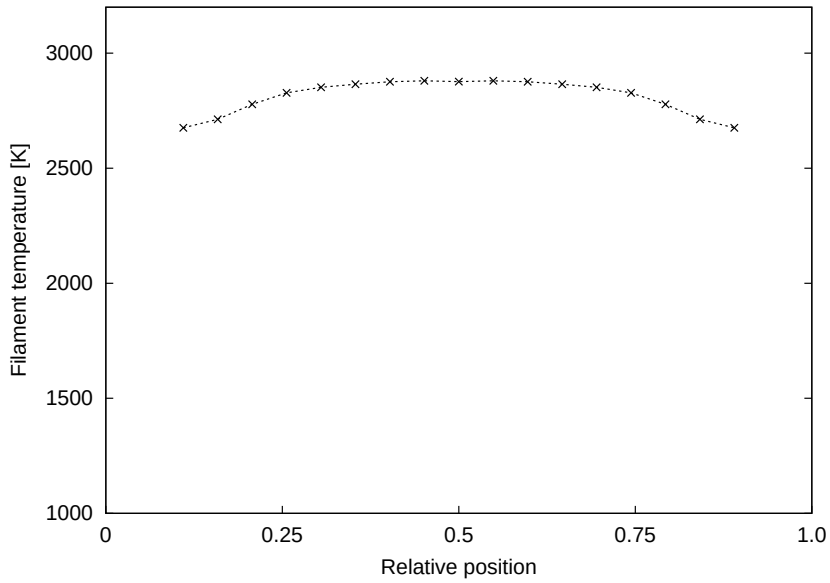

Figure 3.14.: Temperature distribution over the entire length of the filament. By means of two-wavelength spectral thermometry, the temperature on each sampled area element is derived. In the center it reaches 2880 K.

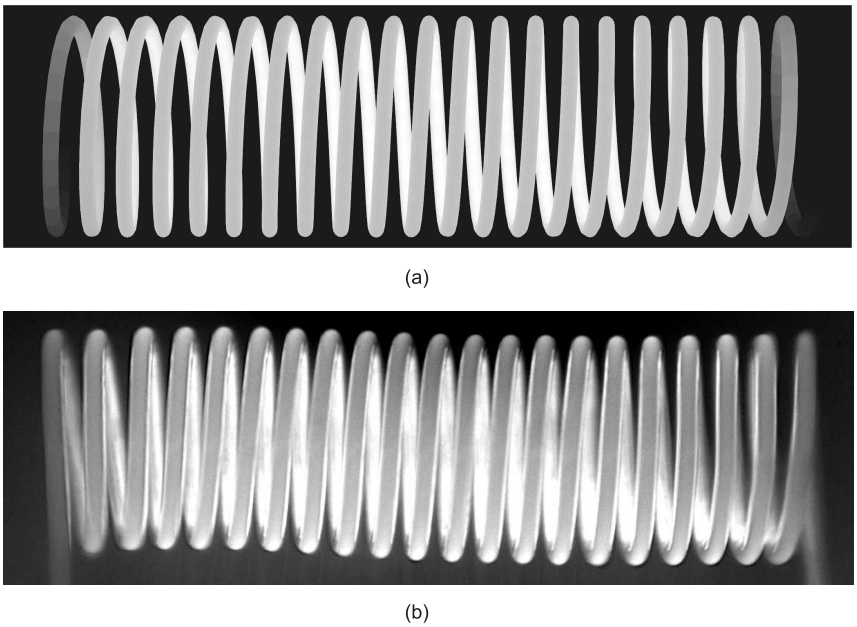

Figure 3.15.: (a) Modelled radiance of the filament lamp and (b) photograph of the intensity distribution of the filament lamp.

Fig. 3.15 (b) shows a photograph of the actual lamp taken with a high resolution CCD camera with an interference filter at 650 nm.

Figure 3.16 shows a comparison between the radiance predicated by the model of

the filament lamp (solid curve) and the measured radiance (points) from spectroscopic measurements.

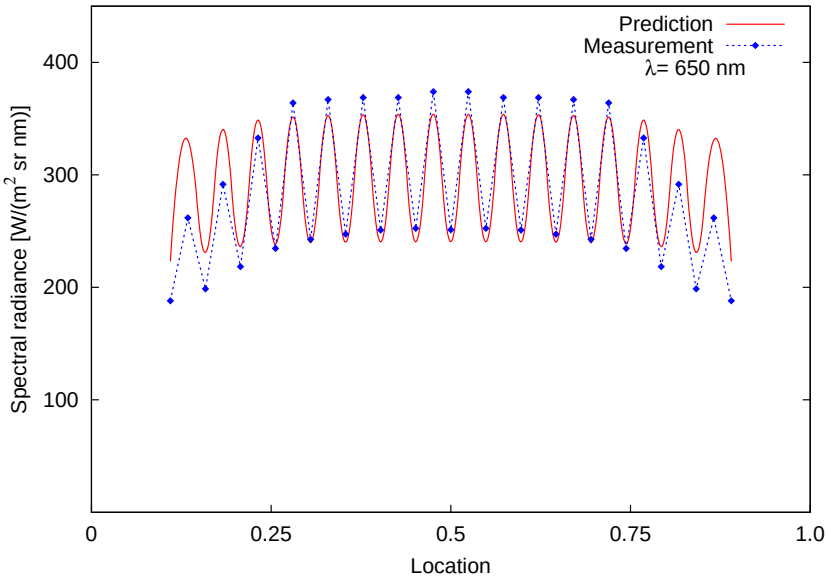

Figure 3.16.: Comparison between modelled radiance and experimental spectroscopic measurement. The considered surface elements, bright points on the inside the filament and neighboring less bright points on the outside are measured alternately along the filament. The intensity difference between bright points and neighboring less bright points approximates 30%, due to intrinsic light recycling.

Note that the model correctly describes the following features:

- The decrease in spectral brightness towards the ends of the filament, due to a temperature drop which is in turn caused by heat conduction to the support.
- Variations in spectral brightness between the inside and outside of the coil by as much as 30% due to light recycling.
- Spectral distribution in absolute terms, consistent with Planck's law and Kirchhoff's law.
- Observed voltage under operating conditions.

Far-field distribution

The detail model Eq. (3.26) can be integrated to predict the far-field spectral intensity distribution E that would be observed, e. g. in the direction specified by the

unit vector $\mathbf{d}$

$$E(\lambda, \mathbf{d}) = \int_{x=0}^{x=L} \int_{\phi=0}^{\phi=2\pi} L_\lambda(x, \phi, \lambda) \left(\mathbf{d} \cdot \mathrm{d}\mathbf{a}\right)_+ \ , \tag{3.27}$$

where d$\mathbf{a}$ is the surface element pointing in the direction of the normal vector, as defined by the geometrical model (Eq. (3.3)) and the subscript + indicates that only those surface elements contribute, for which the scalar product is positive (meaning they are visible from direction $\mathbf{d}$).

3.3. Summary

Virtual prototyping of illumination optical systems based on ray tracing needs an accurate model of the light source. This model yields the spectral radiance as a function of all relevant variables which comprise at least two spatial, and two directional coordinates in addition to wavelength, but may include polarization, coherence and others. The phenomenological approach consists of measuring (sampling) the radiance on a suitable grid and interpolating the values. One may also model the thermodynamic behavior of the light source. The advantage of this approach is that it generally needs fewer parameters than the measurement and in addition is capable of correctly modelling light recycling. We developed as an example for thermal light sources the model of a halogen tungsten filament lamp. The model based on thermodynamics, geometry, material and electrical properties is widely applicable for any kind of tungsten filament lamp. In particular, emission, absorption and light recycling properties are taken into consideration. The model starts by calculating the one-dimensional temperature distribution in the filament by solving the time dependent heat transfer equation. From this it creates the five-dimensional radiance distribution based on Planck's law, and the emissivity of the filament. Light recycling due to the coiled filament is a significant effect in this type of lamps. The model is validated with high resolution absolute radiance measurements. The model can easily be integrated into ray-tracing software.

4. Luminescent light sources

4.1. Electroluminescence of LEDs

In the previous Chapters Kirchhoff's law and Planck's law were used to describe the light emission of thermal sources, with the spectral radiance distribution as a function of the emitter's temperature and the emissivity. Being dependent on the temperature, this emission is called thermal radiation. In contrast, non-thermal radiation is recognized by its high intensity, which is too high for the temperature of the body which emits it to be thermal radiation. The non-thermal radiation is termed luminescence, it describes the general process in which energy is absorbed in matter and reemitted as photons, e. g. the emission from glow discharges, luminescent diodes and lasers.

Luminescence in LEDs is termed electroluminescence involving the generation of photons when current passes through a p-n junction of certain solid materials under an applied voltage [4, 40, 66]. In this process electric energy is directly converted into optical energy. Electroluminescence is the result of radiative recombination of electrons and holes in a material.

Radiative recombination and non-radiative recombination

The LED is a type of semiconductor device made of a p-n junction. Due to the nature of the p-n junction, the concentrations of holes and electrons on the p-type side and n-type side are different. An unbiased p-n junction reaches a kinetic equilibrium in the vicinity of the p-n junction due to a built-in electric field (the corresponding potential barrier is termed the diffusion voltage) resulting from the recombination of electrons and holes in this region. The region is named the depletion region for the fact that it is depleted of free carriers. The Fermi energy level on the p-type side is the same as that on the n-type side.

When a forward voltage is applied to the p-n junction, the height of the potential barrier is reduced. As a result, the holes on the p-type side and the electrons on the n-type side are injected into the other side and diffused. This injection of minority carriers (holes and electrons) causes excessively high carrier concentration compared with that in the thermal equilibrium state, resulting in a separation of the Fermi levels on the p-type side and the n-type side, and in turn a recombination

of carriers. Simultaneously, energy is released as photons, with an energy equal to the energy difference between the involved electrons and holes before recombination. The process is called radiative recombination, i. e. luminescence. The photon energy is slightly larger than the bandgap energy E_g of the material, i. e. the energy difference between the bottom of the conduction band E_c and the top of the valence band E_v, if the thermal energy of carriers is very small compared with the bandgap energy, i. e. $k_B T \ll E_g$, where k_B is Boltzmann's constant (defined in the previous chapters), T is the ambient temperature.

The bandgap energy E_g defines the maximal wavelength of the emission spectrum λ_{max} (corresponding to the characteristic frequency), according to $E_g = hc/\lambda_{max}$.

The edges of the conduction band and the valence band are populated by most electrons and holes. During the radiative recombination of the carriers the released energy is not constant, it depends on the density of states in the conduction band and in the valence band, Boltzmann distribution [57]. The emission spectrum as a function of energy E is given by

$$I(E) \propto \sqrt{E - E_g}\, \exp\left(-\frac{E}{k_B T}\right) . \tag{4.1}$$

The full width at half maximum (FWHM) of the emission spectrum is derived from Eq. (4.1) as $\Delta E = 1.8\, k_B T$, corresponding to tens of nanometers in the visible light at room temperature. The emitted light can be assumed monochromatic in terms of the perception of the human eye.

The radiative recombination is dominant in LEDs. However, non-radiative recombination of electrons and holes also occurs due to the defects of materials and the bonding structure, in which the electron energy is converted to vibrational energy of lattice atoms, i. e. phonons, consequently into heat [59]. An increased temperature will boost the rate of non-radiative recombination, but diminish the rate of radiative recombination. As a consequence, the probability of the radiative recombination or internal quantum efficiency (see Sec. 4.2.3) drops since is the ratio of the probability of radiative recombination to the total probability of recombinations consisting of radiative and non-radiative processes [31], leading to a reduction of light emission. The undesirable non-radiative recombination can be reduced, but can never be entirely avoided.

The ideal luminescent spectrum

A generalization of Planck's equation for luminescence [53, 54, 68] is used to describe the luminescent spectrum of an ideal LED, in which the temperature of the radiation T is the actual temperature of the emitter that affects the intensity and determines the shape of the spectrum. The applied voltage V of an LED is combined with the

photon energy to affect mainly the light intensity, expressed as

$$L_{\mathrm{lum}}^{\mathrm{eq}}(\lambda, T, V) = \frac{2hc^2}{\lambda^5} \frac{1}{\exp\left(\frac{hc/\lambda - qV}{k_{\mathrm{B}} T}\right) - 1} \,. \tag{4.2}$$

As we know, thermal radiation can be emitted by any material. Its spectrum may contain photons with any energy greater than zero and smaller than a temperature-dependent maximum. In contrast, the spectrum of luminescent radiation of LEDs is characterized by the bandgap energy, with photons of smaller energy missing. Whether a semiconductor at a given temperature emits thermal radiation or luminescent radiation is determined by the concentrations of electrons in the conduction band and holes in the valence band, which depends not only on the temperature but also on the applied voltage. The emission of LEDs is dominated by the luminescent radiation due to the effect of high doping and a forward bias.

Equation (4.2) describes both types of thermal and luminescent radiation. It contains the Planck's equation for thermal blackbody radiation in Eq. (2.12) as a special case, in which the applied voltage equals zero.

4.2. Physical modelling of LEDs

The key issue in this work is to investigate light recycling in light sources, especially LEDs, aiming at increasing the output brightness of the light source. For this purpose a physical model yielding the spectral radiation of LEDs with respect to position, wavelength and applied voltage is built. The physical model includes the following submodules:

- the geometrical model for defining the light-emitting surface based on an accurate microscopic measurement;
- the electrical model for a derivation of the I−V characteristics of an LED. The experimental I−V characteristics and the ideal I−V characteristics derived from the ideal spectral radiation of LEDs are compared in Sec. 4.2.2;
- the material model for deriving the intrinsic properties of the semiconductor material of an LED. The material properties consist of the emissivity/absorptivity (see Sec. 4.2.3), the quantum efficiency, the bandgap energy and the refractive index of the material. These properties vary for LEDs of different types and different materials. For deriving the values of these properties, absolute measurements of the spectral radiation of LEDs are needed;
- the thermal model for defining the actual temperature of the LEDs and parameters required for defining the thermal effect on the radiation;

- the radiation model for combining these submodules based on the generalization of Kirchhoff's law and Planck's law, in turn yielding the spectral radiance $L(x, y, \lambda, V, T)$, where (x, y) is the location on the light-emitting surface, λ is the wavelength of the emitted light, V is the forward voltage, and T is the temperature of the material (Sec. 4.2.3).

The interdependence of the submodules used in the model of LEDs is briefly presented in Fig. 4.1.

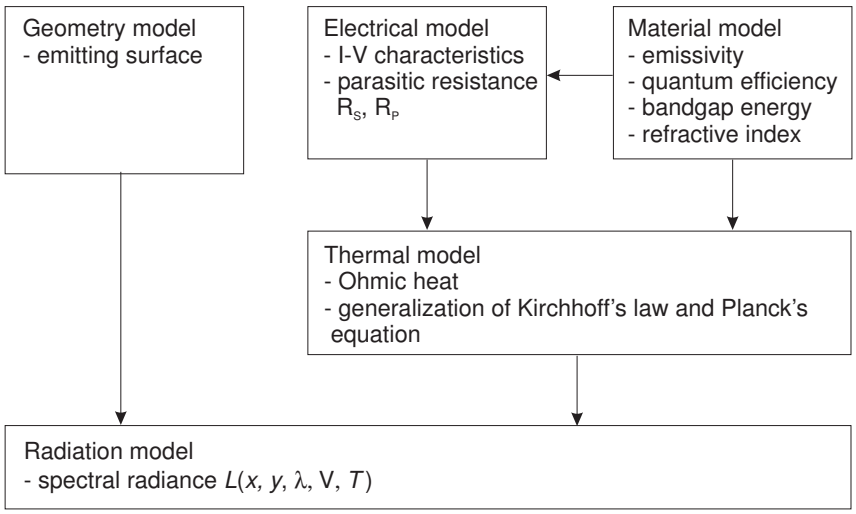

Figure 4.1.: Flow chart of the physical modelling of LEDs.

4.2.1. Geometrical model of the light-emitting surface

An LED is a volume emitter. Light is emitted from a slab of semiconductor which has a uniform thickness. The thickness (one to a few microns) is very small compared with the length and the width of the light-emitting surface. Light emitted from the active region of the substrate travels through the other layers which have small optical thickness (Fig. 4.2). The net intensity change can be assumed negligible due to the concurrent absorption and reemission at the same rate in an LED with a high internal quantum efficiency (especially for an ideal LED with an internal quantum efficiency of unity). For these reasons, we are allowed to model the light emitting from a two-dimensional light-emitting surface instead of a three-dimensional volume.

The light-emitting surface of an LED consists of a current-conducting metal and emitting area in between and around. The emittance of the grid, due to its low temperature, does not contribute to the radiance of the LED.

In order to model the geometry of the LED, a boolean function $g(P)$ and a vector

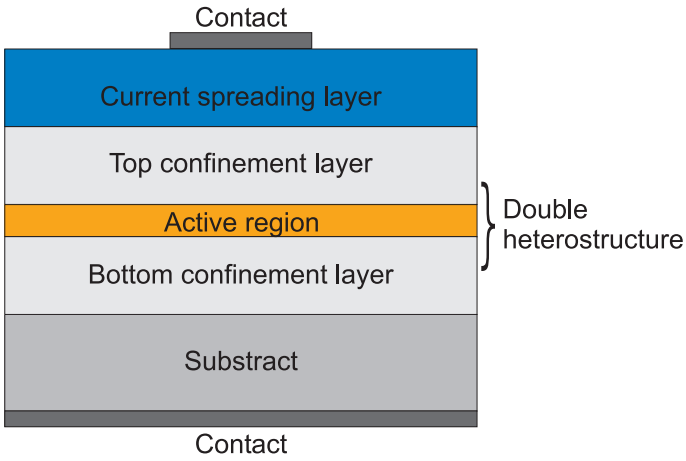

Figure 4.2.: Schematic of a double heterostructure LED. Light is emitted from the active region and travels through the other layers. The confinement layers prevent carriers from escaping from the active region aiming at attaining a high internal quantum efficiency.

method is used to define any point P on the emitting surface, expressed as

$$g(P) = \begin{cases} 1 & d > d_0/2 \\ 0 & d \leq d_0/2 \end{cases} \tag{4.3}$$

where d is the distance from a point P to the axis of a metal lead P_1P_2 (in Fig. 4.3), d_0 is the thickness of the metal lead. This would tell whether a point emits light, or not.

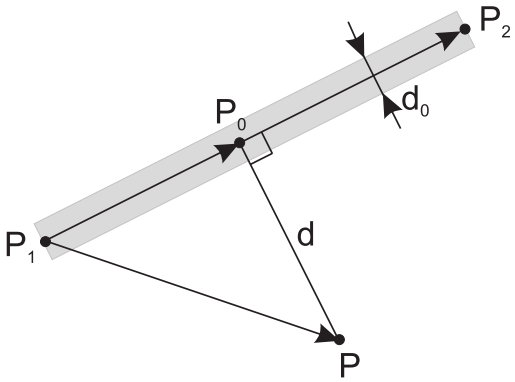

Figure 4.3.: The geometrical principle for deriving the distance from a point P to a line P_1P_2. Project vector $\mathbf{P}_1\mathbf{P}$ onto the vector $\mathbf{P}_1\mathbf{P}_2$ and derive the normalized length p of $|\mathbf{P}_1\mathbf{P}_0|$ with respect to $|\mathbf{P}_1\mathbf{P}_2|$ with Eq. (4.4). The projected point P_0 is calculated with Eq. (4.6). In the case of the light-emitting surface of an LED, P_1P_2 indicates the axis of a metal lead with a thickness of d_0.

Figure 4.3 shows the geometrical principle of deriving the distance from any point to a line. The vector $\mathbf{P}_1\mathbf{P}$ is projected onto the vector $\mathbf{P}_1\mathbf{P}_2$, the length component p of the projection $\mathbf{P}_1\mathbf{P}_0$ is normalized with respect to $|\mathbf{P}_1\mathbf{P}_2|$ as

$$p = \frac{\mathbf{P}_1\mathbf{P}_2 \cdot \mathbf{P}_1\mathbf{P}}{|\mathbf{P}_1\mathbf{P}_2|^2} , \quad \text{with} \quad p \in [0,1] . \tag{4.4}$$

A special case for Eq. (4.4) is defined as

$$p = 1 , \quad \text{if} \quad |\mathbf{P}_1\mathbf{P}_2| = 0 . \tag{4.5}$$

This is the case when P_1 coincides with P_2, i. e. a rectangular cross-section of metal lead evolves into a circular disk centered at P_1. Summarizing Eqs. (4.4) and (4.5) yields the projected point P_0

$$P_0 = (1-p)\,P_1 + p\,P_2 . \tag{4.6}$$

With P given and P_0 derived, the distance d required for the boolean function is calculated as $d = |\mathbf{P}\mathbf{P}_0|$.

This method is applicable to any chip with any grid geometry. A geometrical model of the light-emitting surface a surface-mounted diode (SMD) NovaLED175 [47] is shown in Fig. 4.4 (a). As comparison a microscopic photograph of the same LED is illustrated in Fig. 4.4 (b).

In this method, the effective emitting area (without including the metal contact) can be derived via defining the area of one pixel and counting the number of emitting pixels.

4.2.2. Electrical model

Current−voltage (I−V) characteristics of LEDs

The bandgap energy of any semiconductor corresponds to an applied voltage, at which the forward current flowing through the p-n junction strongly increases. This applied voltage is termed the threshold voltage V_{th}. Considering the investigated NovaLED175 LED (AlInGaP) with a theoretical bandgap energy of 2.05 eV [47], the corresponding threshold voltage $V_{\mathrm{th}} \approx 2.05\,V$.

The I−V characteristics of an ideal LED with an emitting area of A_{s} (derived from the geometrical model) can be derived from the ideal luminescent spectrum according to Eq. (4.2) [53], expressed as

$$\begin{aligned} I_0(V,T_0) &= A_{\mathrm{s}}\pi q \int_0^{\lambda_{\max}} \left(\frac{L_{\mathrm{lum}}^{\mathrm{eq}}(\lambda,T_0,V) - L_{\lambda}^{\mathrm{Pl}}(T_0)}{hc/\lambda} \right) \mathrm{d}\lambda \\ &= 2A_{\mathrm{s}}\pi qc \int_0^{\lambda_{\max}} \left(\frac{\lambda^{-4}}{\exp\left(\frac{hc/\lambda - qV}{k_{\mathrm{B}}T_0}\right) - 1} - \frac{\lambda^{-4}}{\exp\left(\frac{hc/\lambda}{k_{\mathrm{B}}T_0}\right) - 1} \right) \mathrm{d}\lambda , \end{aligned} \tag{4.7}$$

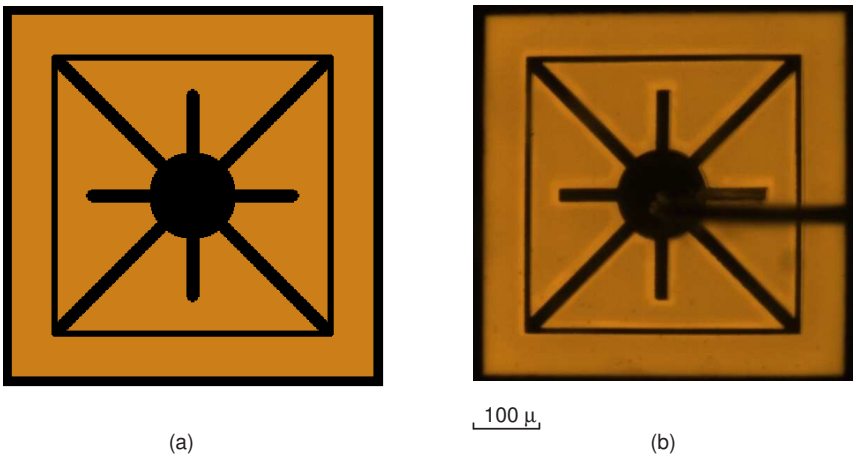

Figure 4.4.: (a) Geometrical model of the light-emitting surface of an amber LED, a surface-mounted diode (SMD) NovaLED175 with an effective light-emitting area of 0.235 mm^2, (b) a microscopic photograph of the NovaLED175 LED, the black thick line in the middle right-hand side is a contact wire which does not belong to the light-emitting surface.

with

$$\lambda_{\max} = hc/E_{\mathrm{g}} \ ,$$

where T_0 is the ambient temperature.

Using Eq. (4.7) to describe the I−V characteristics of LEDs instead of the commonly used Shockley equation [58] has the advantage that Eq. (4.7) is an accurate theoretical equation based on the thermodynamic laws, while the Shockley equation is an empirical derivation. Eq. (4.7) connects the light emission spectrum of the LED with the applied voltage (in turn with the current) and it does not need any approximation, whereas the Shockley equation requires the reverse saturation current and the ideality factor of the material.

As comparison, the I−V characteristics of the real LED are measured with the experimental setup in Fig. 4.5. The experimental I−V characteristics and the ideal I−V characteristics are illustrated in Fig. 4.6. In comparison with the ideal I−V characteristics, the curve of the experimental I−V characteristics shifts to a higher voltage, this voltage shift increases with the current, resulting from a series resistance effect. At a high voltage range, the ratio of the voltage shift (at the same current) to the corresponding current value yields the series resistance R_{s}. For the measured NovaLED175 LED, the derived series resistance is about 0.1 Ω.

The parasitic resistances of a real LED consist of a parallel resistance R_{p} (parallel to the ideal diode) and a series resistance R_{s} (in series with the ideal LED and R_{p}), shown in Fig. 4.6. Taking R_{p} and R_{s} into account, the I−V characteristics of the

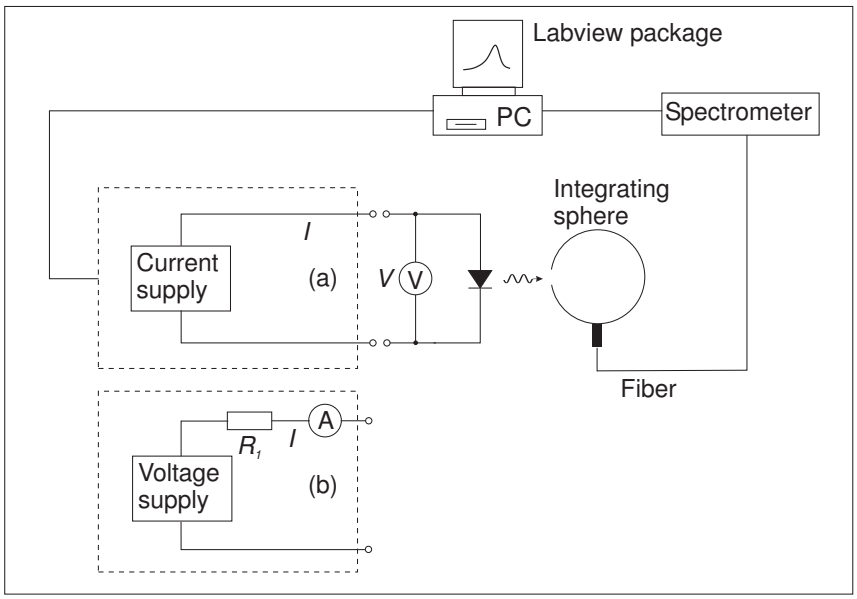

Figure 4.5.: Experimental setup for measuring I−V characteristics and the optical flux of LEDs. The two circuits in the dashed frame are alternative: (a) powered with a current source, (b) powered with a voltage source, R_1 acts as a current limiting resistor in series with the voltage source and the Amperemeter. The forward voltage V as a function of the current I is measured, because the current is easily controlled. The integrating sphere connected to the spectrometer is used to measure the optical flux of the LED. The measurements are executed automatically under the control of a LabVIEW$^{\mathrm{TM}}$ package.

LED are modified as

$$I - \frac{V - I R_\mathrm{s}}{R_\mathrm{p}} = I_0 \left(V - I\, R_\mathrm{s}, T_0\right) \ . \tag{4.8}$$

The parallel resistance takes effect at a low current. Fig. 4.6 shows that the two curves of the I−V characteristics overlap at the low current range, resulting from a large parallel resistance, i. e. $R_\mathrm{p} \to \infty$.

4.2.3. Material and radiation model

The material model consists of the material properties required for the physical model, it is combined with the radiation model.

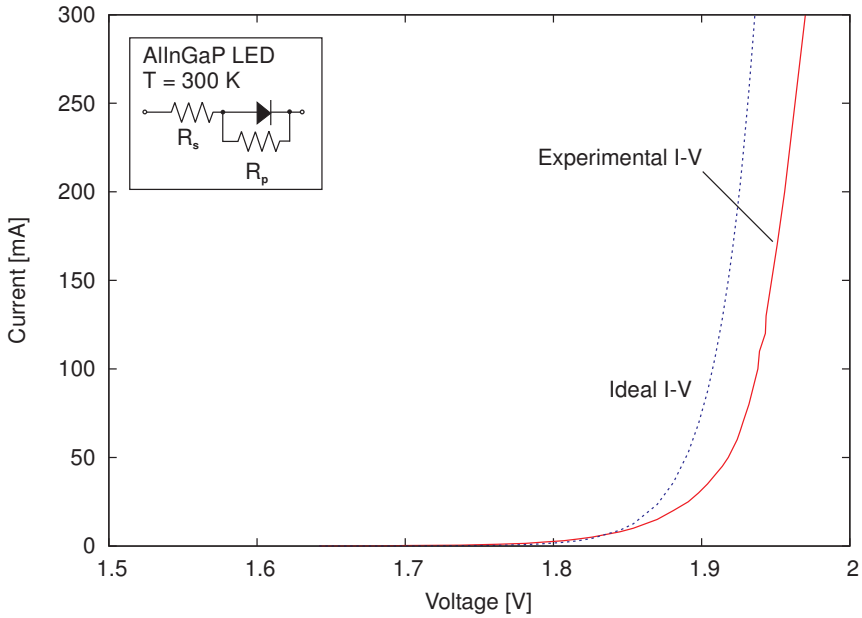

Figure 4.6.: Current−voltage (I−V) characteristics of the p-n junction of the NovaLED175 LED. The ideal I−V characteristics are calculated with Eq. (4.7). The discrepancy between the two characteristics results from a series resistance R_s. At a low voltage range, the experimental I−V characteristics are in agreement with the ideal I−V characteristics, resulting from a large parallel resistance R_p.

Generalized Kirchhoff's law for luminescence

Kirchhoff's law of thermal radiation states that a non-black body has the same emissivity as the absorptivity at the same temperature and the at same wavelength. It relates the light emission of the non-black body to the thermal radiation of the black body at the same temperature by means of its thermal emissivity/absorptivity, clarified in Sec. 2.2.

As for the quantum absorptivity and emissivity of non-thermal radiation from a non-black body, earlier work has proven that macroscopic quantum absorptivity and emissivity are equal for any given wavelength [1, 44, 54], similar to thermal emissivity and absorptivity. The quantum absorptivity-emissivity usually depends strongly on the wavelength and it also depends on the state of excitation, i. e. on the applied voltage and the temperature in case of the luminescent source, LEDs.

As a result, Kirchhoff's law is extended to the case where a non-black body emits non-thermal radiation into an environment of different temperature and different applied voltage of LEDs (non-equilibrium case) by using the emissivity/absorptivity $\alpha(\lambda, T, V)$ of the involved emitter, given by

$$L_\mathrm{lum}(\lambda, T, V) = \alpha(\lambda, T, V)\, L^\mathrm{eq}_\mathrm{lum}(\lambda, T, V)\ , \tag{4.9}$$

where the last term is given by Eq. (4.2),

Absorptivity-emissivity

In order to derive the absorption coefficient τ, in turn the absorptivity/emissivity, we assume that in a simplified two-level system only one molecular transitions between a lower level and a higher level contribute to the absorption and emission of photons of a certain energy [41].

The concentrations of molecules in the higher level C_{H} and in the lower level C_{L} are related by Boltzmann distribution [36]

$$\frac{C_{\mathrm{H}}}{C_{\mathrm{L}}} = \exp\left(-\frac{hc/\lambda - qV}{k_{\mathrm{B}}\,T}\right) . \tag{4.10}$$

Earlier work [54, 69] proved that the absorption coefficient τ is proportional to the difference of the two concentrations $C_{\mathrm{L}} - C_{\mathrm{H}}$. Since the total concentration of molecules is constant, the absorption coefficient can be expressed as

$$\tau \propto C_{\mathrm{L}} - C_{\mathrm{H}} \propto \frac{C_{\mathrm{L}} - C_{\mathrm{H}}}{C_{\mathrm{L}} + C_{\mathrm{H}}} = \frac{\exp\left(\frac{hc/\lambda - qV}{k_{\mathrm{B}}T}\right) - 1}{\exp\left(\frac{hc/\lambda - qV}{k_{\mathrm{B}}T}\right) + 1} = \tanh\left(\frac{hc/\lambda - qV}{2\,k_{\mathrm{B}}T}\right) . \tag{4.11}$$

Note that the last term in Eq. (4.11) is a hyperbolic tangent function, related to the exponential function by

$$\tanh(x) = \frac{1 - \exp\left(-2x\right)}{1 + \exp\left(-2x\right)} , \tag{4.12}$$

when the variable x varies in the range $(-\infty, \infty)$, the value of the hyperbolic tangent function changes from -1 to 1 through zero.

The absorptivity $\alpha(\lambda, T, V)$ is connected to the absorption coefficient by Lambert-Beer's law

$$\alpha = 1 - \exp\left(-\Delta_0 \tanh\left(\frac{hc/\lambda - q\,V}{2\,k_{\mathrm{B}}T}\right)\right) , \quad \text{with} \quad \Delta_0 = \tau_0\, d\,, \tag{4.13}$$

where τ_0 is the absorption coefficient in the absence of excitations, d is the thickness of the source, Δ_0 is the optical thickness of the source, evaluated at zero voltage.

For an optically thick source $\Delta_0 \to \infty$, the absorptivity is given by

$$\alpha = \begin{cases} 1 & \frac{hc/\lambda - q\,V}{k_{\mathrm{B}}\,T} > 0 \\ 0 & \frac{hc/\lambda - q\,V}{k_{\mathrm{B}}\,T} = 0 \\ -\infty & \frac{hc/\lambda - q\,V}{k_{\mathrm{B}}\,T} < 0 \end{cases} \tag{4.14}$$

For most cases $(hc/\lambda - q\,V)/k_\mathrm{B}T \gg 1$, and the absorptivity in Eq. (4.13) is simplified as $\alpha = 1 - \exp(-\Delta_0)$.

For a real LED with a finite optical thickness ($\Delta_0 < \infty$), summarizing Eqs. (4.9) and (4.13) yields the luminescent spectrum of a real LED as

$$L_\mathrm{lum}(\lambda, T, V) = \frac{2hc^2}{\lambda^5} \frac{1 - \exp\left(-\Delta_0 \tanh\left(\frac{hc/\lambda - q\,V}{2\,k_\mathrm{B}T}\right)\right)}{\exp\left(\frac{hc/\lambda - q\,V}{k_\mathrm{B}T}\right) - 1} \,. \tag{4.15}$$

This is a continuous, bounded function of $(hc/\lambda - q\,V)$ for both positive and negative values and can be continued to $hc/\lambda - q\,V = 0$, with the limit

$$\lim_{\frac{hc/\lambda - q\,V}{k_\mathrm{B}T} \to 0} \alpha\, L_\mathrm{lum}^\mathrm{eq} = \frac{hc^2\Delta_0}{\lambda^5} \,. \tag{4.16}$$

The optical thickness is an intrinsic property of the source. It varies for LEDs of different types and different materials. In order to derive the optical thickness and apply it to the physical model of the spectral radiation of LEDs, we compare a real luminescent spectrum $L_\mathrm{lum}^\mathrm{m}$ of the LED from measurements with an ideal luminescent spectrum given by Eq. (4.2) under identical conditions (the same temperature and the same applied voltage). The optical thickness is derived as

$$\Delta_0 = -\ln\left(1 - \frac{L_\mathrm{lum}^\mathrm{m}}{L_\mathrm{lum}^\mathrm{eq}}\right) \coth\left(\frac{hc/\lambda - q\,V}{2\,k_\mathrm{B}T}\right) \,. \tag{4.17}$$

The second multiplier is a hyperbolic cotangent function, the reciprocal of the hyperbolic tangent function. Fig. 4.7 shows the calculated optical thickness of the NovaLED175 LED. Accordingly, the absorptivity at any applied voltage can be calculated with Eq. (4.13) by giving the value of the applied voltage.

Efficiencies

- Internal quantum efficiency η_iq

  The ratio of the number of photons emitted from the active region (in which radiative and non-radiative recombination occurs) to the number of electrons injected into an LED, expressed as

  $$\eta_\mathrm{iq} = \frac{\Phi_\mathrm{i}/(h\nu)}{I/q} \,, \tag{4.18}$$

  where Φ_i is the light power emitted from the active region, I is the forward current, $h\nu$ is the photon energy. An ideal LED has an internal quantum efficiency of unity, the active region emits one photon for each electron injected.

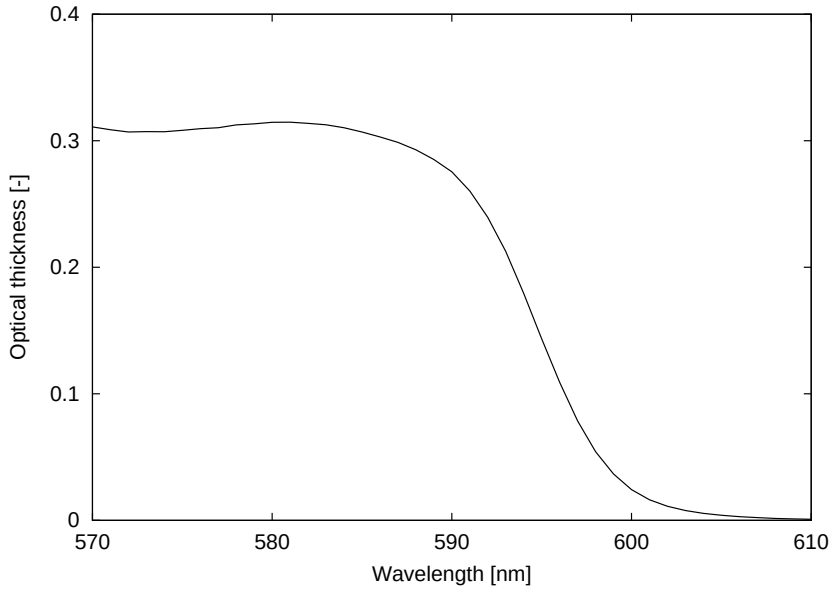

Figure 4.7.: Optical thickness of the NovaLED175 LED is evaluated at a very low current according to Eq. (4.17).

The internal quantum efficiency of a real LED is less than unity due to non-radiative recombination. Two general possibilities to increase the internal quantum efficiency are enhancing the radiative recombination and decreasing the non-radiative recombination: by using a double heterostructure consisting of the active region (light emitting region) and claddings for preventing carriers from escaping from the active region [64].

- Light extraction efficiency η_{ex}

  The ratio of the number of photons emitted into free space to the number of photons emitted from the active region, indicated as

$$\eta_{\mathrm{ex}} = \frac{\Phi_{\mathrm{e}}/(h\nu)}{\Phi_{\mathrm{i}}/(h\nu)} = \frac{\Phi_{\mathrm{e}}}{\Phi_{\mathrm{i}}} \,, \tag{4.19}$$

  where Φ_{e} is the radiant power emitted into free space. An ideal LED has $\eta_{\mathrm{ex}} = 1$. The light extraction efficiency of real LEDs is much lower than unity due to the absorption of the substrate and the metallic contact surface, Fresnel reflection loss and total internal reflection (TIR) at the semiconductor-air interface. The light extraction efficiency is a severe limitation for high performance LEDs.

  The loss resulting from the absorption of the substrate can be decreased by compromising the doping and the thickness of the transparent substrate. A high doping of carriers may increase the radiative efficiency. On the other hand it may introduce defects, leading to unwanted non-radiative recombination.

Doping may also increase the absorption coefficient, in turn the absorption will increase exponentially as a function of the optical thickness.

The absorption caused by the metallic contact can be reduced via utilizing reflective and transparent contacts and flip-chip packaging [34, 65].

Fresnel reflection can be reduced by using anti-reflection coating of an optimized thickness and refractive index.

In case of TIR, the fraction of light extraction constricted by TIR at the semiconductor-air interface (with refractive indices N_s and N_0 respectively) is approximately $N_0^2/(4N_s^2)$. This fraction is quite low due to the large contrast between the two refractive indices (generally $2.5:1$, or even higher). TIR is a main issue that limits the light extraction efficiency.

Several approaches were presented to increase the light extraction limited by TIR, e. g. a domed transparent epoxy encapsulation, LED chips-shaping (a hemispherical dome [9], a truncated inverted pyramid [35], truncated inverted cones [15]), textured surfaces [21, 56, 67], an omnidirectional reflector [32], a diffuse reflector-cup [42]. With these methods, the light extraction efficiency can be increased.

- External quantum efficiency η_{eq}

  The ratio of the number of photons emitted into free space to the number of injected electrons, indicated as

$$\eta_{eq} = \frac{\Phi_e/(h\nu)}{I/q} = \eta_{iq}\,\eta_{ex}\ . \tag{4.20}$$

- Power efficiency η_e

  The power efficiency η_e is defined in Eq. (2.4). The power efficiency is the overall efficiency of the LED. Generally the power efficiency is slightly lower than the external quantum efficiency due to the effect of a series resistance in LEDs. η_e is an important value for evaluating the performance of LEDs.

The experimental spectral distribution of the NovaLED175 LED at an applied current of 100 mA and at room temperature 300 K is shown in Fig. 4.8. The linewidth of the LED emitting at the peak wavelength of 595 nm is 14 nm (FWHM), in agreement with the derived linewidth from Eq. (4.1), $\Delta E = 1.8\,k_B T = 46$ meV at room temperature. Light power over the spectral range $560-620$ nm, over the total emitting area and over a solid angle of π is 8.3 mW.

The light output power versus current (L−I) characteristics of the NovaLED175 LED are illustrated in Fig. 4.9. The light output increases less than linearly with the current as a result of a carrier saturation effect in the small light-emitting region.

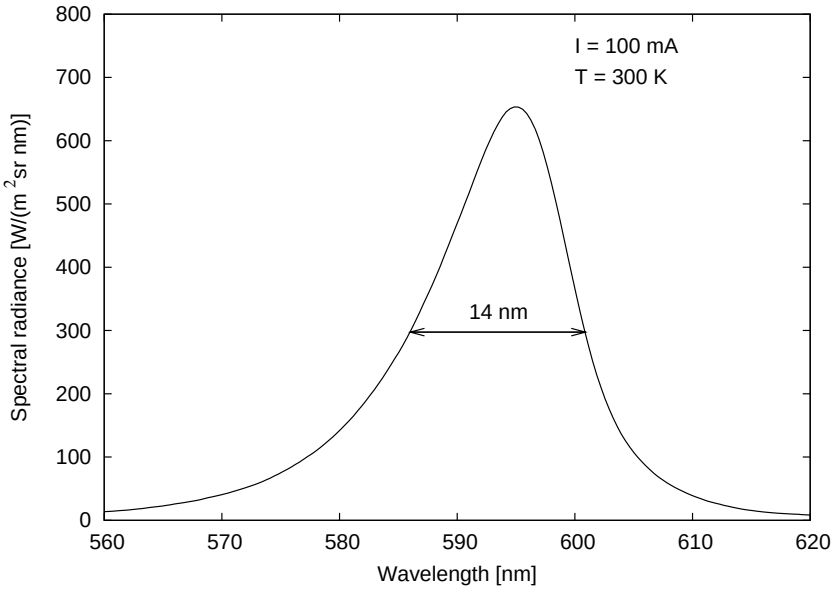

Figure 4.8.: Spectral distribution of the NovaLED175 LED at a current of 100 mA. The full width at half maximum is 14 nm. The peak wavelength is 595 nm. Light power over the spectral range 560−620 nm, over the total emitting area and over a solid angle of π is 8.3 mW.

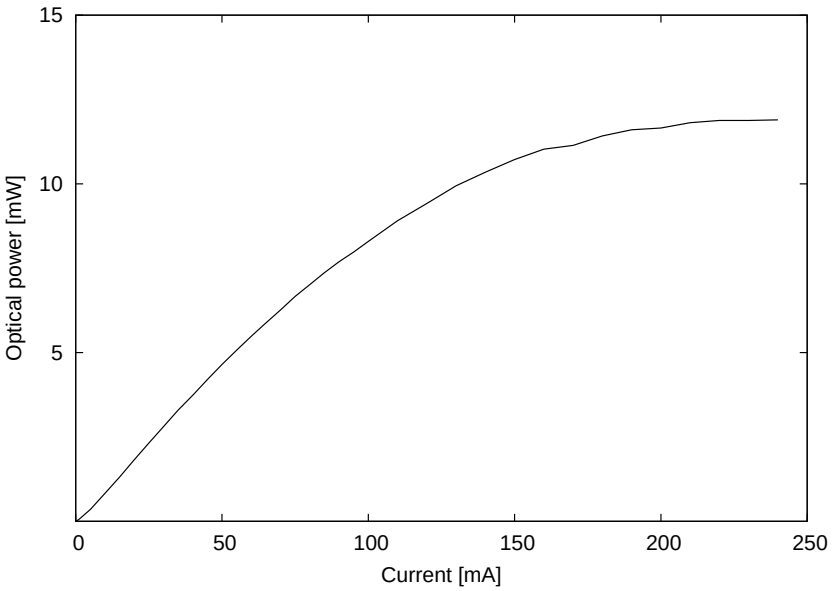

Figure 4.9.: Light output versus current characteristics of the NovaLED175 LED. The light output increases less than linearly with the current as a result of a carrier saturation effect in the small light-emitting region.

The measured external quantum efficiency versus current is illustrated in Fig. 4.10. At a low current (< 40 mA) the quantum efficiency increases with the current up to

a maximum, then drops due to the thermal effect on the p-n junction.

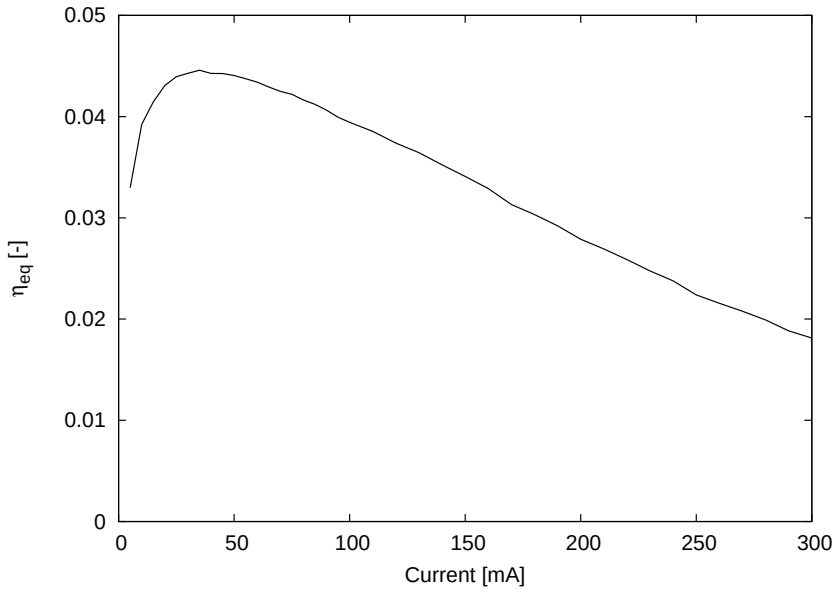

Figure 4.10.: External quantum efficiency η_{eq} versus current of the NovaLED175 LED from measurement. At a low current ($< 40\,\mathrm{mA}$) the external quantum efficiency increases with the current up to a maximum, then drops due to the thermal effect on the p-n junction.

As an example, the external quantum efficiency of the LED at an applied current of 100 mA is calculated with the measured luminescent spectrum $L^{\mathrm{m}}_{\mathrm{lum}}$ and Eq. (4.20) as

$$\begin{aligned}\eta_{\mathrm{eq}} &= \frac{A_{\mathrm{s}}\Omega_{\mathrm{p}}}{I/q}\int_{\lambda_{\min}}^{\lambda_{\max}}\frac{L^{\mathrm{m}}_{\mathrm{lum}}(\lambda,T,V)}{hc/\lambda}\mathrm{d}\lambda \\ &= \frac{0.235\,\mathrm{mm}^2\,\pi}{100\,\mathrm{mA}/q}\int_{560}^{620}\frac{L^{\mathrm{m}}_{\mathrm{lum}}(\lambda,T,V)}{hc/\lambda}\mathrm{d}\lambda \\ &= 4.4\%\ ,\end{aligned}$$

where the projected solid angle Ω_{p} of the LED (a Lambertian emitter) is π.

The power efficiency is calculated with Eq. (2.4) as

$$\begin{aligned}\eta_{\mathrm{e}} &= \frac{A_{\mathrm{s}}\Omega_{\mathrm{p}}}{VI}\int_{\lambda_{\min}}^{\lambda_{\max}}L^{\mathrm{m}}_{\mathrm{lum}}(\lambda,T,V)\mathrm{d}\lambda \\ &= \frac{0.235\,\mathrm{mm}^2\pi}{1.938\,\mathrm{V}\cdot 100\,\mathrm{mA}}\int_{560}^{620}L^{\mathrm{m}}_{\mathrm{lum}}(\lambda,T,V)\mathrm{d}\lambda \\ &= 4.3\%\ .\end{aligned}$$

The power efficiency is slightly lower than the external quantum efficiency due to the effect of a series resistance.

In addition, applying the measured data to Eq. (2.5) yields the luminous efficacy $\eta_v = 21\,\mathrm{lm/W}$. The low external quantum efficiency, power efficiency and luminous efficacy are results of the low light extraction efficiency.

Temperature dependence of emission

Previous research [10, 26] showed that the bandgap energy of certain types of LEDs decreases with temperature. The peak wavelength of the LED shifts to longer wavelengths with increasing current. The peak wavelength of the NovaLED175 LED increases linearly with the forward current, shown in Fig. 4.11. The current increase leads to a temperature increase of the p-n junction, as a consequence the temperature-dependent bandgap energy drops proportionally to the current [62]. As a result, the linewidth (FWHM) of the NovaLED175 LED increases linearly with the forward current, shown in Fig. 4.12.

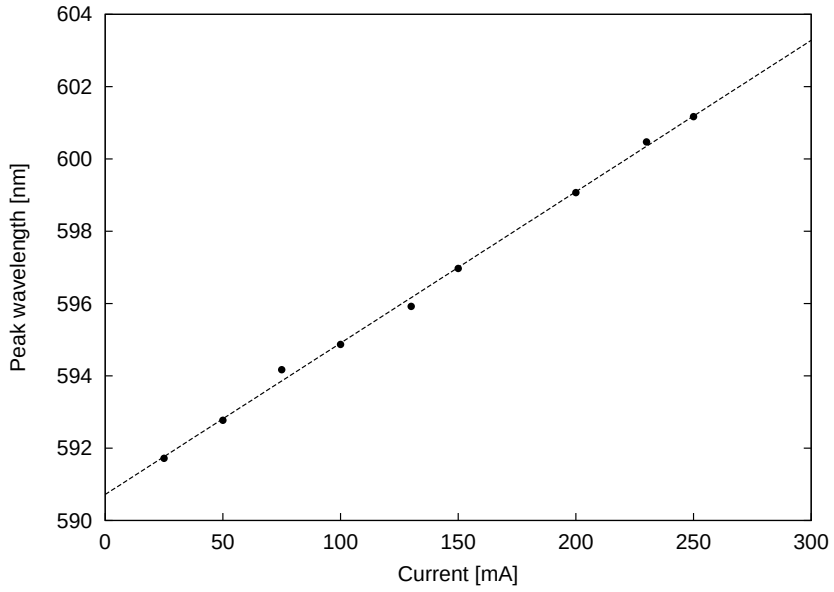

Figure 4.11.: Peak wavelength increases linearly with the forward current in the NovaLED175 LED.

The radiant flux of the LED decreases with temperature. The decrease of the emission intensity is due to several temperature-dependent factors consisting of (1) non-radiative recombination, (2) surface recombination, and (3) carrier loss over barriers [57].

The temperature dependence of the emission of LEDs near room temperature is expressed as a function of the temperature T

$$\Phi_e(T) = \Phi_e(T_0)\,\exp\left(-\frac{T - T_0}{T_{\mathrm{char}}}\right)\,, \tag{4.21}$$

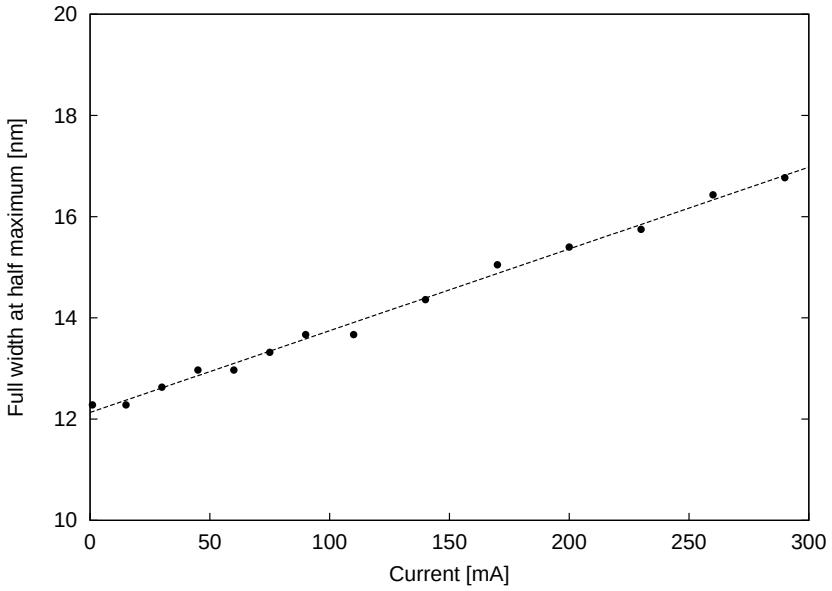

Figure 4.12.: The full width at half maximum (FWHM) increases linearly with the forward current in the NovaLED175 LED, in agreement with $\Delta E = 1.8\, k_\mathrm{B}\, T$.

where $\Phi_\mathrm{e}(T_0)$ is the light emission at room temperature T_0. The characteristic temperature T_char describes the temperature dependence of the emission. A high characteristic temperature is desirable, which implies a small temperature dependence. T_char can be obtained via measuring the respective light emission at room temperature and at another temperature T. The thermal effect on the emission at any temperature in between can be obtained with Eq. (4.21).

The thermal effect is included in the physical model.

The far-field radiation

The NovaLED175 LED is a Lambertian emitter. In order to measure the far-field radiation of light sources, a goniometer is used. Generally two kinds of goniometers are applied, either with a movable detector or with a movable source, depending on the measuring space and the size of the source and the detector.

Figure 4.13 shows the schematic mechanism of a goniometer with a movable detector. A source is placed in the center of the equator plane of the hemisphere. This is the reference point. A detector is spatially adjustable by giving an azimuth angle ϕ and a zenith angle θ. For most sources with symmetrical radiation, the measurement is only needed to be done in the cross section with $\phi = 0$ and θ from 0 to 90°. For sources with asymmetrical radiation pattern, measurements covering the entire hemisphere are necessary. In our experiment, all measurements are automatically

controlled by a LabVIEW package.

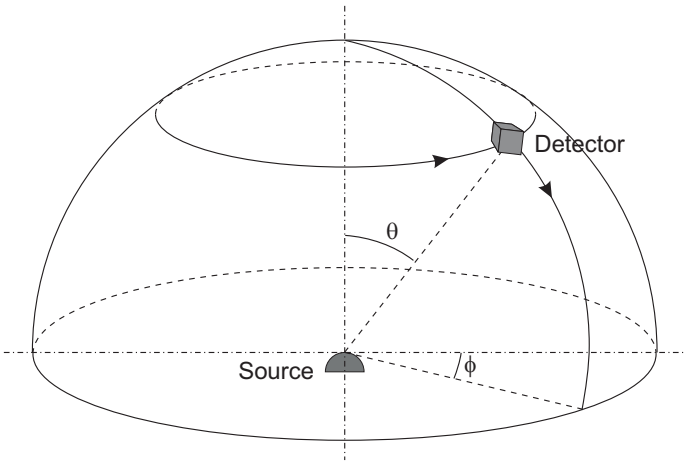

Figure 4.13.: Schematic mechanism of a goniometer with a movable detector. The source is in the center of the equator plane of the hemisphere. The detector is adjustable by giving an azimuth angle ϕ and a zenith angle θ. For a source with symmetrical radiation, the measurement only needs to be taken in the cross-section with $\phi = 0$ and θ from 0 to 90°.

The far-field radiation distribution of the NovaLED175 LED has a rotational symmetry. The radiation in one cross section vertical to the light-emitting surface is measured continuously. Fig. 4.14 shows a two-dimensional radiation distribution, presented in a polar plot. The intensity is normalized to the value perpendicular to the light-emitting surface of the source. The distribution shows that the NovaLED175 LED is a Lambertian emitter.

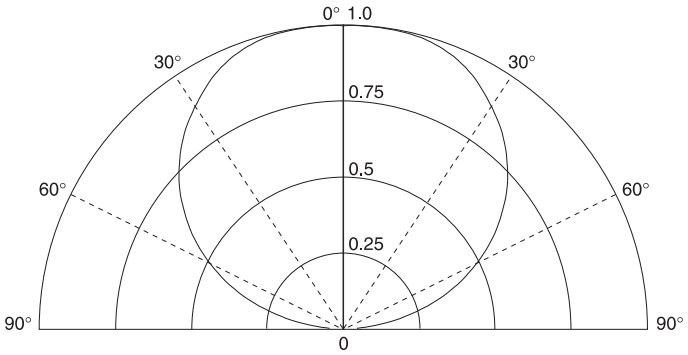

Figure 4.14.: Far-field emission distribution (relative intensity vs. angle) of the NovaLED175 LED in a polar plot. The distribution shows a Lambertian emission.

A three-dimensional radiation distribution of the LED is shown in Fig. 4.15, it has a rotational symmetry. The intensity is normalized with respect to the value for

the angle normal to the light-emitting surface of the LED. For the measured LED, the maximal intensity is in the center. In case of some LEDs, the maximal intensity is not on the mechanical axis.

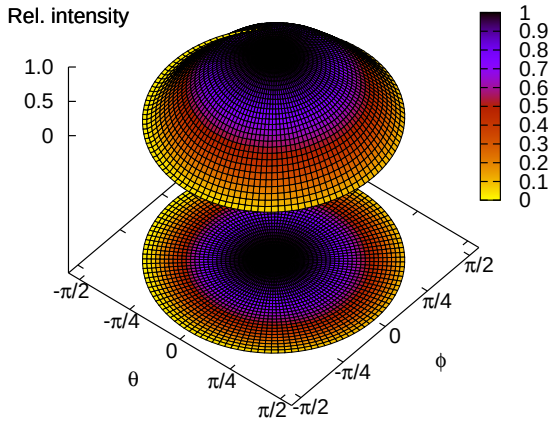

Figure 4.15.: Three-dimensional far-field emission distribution of the NovaLED175 LED. The intensity is normalized with respect to the intensity for the angle normal to the light-emitting surface of the LED. The emission distribution has a rotational symmetry.

Combining the geometrical, electrical, material and radiation submodules yields the physical model of light emission of LEDs.

4.3. Light recycling with an LED

4.3.1. Experimental method and setup

An LED can both emit light and reflect light. Fig. 4.16 (a) illustrates an LED emitting light, (b) shows the same LED reflecting light. The light directed on the LED may come from other LEDs or from the same LED that is reflected onto itself. The reflected light is superposed to the emitted light, leading to an increased brightness of the LED. The intrinsic reflectivity of the LED is utilized when the reflection occurs at the air-semiconductor interface.

In order to investigate the light recycling effect in LEDs and achieve brightness increase of LEDs via light recycling by utilizing the intrinsic reflectivity of LEDs, an experimental setup (Fig. 4.17) is used for measurements. An aspheric condenser

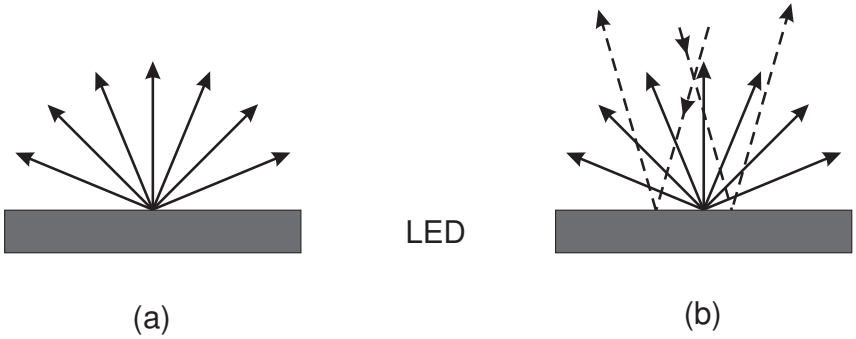

Figure 4.16.: (a) shows light emission from the light-emitting surface of an LED, (b) shows light reflection from the same LED. The light directed on the LED may come from other LEDs or from the same LED that is reflected to itself by a reflector. The reflected light is superposed onto the emitted light, leading to an increased brightness of the LED, i. e. the LED on the right-hand side is brighter than the LED on the left-hand side.

is used to collimate the emitted light from the NovaLED175 LED. A flat mirror returns the light back onto the LED. A beam splitter placed in between is used to extract the light and redirect the light to a diffusor, in turn to the aperture of the fiber and the spectrometer. For seeking brightness enhancement due to light recycling, the light emissions are measured twice for a comparison, i. e. once with the mirror, once without the mirror. The ratio of the two measurements yields the light enhancement.

Note that the diffusor is used for offering an average brightness and an average brightness enhancement, since the emission and reflecting properties of an LED are not uniform across the LED output surface. The overall LED reflectivity depends on several design factors including the reflectivity of any top metal contacts, the reflectivity of the mirror surface on the back side of the LED, the absorption of light by the semiconductor layers and the number and type of light extracting elements incorporated in the LED design [3]. From a practical standpoint, the most important brightness values are the average brightness of the LED and the average brightness enhancement contributed by the entire LED surface but not only by the brighter parts of the output surface.

As comparison, this experiment is modelled via ray-tracing. Fig. 4.18 shows a rendering of the model including some sample rays.

The light emissions on the entrance of the spectrometer are denoted with L_{no} (in the absence of the flat mirror) and L_{with} (with the mirror), respectively. They are expressed as

$$L_{\mathrm{no}} \;=\; L^{0}_{\mathrm{lum}}\, t_2\, r_3 \;,$$

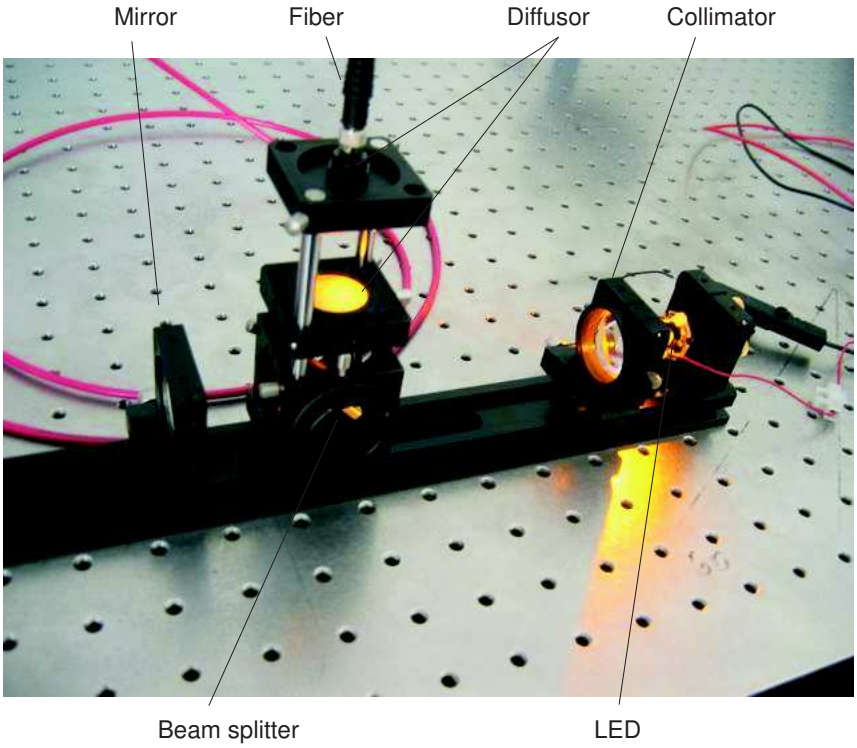

Figure 4.17.: Experimental setup for light recycling with an LED. Light emitted by an LED is collimated by an aspheric condenser. A flat mirror returns the light back to the LED. A beam splitter placed in between is used to extract the light and redirect the light to a diffusor, in turn to the aperture of the fiber and the spectrometer. We measure the light emission twice, i. e. once with the mirror (with light recycling), once without the mirror. The ratio of the two measured results implies brightness enhancement.

$$L_{\text{with}} \;=\; L^0_{\text{lum}}\, t_2\, r_3 \left(1 + r_1\, r_4\, t_2^2\, t_3^2 + \left(r_1\, r_4\, t_2^2\, t_3^2\right)^2 + \;...\right) \;, \tag{4.22}$$

where the subscripts 1, 2, 3, 4 indicate the LED, the collimator, the beam splitter and the mirror, respectively. The other parameters are: L^0_{lum} is the original light emission from the output surface of the LED, r_1 is the reflectivity of the LED, t_2 is the transmissivity of the collimator, r_3 and t_3 are the reflectivity and the transmissivity of the beam splitter, respectively, r_4 is the reflectivity of the mirror. L_{with} results from multiple recycling (due to the reflection of the mirror) constituting an infinite geometric series.

The ratio of L_{with} to L_{no} yields an average brightness enhancement, expressed as

$$\eta = \frac{L_{\text{with}}}{L_{\text{no}}} = \frac{1}{1 - r_1\, r_4\, t_2^2\, t_3^2} \;. \tag{4.23}$$

The term $r_1\, r_4\, t_2^2\, t_3^2$ in Eq. (4.23) indicates the capability of light recycling of the

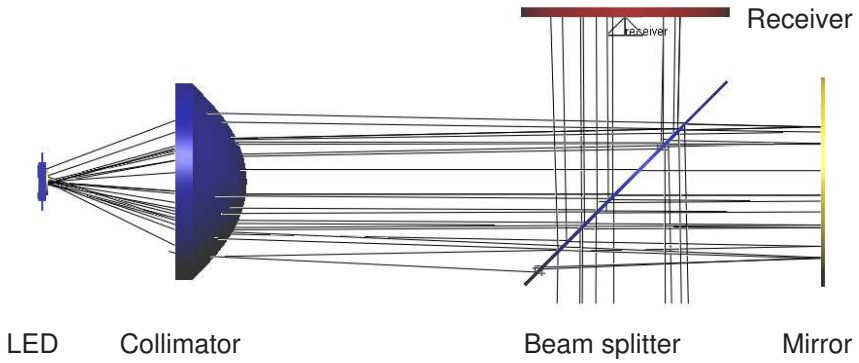

Figure 4.18.: Simulation of light recycling in an LED via ray-tracing. The figure shows a rendering of the model including some sample rays. The values of the reflectivity and the transmissivity are listed in Table 4.1.

system, i. e. after one cycle the fraction of the light that escapes absorption and re-emerges in the same phase space as the direct radiation (the fraction without being recycled). It is termed light recycling factor

$$\xi = r_1\, r_4\, t_2^2\, t_3^2\ . \tag{4.24}$$

This recycling factor is equivalent to the fraction of transmitted light after one transit through the source according to Lambert-Beer's law (see Sec. 2.2).

The brightness enhancement η is a function of ξ. A high recycling factor facilitates light increase. This conclusion is proven in the experiments by using two beam splitters with different reflectivity-transmissivity ratios (0.5 : 0.5, 0.1 : 0.9) respectively, keeping other factors constant. The ideal brightness enhancement can approach infinity, if the recycling factor approaches unity. This is in agreement with the conclusion in Sec. 2.2 that an optically thin source offers a large potential for brightness increase via light recycling.

4.3.2. Results and discussion

Figure 4.19 illustrates the brightness enhancement of the spectral radiation due to light recycling with a beam splitter of a transmissivity of 0.9. The brightness enhancement factor approaches 1.3−1.4 on average. A similar effect is found for the same source with a beam splitter of 0.5 transmissivity. The results are listed in Table 4.1.

The results show that brightness enhancement is achieved via light recycling. Using a beam splitter with a higher transmissivity yields a larger brightness enhancement factor, since more light is used for light recycling.

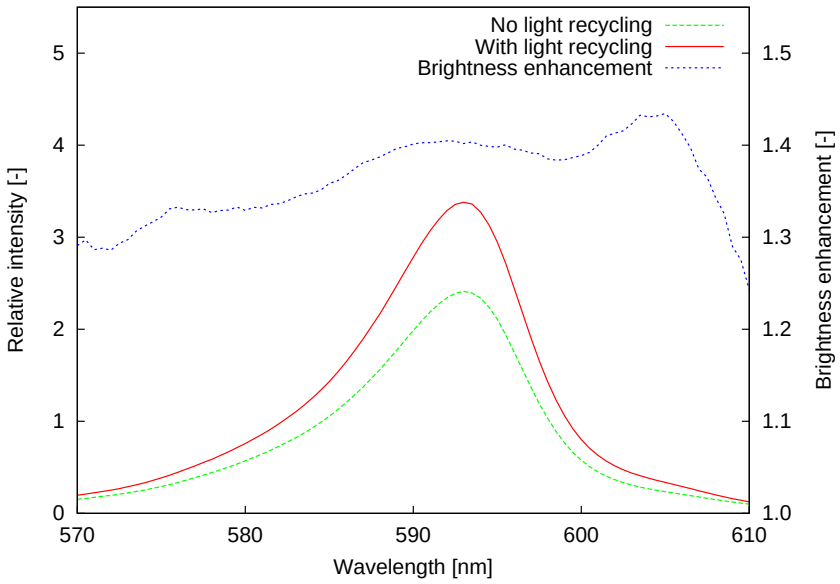

Figure 4.19.: Brightness enhancement results from light recycling with a beam splitter of a transmissivity of 0.9. The radiance is increased by 38% on average with a tendency of larger increase for longer wavelengths. Beyond the bandgap, the enhancement factor drops.

Table 4.1.: Results of brightness enhancement for light recycling with the Nova-LED175 LED. Two beam splitters with different transmissivity are used. The values of the reflectivity and the transmissivity for each device are listed.

Brightness enhancement	Beam splitter ($r_3 : t_3$)	
	0.5 : 0.5	0.1 : 0.9
Experiment	1.10	1.38
Simulation	1.10	1.40
Calculation with Eq. (4.23)	1.11	1.49

LED reflectivity $r_1 = 0.5$, mirror reflectivity $r_4 = 0.96$, collimator transmissivity $t_2 = 0.92$

The brightness enhancement factor increases with the emitted wavelength close to the bandgap energy due to a decreased absorption and an increased reflectivity. Eq. (4.14) shows zero absorption at the bandgap energy for an ideal semiconductor. As a consequence, the reflectivity approaches unity.

The calculated brightness enhancement factors are higher than the measured results. The difference is caused mainly by the reflectivity of the LED. Compared with

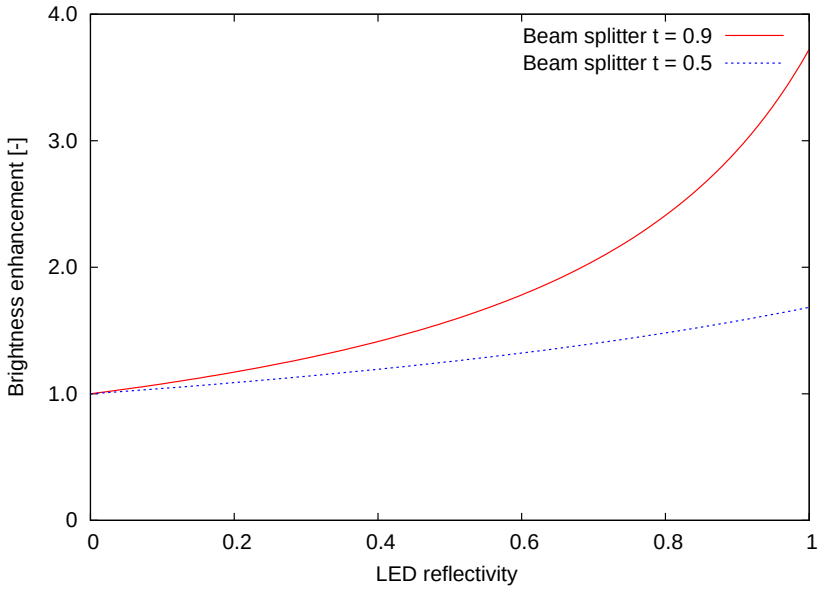

Figure 4.20.: Calculated brightness enhancement vs. reflectivity of the LED according to Eq. (4.23). Two cases are illustrated, one with a beam splitter of a transmissivity of 0.9, the other with 0.1. Other used values are: mirror reflectivity 0.96, collimator transmissivity 0.92.

other parameters constituting the light recycling factor in Eq. (4.24), the reflectivity of the LED is low, leading to a low recycling factor. The brightness enhancement factor as a function of the LED reflectivity is illustrated in Fig. 4.20, keeping other factors constant. Two cases are illustrated, one with a beam splitter of 0.9 transmissivity, the other with a beam splitter of 0.5 transmissivity. The reflectivity of the LED was measured in the experiment. An average reflectivity over the total output surface is used. However, the model (Fig. 4.18) and the experiment showed that only part of the light output surface is used, since part of the light escapes out of the system as loss.

In addition, the accumulated collimation error due to the multiple light reflections and the increased optical path length would defocus the recycled rays, in turn reduce the contribution of the total light emission to light recycling by about 12%.

4.4. Summary

Based on the experiments, the simulation and the discussion on light recycling of LEDs, we draw the conclusions:

- the reflectivity of the LED is the main issue in light recycling. This reflectivity is expected to be improved with the development of material and fabrication,

or via incorporating specially designed optics, e. g. a backside mirror.

- a large light recycling factor (the efficiency of one cycle) is desirable for brightness enhancement.
- driving the LED close to the bandgap energy is favorable for seeking a low absorptivity, and in turn a high reflectivity.
- high external quantum efficiencies of LEDs are required, not only for achieving brightness enhancement, but for high brightness for practical illumination.

5. Optical device for light recycling–Carambola

5.1. Optical principle

Light recycling in thermal sources and luminescent sources has been discussed theoretically and proven experimentally. In order to apply light recycling to practical applications, an optical device for achieving brightness enhancement of light sources via deterministic and multiple light recycling, the Carambola, is designed based on the principle of light recycling (see Sec. 2.2). A rendering of a five-point Carambola is shown in Fig. 5.1.

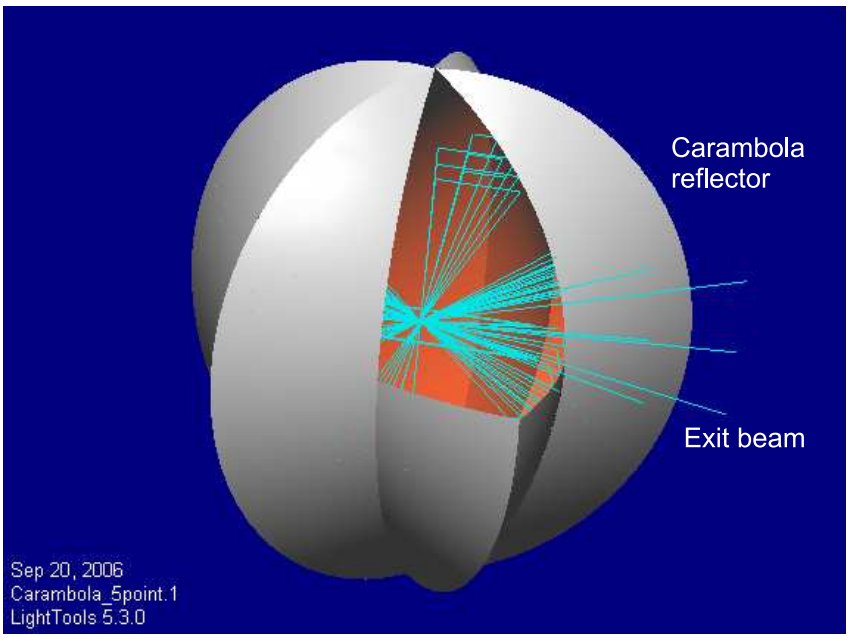

Figure 5.1.: Rendering of a five-point Carambola for deterministic and multiple light recycling. One rib remains half open. Rays emitted from the source situated in the center of the Carambola are reflected from the walls and transit through the source multiplely. The rays are redirected to the exit of the device, and superposed onto the direct radiation in the same phase space, leading to an increase of the brightness.

Due to the geometry of the Carambola, rays emitted from the source situated in the center of the Carambola are reflected from the walls and transit through the source multiplely. The rays are redirected to the exit of the device, and superposed onto the direct radiation in the same phase space, leading to an increase of the collected flux and an enhanced brightness. The cost is a reduction of the total radiated flux due to the absorption in the source in the process of light transits through the source. Multiple transits through the source are equivalent to increasing the optical thickness of the source.

The device is named *Carambola* for its resemblance to the shape of the Star Fruit, which often has five points. The principle is applicable to any similar designed geometry of odd number of points, due to the need for rotation.

A three-dimensional Carambola is a geometrical combination of a dual-paraboloidal mirrors [38, 39]. The globe-like geometry allows rays to recirculate alternately between the upper half and the lower half in the Carambola (Fig. 5.1). The dual-paraboloidal mirrors can focus rays towards the center due to the cofocus of the system.

For a clear understanding of the working principle and the function of the Carambola, one can resort to a commonly used optical device for radiometric measurements, an integrating sphere. An integrating sphere is used for yielding a uniform light distribution over the interior by reflecting the incident rays many times. By means of this stochastic reflection, each ray contributes equally to the ultimate light distribution, leading to a Lamtertian distribution over the interior. Generally, using an integrating sphere one cannot increase radiance of the source because the resulting étendue of the system is not reduced.

The reflection of rays in the Carambola happens in deterministic fashion. Incident rays are reflected and redirected a number of times through the source in the center, and are extracted from the exit. In the phase space of the exit, the collected flux is increased compared with the case in the absence of the Carambola. Under an assumption of a highly reflective interior of the Carambola, an increased radiance can be achieved at a reduced phase space (compared with the case of a naked source). In systems which feature compact size and high brightness, using the Carambola as part of the illumination system is a viable option.

5.2. Prototyping

5.2.1. Geometry

The geometry of the Carambola is a combination of paraboloids. Consider the case of a five-point Carambola illustrated in Fig. 5.2: (a) shows the cross section in the equator plane, it is a combination of five pieces of dual-parabolas (defined as

baseline) equiangularly distributed around the center S and cofocused to S. Each dual-parabola consists of two identical parabolas and is symmetric with respect to the latus rectum of the involved pair of parabolas. Each parabola intersects the respective latus rectum at a point, actually two points (A and C), but point C is omitted, as only odd number of points are allowed for reasons of the rotation of the recycled rays (see below). Point A is defined as the point of the Carambola. This point is also the intersection of the dual-parabola. All intersection points are located on a circle of radius R_0 (the semilatus rectum of the involved parabolas). R_0 defines the dimension of the Carambola.

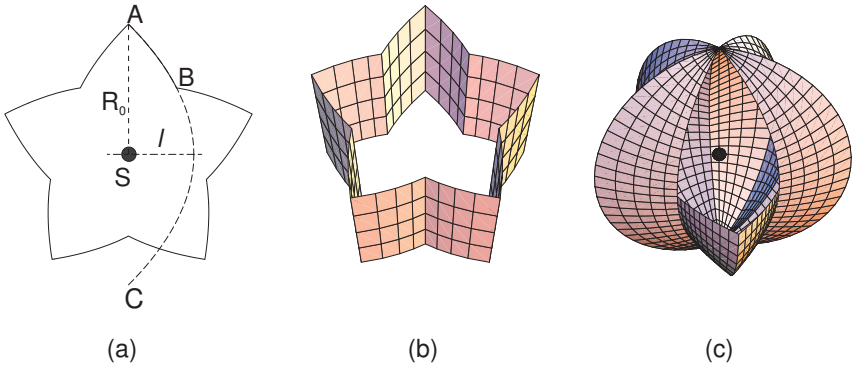

Figure 5.2.: Geometry of a five-point reflective Carambola. (a) the cross section in the equator plane is a combination of five pieces of dual-parabolas (defined as baseline) equiangularly distributed around the center S and cofocused to the point S. Each dual-parabola consists of two identical parabolas and is symmetric with respect to the semilatus rectum R_0 of the involved pair of parabolas. Consider the uppermost dual-parabolas, arc AB is a part of the parabola AC with its axis passing through the center S of the geometry. The parabola intersects the semilatus rectum $\overline{AS}$ at point A, defined as one point of the Carambola. R_0 defines the dimension of the Carambola. (b) a longitudinal translation of the cross section yields a two-dimensional Carambola. (c) the cross section is revolved around the center becoming sections of paraboloids which join along circular edges. The Carambola has a half opening on one of the dual-paraboloids. Upon each pass through the source (placed in the center) a ray alternates between the upper half and the lower half of the Carambola.

A longitudinal translation of the cross section yields a two-dimensional Carambola illustrated in Fig. 5.2 (b), which matches a cylindrical source with the same length as the Carambola.

The principle of the Carambola can be generalized from two-dimensional space into three-dimensional space. The reflectors are revolved around the source becoming sections of paraboloids which join along circular edges. Fig. 5.2 (c) illustrates a

three-dimensional reflective Carambola. Upon each pass through the source (placed in the center) a ray alternates between the upper half and the lower half of the Carambola.

The design of a reflective version needs two parameters: the odd number of the ribs (or points) n and the semilatus rectum R_0 (twice as long as the focal length of the parabola). For a refractive version, the refractive index needs to be taken into account.

The locus function of a parabola in a three-dimensional space is parameterized by the azimuth angle θ and zenith angle ϕ, expressed as

$$\mathbf{Z}(\theta,\phi) = \frac{2R_0\,\mathbf{P}(\theta,\phi)}{1-\mathbf{K}(\theta)\cdot\mathbf{P}(\theta,\phi)}\ , \tag{5.1}$$

with $0 \le \theta \le 2\pi,\ 0 \le \phi \le \pi$, $\mathbf{P}(\theta,\phi)$ is the unit position vector, $\mathbf{K}(\theta)$ is the unit vector of the axis of a parabola. Eq. (5.1) is a general form of the function of a paraboloid. Any paraboloid can be created by defining the corresponding $\mathbf{P}$ and $\mathbf{K}$, which do not need to be parameterized by θ and ϕ. In terms of the designed Carambola, for the purpose of combining the function of a sphere in Eq. (5.1), we define the unit vector of each parabola's axis and the position vector of the geometry by using the position vector of a sphere as

$$\begin{aligned}
\mathbf{K}(\theta) &= \begin{cases} (-\cos(n_{\rm s}\,d\theta),\ \sin(n_{\rm s}\,d\theta),\ 0) & n_{\rm s} \le \theta/d\theta \\ (\cos(n_{\rm s}\,d\theta),\ -\sin(n_{\rm s}\,d\theta),\ 0) & n_{\rm s} > \theta/d\theta \end{cases}\ , \\
\mathbf{P}(\theta,\phi) &= (\sin\theta\sin\phi,\ \cos\theta\sin\phi,\ \cos\phi)\ ,
\end{aligned} \tag{5.2}$$

with

$$\begin{aligned}
d\theta &= 2\pi/n\ , \\
n_{\rm s} &= \text{round}\,(\theta/d\theta)\ ,
\end{aligned}$$

where $d\theta$ is the subtended angle by each dual-parabola, $n_{\rm s}$ is an integer, used for defining the azimuth angle of each parabola's axis.

Equation (5.1) is a general function of a three-dimensional Carambola. Summarizing Eqs. (5.1), (5.2) and defining n and R_0 yields the three-dimensional Carambola in Fig. 5.2 (c).

A two-dimensional Carambola illustrated in Fig. 5.2 (b) is a special case of Eq. (5.1) with $\phi = \pi/2$ and with a translation length z added, expressed as

$$\mathbf{Z}_{\rm 2D}(\theta,\phi,z) = \mathbf{Z}(\theta,\pi/2) + (0,\ 0,\ z)\ . \tag{5.3}$$

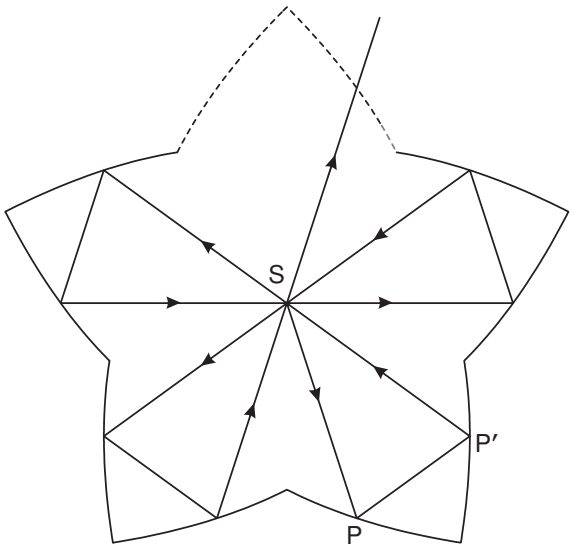

Figure 5.3.: Two-dimensional five-point reflective Carambola consists of five dual-paraboloid reflectors as designed. In order to extract the light out of the device, one of the dual-paraboloid reflectors (dashed line) is removed. Any ray emitted from the source in the center passes precisely 1, 2,...n times through the assumed transparent source S in the center and is reflected 2, 4,...$2\,(n-1)$ times before reemerging through the exit. n needs to be odd, due to the need for light circulation.

5.2.2. Reflective version

Two-dimensional version

In deterministic recycling rays are recycled a certain number of times before they finally exit the Carambola. Assume a light source in two-dimensional space as indicated in Fig. 5.3. Any ray emitted by the source S is reflected at point P, with a reflected direction parallel to the optical axis of the involved dual-paraboloid reflector. The reflected ray PP' will be reflected again at point P' towards the focus due to the cofocus of the dual-paraboloid reflector, and hit the opposite reflector. In turn the ray is recycled through the source.

For the Carambola with an odd number of ribs and same number of dual-paraboloid reflectors n, in two-dimensional space the maximal number of reflections of any ray is given by

$$m_{\mathrm{2D}} = 2\,(n-1)\,, \tag{5.4}$$

since one rib serves as exit. The transit only happens between two not neighboring dual-paraboloids (except the case $n = 3$, in which the transits always happen between the neighboring dual-paraboloids). A schematic approach illustrated in Fig. 5.4 is used to count the possible reflection number and the transit number.

Fig. 5.4 (a) shows that in a two-dimensional five-point Carambola transits only happen between the two connected points (note that each point indicates a dual-paraboloid) which are not next to each other, between the neighboring points no transit happens. Following this principle, the possible reflection number of any arbitrary ray is an arithmetic series: 2, 4, ..., $2\,(n-1)$. The average number of reflections for any ray is expressed as

$$\overline{m}_{2\mathrm{D}} = \frac{2+4+...+2\,(n-1)}{n} = n-1\ . \tag{5.5}$$

Each transit through the source is accompanied by double reflections, leading to the average number of transits of $(n-1)/2$. The number of transit through the center and the number of reflection are the required parameters for modelling the light recycling effect in the Carambola.

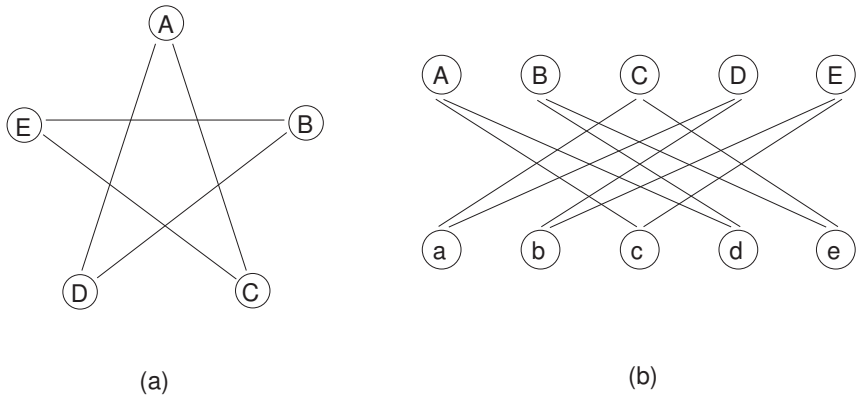

Figure 5.4.: (a) Schematic of the possible transits through the source between two not neighboring dual-paraboloids in a two-dimensional Carambola, the points indicate the dual-paraboloids. Assuming one pair is removed, i. e. one point is missing, the maximal number of transits is given by $n-1$ and the maximal number of reflection is $2n-2$; (b) illustrates the alternate transits through the source between two not neighboring dual-paraboloids which are in the upper and lower halves respectively in a three-dimensional Carambola. The two rows of letters indicate the dual-paraboloid mirrors in the upper half and the lower half, respectively. Assume that one pair in the upper space is removed, the maximal number of transits is $2n-1=9$, the maximal number of reflections is $4n-2=18$. If one total pair extending from the upper half to the lower half is missing, the maximal number of transits and reflections are similar to the two-dimensional case in (a).

In a closed Carambola without an opening any ray is recirculated infinitely until being absorbed due to the infinite number of transits through the source. However, the number of the hits is not infinity, but a specific number, i. e. a ray will return

to its start point after one complete circulation (generally, for a two-dimensional Carambola $4\,n$ hits, for a three-dimensional Carambola $8\,n$ hits). This is the essence of deterministic reflection.

A two-dimensional translated Carambola matches a cylindrical source which can be placed on the optical axis of the sphere.

Three-dimensional version

The global shape of the three-dimensional Carambola is spherical. Its dimension is confined by the radii of the ribs. The exit aperture in the direct generalization extends in zenith $0 < \phi < \pi$ and azimuth $\theta_0 < \theta < \theta_0 + 2\pi/n$, with $0 < \theta_0 < 2\pi$. Alternatively the lower half of the exit aperture may be closed with a pair of reflectors extending only up to $\phi = \pi/2$, the case in Fig. 5.2 (c). Because upon each pass through the source a ray alternates between the upper and the lower half of the system illustrated in Fig. 5.4, which increases the maximum number of reflections to

$$m_{3\mathrm{D}} = 4n - 2\ . \tag{5.6}$$

A derivation similar to Eq. (5.5) results in the number of reflections of an arbitrary ray in the three-dimensional Carambola as an arithmetic series with $2n - 1$ terms: 2, 4, ..., $2\,(n-1)$, yielding the average number of reflections $\overline{m}_{3\mathrm{D}} = 2\,n - 1$, the average number of transits $2n - 1/2$.

In comparison with a Carambola used for a transparent source emitting globally, for a source with a hemispherical emitting space, e. g. a surface-mounted LED, only the upper half of the Carambola is needed, the intrinsic reflectivity of the LED can be utilized in order to achieve light recycling, shown in Fig. 5.5.

5.2.3. Refractive version

The rotation of the direction vector of the recirculated light in transit through the source is a necessary condition for the Carambola optics. Rotation can be achieved by refractive optics, too. The light ray must be refracted in such a way that it propagates as secant radially.

The Porro prism consists of an aspheric front surface, and two symmetrical back surfaces with a right angle between them. In Fig. 5.6, the uppermost aspheric lens images the light from the source S into infinity. Rotation takes place during two reflections, and the direction of the ray is turned reversely, resulting from the optical property of the Porro prism. Coming from infinity, light is focused into the source by the same aspheric lens. The two reflections inside the prism follow total internal reflection, which requires the refractive index $N > 1/\sin(\pi/4) = 1.414$.

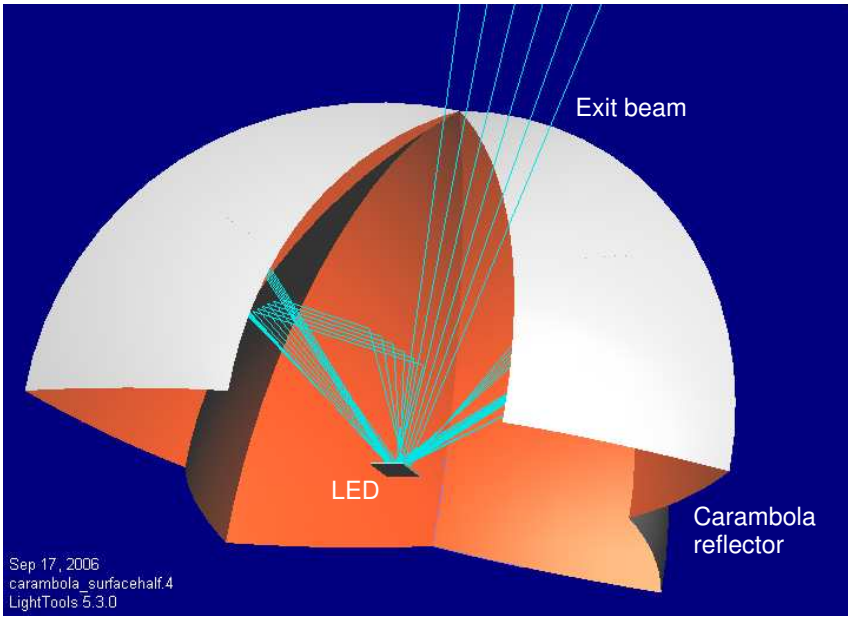

Figure 5.5.: Three-dimensional hemispherical Carambola with an LED for light recycling. The LED is placed in the center of the equator plane. Light emitted from the LED is reflected back to the LED off the walls, in turn the light can be reflected again from the LED due to its intrinsic reflecting property. The light escaping absorption is circulated between the dual-paraboloids and finally redirected to the exit. The beam in this example is circulated and hits each dual-paraboloid once, before exiting the Carambola. The collected flux in the phase space passing the exit is increased, compared with the case of the absence of the Carambola. The total radiant flux is decreased by the amount of absorption on the LED and on the walls. The brightness of the LED in the phase space is increased.

The prism does not have to be a Porro prism, but the two symmetrical back surfaces must be tailored to match the front surface. The back surfaces are straight walls for an aspheric front surface.

5.3. Light recycling in the Carambola

5.3.1. Source

In order to direct transiting light through the source, the geometrical size of the source is constricted by the number of points and the size of the Carambola. The relation between the three parameters can be estimated by means of the optical path length. The optical thickness of the source can be derived as well.

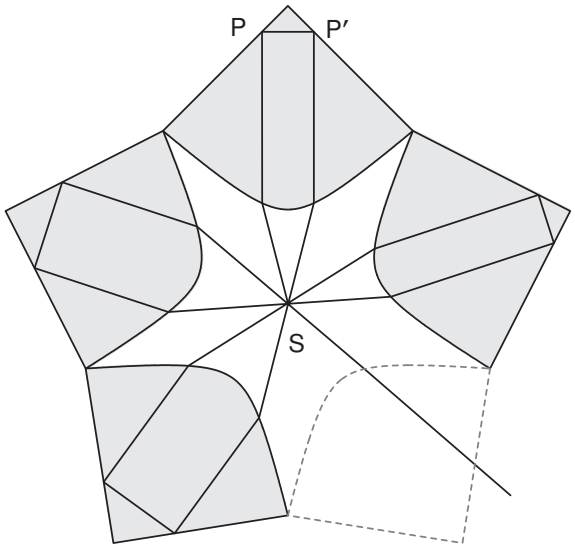

Figure 5.6.: Two-dimensional five-point refractive Carambola with four recirculations. Ray-tracing simulation of central ray from source S through point P. The Carambola has $n = 5$ points (one remains open as exit, dashed line). The refractive index of the lens material is $N = 1.51$. All reflections follow total internal reflection.

Geometrical size

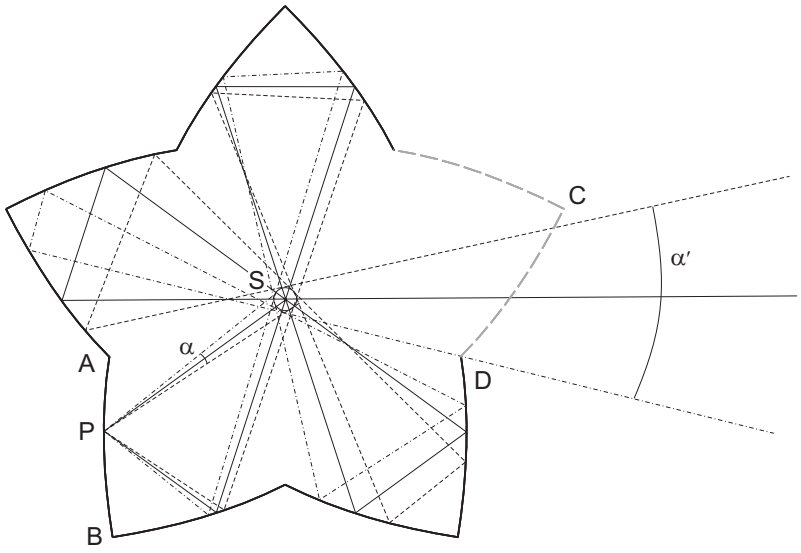

Figure 5.7.: Light recycling in a two-dimensional five-point reflective Carambola. Ray-tracing simulation of edge-rays through point P. The source appears at an angle $\alpha = 6°$, filling nearly the total exit aperture between points C and D. The central ray SP bisects the angle ASB.

The geometrical size of the source placed in the center of the Carambola can be approximated as a function of the optical path length over which an average ray travels within the optics, using the ray with the maximum number of reflections in Eq. (5.4) for the upper limit of the size of the source. The average ray is defined as the central ray which bisects the angle ASB in Fig. 5.7. Its length $\overline{SP}$ is calculated as

$$\overline{SP} = \frac{R_0}{1 + \sin(\pi/2n)} , \tag{5.7}$$

which can be understood as being the average radius of the Carambola. For an accurate derivation, the average radius is derived by calculating the radius of a circle which has the same area as the Carambola.

In Fig. 5.7 the source appears with an opening angle α from point P, limited by two edge-rays. This angle does not change significantly during the following seven reflections due to a small curvature of the wall of the reflectors. The image size of the source increases approximately proportionally to the distance travelled, its maximum size must fit the exit of the Carambola, guarded by the points C and D.

The optical path is folded within the Carambola. After $m_{2D} = 8$ reflections, the optical path length of $m_{2D}R_0$ is derived according to Fermat's law [6].

The image of the source must pass the exit, an empirical result of the source size R_s for the reflective version is given by

$$R_s \leq \frac{R_0 \sin(\pi/n)}{2\, m_{2D}} , \tag{5.8}$$

where R_0 is defined in Eq. (5.1). Note that this relation is established for the maximum number of reflections, resulting in a conservative estimate of the maximum size of the source.

In case of the refractive Carambola, the optical path length depends on the refractive index N of the material the light travels in, as shown in Fig. 5.8. The optical path length increases, and Eq. (5.8) changes for the refractive version to

$$R_s \leq \frac{R_0 \sin(\pi/n)}{2N\, m_{2D}} . \tag{5.9}$$

The opening angle α of the source in Fig. 5.7 is significantly larger than the same angle in Fig. 5.8, i. e. 6° and 2.75° for the reflective and the refractive versions, respectively. The refractive Carambola is more sensitive to the source size and optical errors, e. g. slope errors of the aspherical surface.

It is interesting to note that the left-hand rim and the right-hand rim of the image of the source in any reflection are alternatively formed by the edge-rays incident in P. Upon transit through the source, the double reflections in each point of the Carambola cause its image to be flipped. In both Figs. 5.7 and 5.8, the caustics

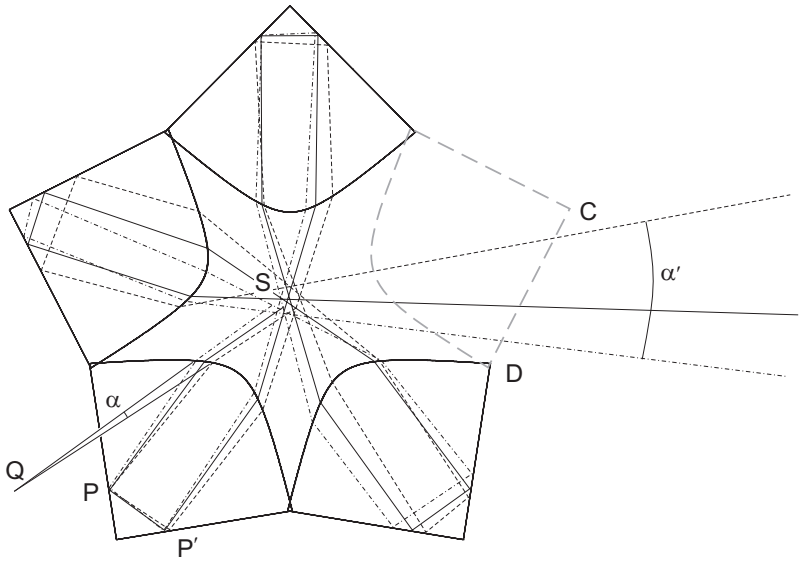

Figure 5.8.: Light recycling in a two-dimensional five-point refractive Carambola. Ray-tracing simulation of edge-rays through point P. The source appears at an angle $\alpha = 2.75°$ at Q. The refractive version of the Carambola is more sensitive to the size of the source than the reflective version due to the increased optical path length by a factor given by the refractive index of the lens material $N = 1.51$.

formed by the edge rays move closer to the source. With the edge-rays tangent to the source, the image of the source is of identical size with the source at the location of the source.

The light at the exit of the Carambola comes either directly from the source, or passes the source on all transits. The recycled light is emitted in the same phase space as the original light.

Optical thickness

The discussion on light recycling in Sec. 2.2 yields the conclusion that light recycling is equivalent to increasing the optical thickness of the source by a factor equal to the number of transits. For deterministic light recycling in the Carambola the optical thickness of the source depends on the number of transits of the recirculated light and the absorption coefficient. For simplicity, the intrinsic optics thickness of the source of one transit Δ_0 (the product of the absorption coefficient and the thickness of the source) is used, without need to consider the two factors separately.

At a two-dimensional Carambola with n points (one is absent for extracting light) and an average number of transits $(n-1)/2$, the typical optical thickness for light emitted from the center of a source (assuming refractive index of unity) with ra-

dius R_s is

$$\Delta_{2D} = n\alpha R_s \ , \tag{5.10}$$

including the original light, observed from the exit of the Carambola.

5.3.2. Brightness enhancement

The average geometrical enhancement factor of a two-dimensional n-point Carambola is derived from the average number of transits of $(n-1)/2$

$$\eta_{2D}^{0} = (n+1)/2 \ . \tag{5.11}$$

The average geometrical enhancement factor is a measure for the recycling capability of the Carambola. As an example, a five-point Carambola has a geometrical average enhancement factor of three, illustrated in the lower curve in Fig. 5.9 in which the optical thickness of the used source is infinitely thin, which is the ideal case for light recycling.

Similarly, a three-dimensional n-point Carambola with a half dual-paraboloid replaced by an exit has an average geometrical enhancement factor of

$$\eta_{3D}^{0} = n + \frac{1}{2} \ . \tag{5.12}$$

If using a real source in the Carambola for light recycling, the brightness enhancement cannot compare with the geometrical enhancement factor according to Eqs. (5.11) and (5.12) due to the absorption in the source and the imperfect reflective quality of the Carambola. Brightness enhancement is a function of the optical thickness, the number of points and the reflectivity of the Carambola. A combination of these three factors should be optimized.

According to the results in Eq. (2.25) in Sec. 2.2 and considering the reflectivity r of the Carambola, the n-th transit yields the maximal brightness enhancement factor as

$$\eta = \sum_{i=1}^{n} r^{2(i-1)} \exp\left(-(i-1)\Delta_0\right) \ . \tag{5.13}$$

Averaging over all light which transits the source one to n times yields the average brightness enhancement as

$$\overline{\eta} = \frac{1}{n} \sum_{j=1}^{n} \sum_{i=1}^{j} r^{2(i-1)} \exp\left(-(i-1)\Delta_0\right) \ . \tag{5.14}$$

The brightness enhancement factor is a function of the reflectivity, the optical thickness and the number of points of the Carambola. It decreases exponentially with the optical thickness, illustrated in Fig. 5.9. A small optical thickness facilitates

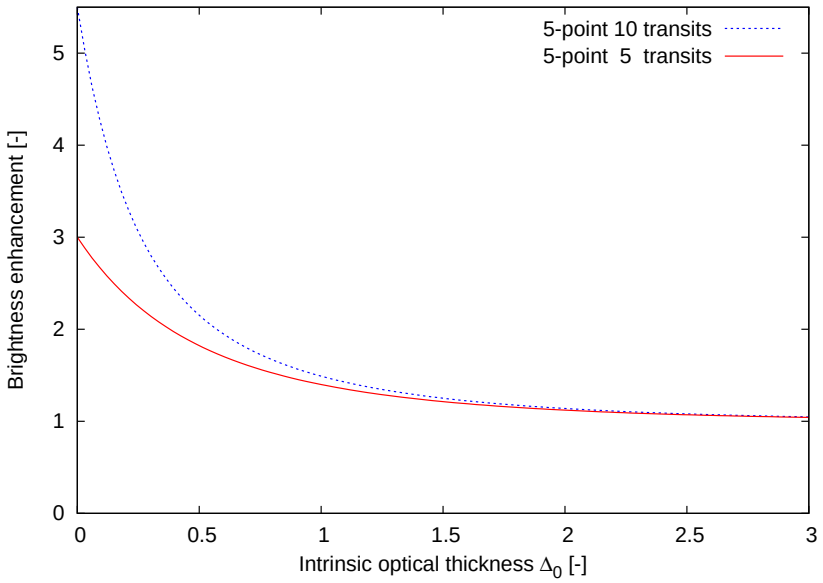

Figure 5.9.: Average brightness enhancement as a function of intrinsic optical thickness with five transits and ten transits in a five-point Carambola including the original emission, assuming unity reflectivity of the reflectors, derived by Eq. (5.14). The case with five transits is either a two-dimensional or three-dimensional five-point Carambola with one total piece replaced by an exit, the case with ten transits is the three-dimensional five-point Carambola with a half dual-paraboloid replaced by the exit.

brightness increase. In the case when Δ_0 is infinitely small, the brightness enhancement factor approaches the average geometrical brightness enhancement factor given by Eqs. (5.11) and (5.12).

The brightness enhancement factor increases with the number of transits, shown in Fig. 5.10.

The brightness enhancement increases with the reflectivity, illustrated in Fig. 5.11. The reflectivity is an important issue in the Carambola, it decides how much of the redirected light can exit. In the case of a Carambola with a low reflectivity, brightness increase can be achieved only with a few transits.

The combined three parameters-dependent (r, Δ_0, n) brightness enhancement yields the principle for designing a Carambola and choosing the matched source: small source with thin optical thickness, high reflectivity and a matched number of points of the Carambola, e. g. a five-point Carambola matches 0.85 reflectivity or higher, a seven-point one fits 0.95 reflectivity.

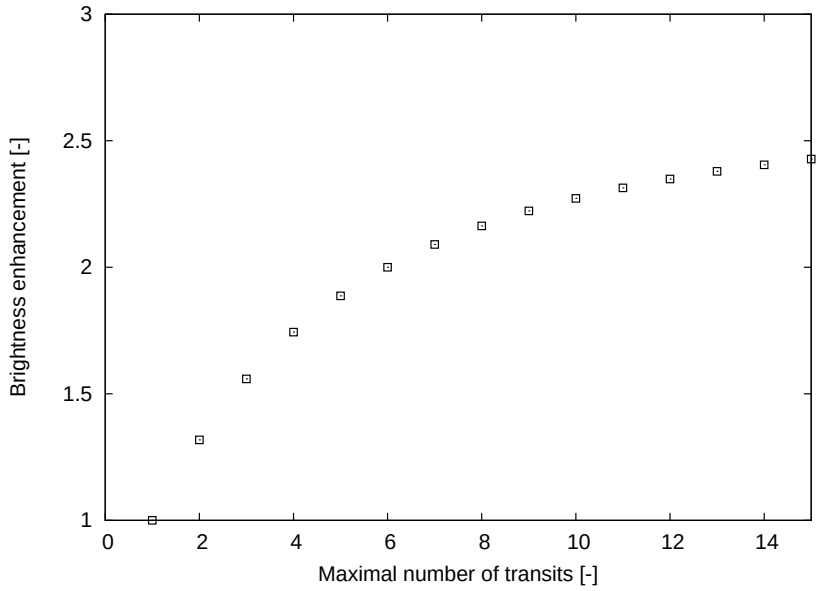

Figure 5.10.: Brightness enhancement as a function of number of transits, with the optical thickness of the source $\Delta_0 = 0.35$ and the reflectivity $r = 0.95$.

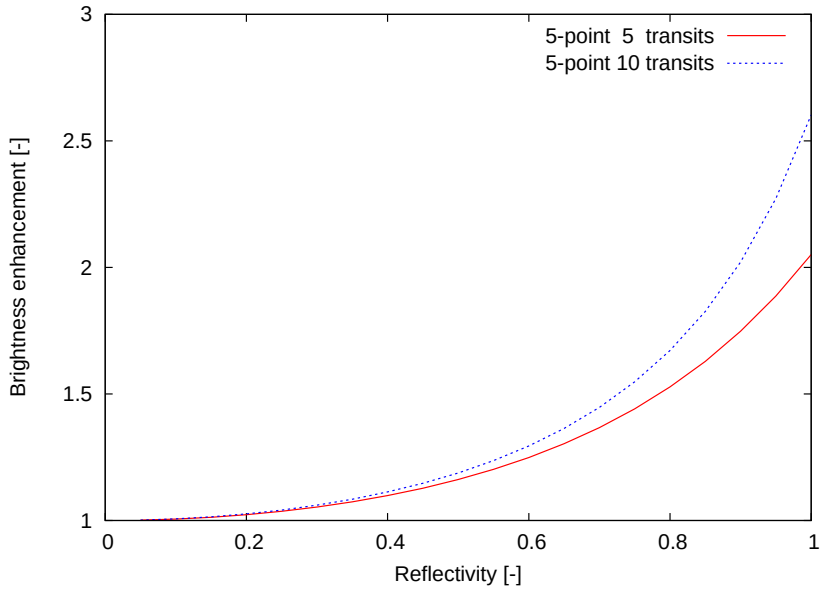

Figure 5.11.: Brightness enhancement as a function of the reflectivity of the Carambola, with the optical thickness of the source $\Delta_0 = 0.35$. Both plotted cases are for a five-point Carambola, one with five transits (two-dimensional Carambola with one exit), the other with ten transits (three-dimensional Carambola with one half dual-paraboloid replaced by the exit).

5.3.3. Results and discussion

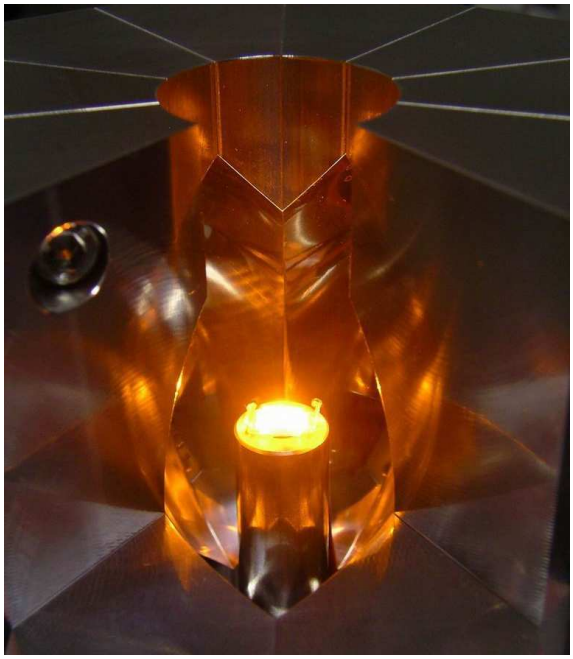

Figure 5.12.: Experimental setup for light recycling with an LED (NovaLED175) in the Carambola. The upper hemisphere of the Carambola is used for light recycling through the source by utilizing the intrinsic reflection of the LED. At the exit the output emission is measured. Comparing the measured quantities with the Carambola and without the Carambola yields the brightness enhancement factor.

A three-dimensional five-point reflective Carambola was designed and fabricated of aluminum. Fig. 5.12 shows a light recycling experiment by using an LED as the source in the Carambola. The upper half of the Carambola is used due to the hemispherically emitting property of the LED. The output emission is measured at the exit. Comparing the measured emission quantities with the Carambola and without the Carambola yields the average brightness enhancement. This effect is investigated in the experiment and modelled via ray-tracing by using different sources including an LED and a short-arc lamp (XBO). In the case of a short-arc lamp as the source, the entire Carambola contributes to the output emission because of the transparency of the source. The results are listed in Table 5.1. Note that all the listed results are the average brightness enhancement covering the entire exit, not the maximal values resulting from the direction-dependent reflection of the involved sources, e. g. LEDs.

Analyzing the results from the measurements we found the low brightness enhancement to be caused by several factors, including

Table 5.1.: Results of brightness enhancement of sources in the Carambola. Two cases are modelled with the reflectivity (r) of 1.0 and 0.67 of each reflecting surface of the Carambola and the LED. The optical thickness of the used XBO lamp is 0.35, derived from the measurement.

Brightness enhancement	Light sources	
	LED	XBO
Simulation ($r = 1.0$)	1.97	2.34
Simulation ($r = 0.67$)	1.31	1.69
Experiment	1.2	1.38

- the reflectivity of the reflecting surfaces of the Carambola (measured Carambola reflectivity 0.67) and the LED. The former can be increased by improving the surface quality via manufacturing and processing. The latter is the intrinsic property of an LED, which is expected to be improved with the development of material. Mirroring the back side of the LED is an approach to increase the reflectivity;

- the size of the source. The LED is too small, and imaging errors of the Carambola is too large;

- the optical thickness of the source. The short-arc lamp XBO is more suitable for light recycling in the Carambola than the HBO lamp, due to a smaller optical thickness of the XBO lamp;

- the external quantum efficiency of LEDs. Using an LED with a high external quantum efficiency is desirable for light recycling for a practical illumination;

- the number of transits or the number of ribs of the Carambola. In principle, a Carambola with more points is suitable for enhancing the output brightness due to the number of transits through the source, assuming a high reflectivity of the reflector and a low absorption of the source. In reality, this enhancement will be traded off by the accumulative absorption in the real source and the low reflectivity of the reflectors.

If using the Carambola with a source for practical illumination, all these factors should be taken into account.

5.4. Summary

The Carambola optics makes the deterministic recycling of light feasible. The rotation of light in a cavity with any odd number of dual-paraboloid reflectors (one is replaced by an opening aperture for light extraction) allows for deterministically emitting light through an exit with the same size as any one of these reflectors. Multiple transits of light through the source and deterministic redirection lead to a superposed emission of direct and recirculated light in the same phase space.

The maximum geometrical size of the source placed in the center of the Carambola is specified by means of the optical path length of the recirculated light. Likewise, the optical thickness of the source can be found. The absorptivity/emissivity characteristics of different light sources according to Kirchhoff's law are tested and modelled, in order to verify the suitability of the Carambola for practical light recycling and for increasing the output brightness of light sources.

The factors that influence light recycling and brightness increase are discussed. The output brightness of the source with the Carambola is expected to be increased by improving the surface quality of the reflectors, using suitable sources with small optical thickness, compact size, (and in the case of LEDs) high intrinsic reflectivity and external quantum efficiency. The Carambola is expected to be put into applications, e. g. high brightness displays.

6. Summary and prospects

In modern illumination systems, compact size and high brightness are important features. Light recycling allows an increase of the spectral radiance (brightness) emitted by a light source for the price of reducing the total radiant power. Light recycling means returning part of the emitted light to the source where part of it will escape absorption. As a result, the output brightness can be increased in a restricted phase space, compared with the intrinsic brightness of the source. In this work the principle of light recycling is applied to artificial light sources in order to achieve brightness enhancement.

Firstly, the feasibilities of increasing the brightness of light sources via light recycling are examined theoretically, based on the fundamental laws of thermodynamics including Kirchhoff's law on radiation, Planck's law, Lambert-Beer's law, the étendue conservation and the brightness theorem. The theory of light recycling can be derived from first principles.

From an experimental viewpoint, the radiation properties of three different kinds of light sources including short-arc lamps, incandescent lamps and LEDs characterized by their light-generating mechanisms are investigated. These three types of sources are used in light recycling experiments, for the purpose of

- validating the intrinsic light recycling effect in light sources, e. g. the intrinsic light recycling effect in incandescent lamps stemming from the coiled filament structure.
- acquiring the required parameters for establishing physical models, e. g. the emissivity/absorptivity of the short-arc lamps, the intrinsic reflectivity and the external quantum efficiency of LEDs.
- laying the foundations for designing optics aimed at brightness enhancement according to the characteristics of the sources and applications.

Based on the fundamental laws and experiments, two physical models for simulating the radiance distribution of light sources are established, one for thermal filament lamps, the other for luminescent sources, LEDs. Both are validated with high resolution measurements. The physical models are capable of analytically modelling the radiance distribution with few required parameters (geometry, material properties and operating conditions). They are widely applicable to any kind of

sources with similar light-emitting mechanisms. Combining the advantages of conciseness, high accuracy and wide applicability, the physical models can be integrated into ray-tracing software.

As validation of the theoretical and experimental investigation of the light recycling effect, an optical device, the Carambola, is designed for achieving deterministic (as opposed to stochastic) and multiple light recycling. The Carambola has the function of a concentrator. In order to achieve the maximum possible brightness enhancement with the Carambola, several combinations of sources and Carambolas are modelled in ray-tracing simulations. Sources with different light-emitting mechanisms and different radiation properties (optical thickness), and Carambolas with different geometries and optical properties are used. It is concluded that a high-pressure xenon lamp is suitable for light recycling with the Carambola due to its moderate optical thickness, its continuous spectrum and its geometrical features. In the ray-tracing simulation, the suitability of the XBO lamp and the Carambola optics for light recycling is confirmed.

A prototype five-point reflective Carambola was manufactured from aluminium, for the purpose of experimentally demonstrating a brightness increase.

The Carambola is tested with different sources. The experimental results are below the theoretical expectation, i. e. the measured brightness enhancement factor is lower than the designed factor and the modelled factor. The discrepancies are explained.

A real Carambola must have a high reflectivity and an accurate shape, if a significant effect of light recycling is to be shown. The brightness enhancement by light recycling with the Carambola is expected to be improved greatly by enhancing the surface quality of the reflectors, using suitable sources with small optical thickness, compact size, (and in the case of LEDs) high intrinsic reflectivity and external quantum efficiency. The Carambola is expected to be utilized in applications such as high brightness displays.

In conclusion, both theoretical investigation and experimental measurements on light recycling demonstrated a significant increase of the brightness of optically thin sources.

A. Symbols and Abbreviations

Symbols

A, A_c, A_s	area
A_HL	transition probability
α, α_c, α_h	absorptivity
c	velocity of light in vacuum
c_p	heat capacity
C	circumference
C_H, C_L	concentration of particles
d	distance; thickness
d_0	thickness
$\mathbf{d}$	unit vector
d$\mathbf{a}$	surface element
δT	temperature difference
$\delta\lambda$	wavelength difference
Δ, Δ_0, Δ_c, Δ_h	optical thickness
E	irradiance; *é*tendue
E_c	energy of conduction band edge
E_g	energy of semiconductor bandgap
E_v	energy of valence band edge
ϵ	emission coefficient
ε	emissivity
ε_eff	effective emissivity
η	brightness enhancement factor
$\overline{\eta}$	average brightness enhancement factor
η_e	power efficiency
η_v	luminous efficacy
η_eq	external quantum efficiency
η_ex	light extraction efficiency
η_iq	internal quantum efficiency
ϕ	angle
Φ_i	light power emitted from the active region (LED)
Φ_e	radiant power

Φ_v	luminous power
g	statistical weight of energy level
$g(P)$	boolean function
Γ	magnification
h	Planck's constant
$h\nu$	photon energy
I	optical intensity; current
I−V	current vs. voltage characteristics
$\mathbf{k}$	normal vector
κ	thermal capacity
k_0	thermal end-coupling factor of filament
k_B	Boltzmann's constant
$\mathbf{K}$	curvature
K_λ	spectral luminous efficiency
l, L	length
L_λ	spectral radiance
L_w	Lorenz number
λ	wavelength
m	number of reflections in the Carambola
M_1, M_2	integer
n	n-type semiconductor material; number of points of the Carambola
N	refractive index
$\mathbf{N}$	normal vector
ν	frequency
Ω	solid angle
obj	objective function
Ω_p	projected solid angle
p	p-type semiconductor material; pressure; length component
$p\,(E)$	occupation probability
P, P_Ω	power
ψ	angle
q	electrical charge
Q	heat
r	reflectivity
$\mathbf{r}$	propagation direction
R_c, R_s, R_w, R_0	radius
R_p	parallel resistance
R_s	series resistance
ρ	electrical resistivity
S	entropy
S_w	slope of filament
σ	Stefan-Boltzmann's constant

$\bar{\sigma}$	standard deviation
t	time; transmissivity
T, T_0, T_{char}	temperature
$\mathbf{T}$	tangent vector
τ	absorption efficient
θ	angle
V	voltage
V_{th}	threshold voltage
V_λ	eye sensitivity function
w	weight factor
W	thermal power
x	position coordinate
ξ	geometric recycling factor
z	position coordinate
$\mathbf{Z}$	vector

Abbreviations

DR	direct radiation
FWHM	half width at half maximum
LED	light-emitting diode
LTE	local thermal equilibrium
RR	reflected radiation
SMD	surface-mounted diode
SR	superposed radiation
TIR	total internal reflection

B. Author's Publications

1. L. Fu, R. Leutz, and H. Ries. Physical modelling of tungsten filament lamps. *J. Appl. Phys.* To be published.

2. R. Leutz, L. Fu, and H. Ries. Carambola optics for light recycling. *Applied Optics*, 45:2572–2575, 2006.

3. L. Fu, R. Leutz, and H. Ries. Spectroscopic measurement of radiation of high-pressure mercury discharge lamps. *J. Appl. Phys.*, 97(1), June 2005. 123302.

4. L. Fu, R. Leutz, and H. Ries. Light recycling in filament light sources. In R. Winston and P. Benitez, editors, *Proceedings of the SPIE Optics and Photonics; Nonimaging Optics and Efficient Illumination Systems III*, volume 6338, San Diego, California, August 2006. SPIE.

5. L. Fu, R. Leutz, and H. Ries. Multiple light recycling with the Carambola. In R. Winston and P. Benitez, editors, *Proceedings of the SPIE Optics and Photonics; Nonimaging Optics and Efficient Illumination Systems III*, volume 6338, San Diego, California, August 2006. SPIE.

6. L. Fu, R. Leutz, and H. Ries. Light recycling in solid state devices. In *Proceedings of the SPIE Optics and Photonics; Illumination Engineering, Fifth International Conference on Solid State Lighting*, volume 5941, San Diego, California, August 2005. SPIE.

7. L. Fu, R. Leutz, and H. Ries. Beating the brightness theorem: Thermodynamics of light recycling (experimental). In *Proceedings of the SPIE 20th Congress of the International Commission for Optics (ICO), Challenging Optics in Science and Technology*, volume 6033, Changchun, China, August 2005. SPIE.

8. L. Fu, R. Leutz, and H. Ries. RIOS: Physikalische Modellierung von thermischen und lumineszenten Lichtquellen. Erster Zwischenbericht: Glühlampen am Beispiel der Halogenlampe. Report, Federal Ministry of Education and Research, Germany, 2005.

9. R. Leutz, L. Fu, and H. Ries. Secondary optics for solar concentrators: Concentration, beam shaping, and illumination uniformity. In *Proceedings of*

the 2nd International Solar Concentrator Conference for the Generation of Electricity or Hydrogen, Alice Springs, Australia, November 2003. U.S. Department of Energy, NREL, CD-520-35349. Invited presentation, slides only.

10. H. Ries, R. Leutz, and L. Fu. Erfindung betreffend Reflektorsysteme (invention related to reflector systems). Patent. Patent application.

Bibliography

[1] Y.B. Band and D.F. Heller. Relationship between the absorption and emission of light in multilevel systems. *Phys. Rev. A.*, 38(4):1885–1895, 1988.

[2] K. Beeson and S. Zimmerman. Illumination systems utilizing highly reflective light emitting diodes and light recycling to enhance output radiance. US-Patent No. 6960872, Nov. 2005.

[3] K. Beeson, S. Zimmerman, and W. Livesay. LED-based light-recycling light sources for projection displays. *SID 06 DIGEST*, page 3701, 2006.

[4] A.A. Bergh and P.J. Dean. *Light Emitting Diodes, Monographs in Electrical and Electronic Engineering.* Claredon Press, Oxford, 1976.

[5] L. Boltzmann. Ableitung des Stefan'schen Gesetzes, betreffend die Abhängigkeit der Wärmestrahlung von der Temperatur aus der electromagnetischen Lichttheorie. *Ann. der Phys. und Chem.*, Bd. 22:291–294, 1884.

[6] M. Born and E. Wolf. *Principles of Optics.* Pergamon, Oxford, 6th edition, 1989.

[7] R.W. Boyd. *Radiometry and the detection of optical radiation.* John Wiley and Sons, USA, 1983.

[8] H.B. Callen. *Thermodynamics and an Introduction to Thermostatics.* John Wiley and Sons, 2nd edition, 1985. pp. 314.

[9] W.N. Carr and G.E. Pittman. One-watt GaAs p-n junction infrared source. *Appl. Phys. Lett.*, 3(10):173, 1963.

[10] S. Chhajed, Y. Xi, Y. Li, T. Gessmann, and E.F. Schubert. Influence of junction temperature on chromaticity and color-rendering properties of trichromatic white-light sources based on light-emitting diodes. *J. Appl. Phys.*, 97, 2005.

[11] R. Clausius. *Théorie Mécanique de la Chaleur.* Lacroix, Paris, 1868.

[12] J.R. Coaton and A.M. Marsden. *Lamps and Lighting.* Arnold, London, 1st edition, 1997.

[13] J.J. Damelincourt, M. Aubes, and P. Fragnac. Effect of modulated high-pressure mercury discharges on the shape of self-reversed lines. *J. Appl. Phys.*, 54(6):3087–3097, 1983.

[14] CIE data of 1978. http://cvision.ucsd.edu, 1978.

[15] A.R. Franklin and R. Newman. Shaped electroluminescent GaAs diodes. *J. Appl. Phys.*, 35(4):1153, 1964.

[16] L. Fu, R. Leutz, and H. Ries. Physical modelling of tungsten filament lamps. *J. Appl. Phys.* To be published.

[17] L. Fu, R. Leutz, and H. Ries. Light recycling in solid state devices. In *Proceedings of the SPIE Optics and Photonics; Illumination Engineering, Fifth International Conference on Solid State Lighting*, volume 5941, San Diego, California, August 2005. SPIE.

[18] L. Fu, R. Leutz, and H. Ries. RIOS: Physikalische Modellierung von thermischen und lumineszenten Lichtquellen. Erster Zwischenbericht: Glühlampen am Beispiel der Halogenlampe. Report, Federal Ministry of Education and Research, Germany, 2005.

[19] L. Fu, R. Leutz, and H. Ries. Spectroscopic measurement of radiation of high-pressure mercury discharge lamps. *J. Appl. Phys.*, 97(1), June 2005. 123302.

[20] J.R. Fuhr and W.L. Wiese. *CRC Handbook of Chemistry and Physics*. Chemical Rubber, Boca Raton, FL, 1994. pp.10-128.

[21] T. Fujii, Y. Gao, R. Sharma, E.L. Hu, S.P. DenBaars, and S. Nakamura. Increase in the extraction efficiency of GaN-based light-emitting diodes via surface roughening. *Appl. Phys. Lett.*, 84(6), 2004.

[22] X. Guo, J. Graff, and E.F. Schubert. Photon recycling semiconductor light emitting diode. *IEDM Technical Digest*, 99:600, 1999.

[23] X. Guo, J. Graff, and E.F. Schubert. Photon-recycling for high brightness LEDs. *Compound Semiconductor*, 6(4), May/June 2000.

[24] G. Hartel and H. Schöpp. Determination of the radial temperature profile in a high-pressure mercury discharge using the electrical conductivity. *J. Phys.D: Appl. Phys.*, 29:2881–2884, 1996.

[25] G. Hartel, H. Schöpp, and H. Hess. Radiation from an alternating current high-pressure mercury discharge: A comparison between experiments and model calculations. *J. Appl. Phys.*, 85(10):7076–7088, 1999.

[26] E. Hong and N. Narendran. A method for projecting useful life of LED lighting systems. In *Proceedings of SPIE 5187; Third International Conference on Solid State Lighting*, San Diego, California, 2004.

[27] http://lighting.sandia.gov/lightingdocs/OIDA_SSL_LED_Roadmap_Full.pdf. Light emitting diodes (LEDs) for general illumination: An OIDA technology roadmap update 2002.

[28] http://www.efunda.com/materials/elements.

[29] http://www.wikipedia.org.

[30] D. Karabourniotis, E. Drakakis, and B. Zacharopoulos. Electron and population temperatures in a non-LTE optically thick plasma. *J. Phys. D: Appl. Phys.*, 25:188–194, 1992.

[31] Y. Kawakami, K. Omae, and A. Kaneta E.L. et. al. Radiative and nonradiative recombination processes in GaN-based semiconductors. *Phys. Stat. Sol.* (a), 183(41):41–50, 2001.

[32] J.K. Kim, T. Gessmann, H. Luo, and E.F. Schubert. GaInN light-emitting diodes with RuO_2/SiO_2/Ag omni-directional reflector. *Appl. Phys. Lett.*, 84(22), May 2004.

[33] G. Kirchhoff. Über das Verhältnis zwischen dem Emissionsvermögen und dem Absorptionsvermögen der Körper für Wärme und Licht. *Ann. Phys.*, 19:275–301, 1860.

[34] M.R. Krames, J. Bhat, and D. Collins. High-power III-nitride emitters for solid-state lighting. *Phys. Stat. Sol.* (a), 192(2):237–245, 2002.

[35] M.R. Krames, M. Ochiai-Holcomb, and G.E. Höfler. High-power truncated-inverted-pyramid $(Al_xGa_{1-x})_{0.5}In_{0.5}P$/GaP light-emitting diodes exhibiting >50% external quantum efficiency. *Appl. Phys. Lett.*, 75:2365–2367, Oct. 1999.

[36] L.D. Landau and E.M. Lifschitz. *Statistische Physik*. Akademie Verlag, Berlin, 1979.

[37] K. Li, S. Sillyman, and S. Inatsugu. Light-piped based projection engine using dual paraboloid reflector system and polarization-recovery system for projection display. *SID 00 DIGEST*, 35(1):954–957, May 2004.

[38] K.K. Li. Illumination engine for a projection display using a tapered light pipe. United States Patent 6739726 B2, 2004.

[39] K.K. Li, S. Sillyman, and S. Inatsugu. Optimization of dual paraboloidal reflector and polarization system for displays using a ray-tracing model. *Optical Engineering*, 43(7):1545–1551, 2004.

[40] O.V. Lossev. Luminous carborundum detector and detection effect and oscillations with crystals. *Philosophical Magazine*, 6(39):1024–1044, 1928.

[41] R. Loudon. *Quantum Theory of Light*. Clarendon, Oxford, 1983.

[42] H. Luo, J.K. Kim, and E.F. Schubert. Analysis of high-power packages for phosphor-based white light emitting diodes. *Appl. Phys. Lett.*, 86(24), June 2005.

[43] D. Malacara. *Color Vision and Colorimetry: Theory and Applications*. SPIE, 2005.

[44] D.E. McCumber. Einstein relations connecting broadband emission and absorption spectra. *Phys. Rev. A.*, 136(4A):954–957, 1964.

[45] T.G. Müller and J. Timmer. Parameter identification techniques for partial differential equations. *International Journal of Bifurcation and Chaos*, 14(6):2053–2060, 2004.

[46] N. Narendran and Y. Gu. Extracting phosphor-scatted photons to improve white LED efficiency. *Phys. Stat. Sol.* (a), 202(6):R60–62, 2005.

[47] optodevices GmbH. Super NovaLED175. http://www.conrad.de. optodevices GmbH, Seekamp 3, 24326 Stocksee, Germany, info@optodevices.de.

[48] L. Piegl and W. Tiller. *The NURBS Book*. Springer, Springer, 2nd edition, 1996. pp. 361.

[49] M. Planck. Über das Gesetz der Energieverteilung im Normalspectrum. *Ann. Phys.*, 4:553–563, 1901.

[50] W.H. Press, B.P. Flannery, S.A. Teukolsky, and W.T. Vetterling. *Numerical Recipes*. Cambridge University Press, Cambridge, 1992.

[51] O. Reeb and F. Bobek. The application of additional mirrors for cinema projection with incandescent lamps and reflectors. *Licht und Lampe Rundschau*, 1926.

[52] J. Richter. In W. Lochte-Holtgreven, editor, *Plasma Diagnostics*, chapter 1, page 20. North-Holland Publishing Company, Amsterdam, 1968.

[53] H. Ries and A.J. McEvoy. Chemical potential and temperature of light. *J. Photochem. Photobiol. A:Chem*, 59:11–18, 1991.

[54] H. Ries and W. Spirkl. A generalized Kirchhoff law for quantum absorption and luminescence. *Solar Energy Materials and Solar Cells*, 38:39–44, 1995.

[55] A. Ritz and H. Mönch. UHP lamps with dichroic coating. In *Light Sources 2004: Proceedings of the 10th International Symposium on the Science and Technology of Light Sources*, Institute of Physics Conference Series 182, page 301, France, 2004.

[56] I. Schnitzer, E. Yablonovitch, and C. Caneau et. al. 30% external quantum efficiency from surface textured, thin-film light-emitting diodes. *Appl. Phys. Lett.*, 63(16):2174–2176, 1993.

[57] E. F. Schubert. *Light-Emitting Diodes.* Cambridge, 1st edition, 2003.

[58] W. Shockely. Detailed balance limit of efficiency of p-n junction solar cells. *Bell System Tech. J.*, 28(435), 1949.

[59] W. Shockely. *Electrons and Holes in Semiconductors.* Van Nostrand, New York, 1950.

[60] G. Sibbald. Improvement in magic-lanterns. US-Patent No. 42412, April 1864.

[61] M. Strojnik and G. Paez. Tungsten lamp as radiation standard and the emissivity effects. In M. Strojnik, editor, *Proceedings of SPIE 5543; Infrared Spaceborne Remote Sensing XII*, Denver, Colorado, November 2004. SPIE.

[62] Y.P. Varshni. Temperature dependence of the energy gap in semiconductors. *Physica*, 34:149–154, 1967.

[63] W.T. Welford and R. Winston. *High Collection Nonimaging Optics.* Academic Press, San Diego, California, 1989.

[64] J.J. Wierer, M.R. Krames, and J.E. Epler. InGaN/GaN quantum-well heterostructure light-emitting diodes employing photonic crystal structures. *Appl. Phys. Lett.*, 84(19), May 2004.

[65] J.J. Wierer, D.A. Steigerwald, and M.R. Krames. High-power AlGaInN flip-chip light-emitting diodes. *Appl. Phys. Lett.*, 78(22), May 2001.

[66] E.W. Williams and R. Hall. *Luminescence and the LED.* Pergamon Press, New York, 1978.

[67] R. Windisch, P. Heremans, and A. Knobloch et. al. Light-emitting diodes with 31% external quantum efficiency by outcoupling of lateral waveguide modes. *Appl. Phys. Lett.*, 74(16), April 1999.

[68] P. Würfel. The chemical potential of radiation. *J. Phys. C*, 15:3967–3985, 1982.

[69] P. Würfel. *Physics of Solar Cells.* Wiley, 2nd edition, 2005.

[70] S. Zimmerman and K. Beeson. Illumination systems utilizing highly reflective light emitting diodes and light recycling to enhance brightness. US-Patent No. 6869206, March 2005.

Acknowledgements

I would like to gratefully acknowledge all the people who gave me support and help to my PhD study and my life during the past years of my stay in Germany.

I would like to gratefully acknowledge my supervisor, Prof. Dr. Harald Ries for hosting me as a PhD student in the group of Optics. His creative supervision and continuous encouragement led me on the way. His extensive knowledge in physics and mathematics, his creative thinking is of great benefit to my study and my research work.

I am especially grateful to Dr. Ralf Leutz for his resourceful guidance and invaluable help and support. He helped me in every detail in my work, from the initial stages of the project design, valuable discussions, to the patient revision of this thesis, letting me find the right way to research work. Thanks for being a sincere friend of mine.

I am grateful to Tobias for his patiently and kindly answering me those theoretical questions.

I grateful thank to Ms. Stani Martini for her warm help to me.

I wish to thank the German Federal Ministry of Education and Research (BMBF) for the financial support.

Forever, grateful thanks to my parents.

Academic Career

from 2003.01	PhD student, Workgroup Optics (Prof. H. Ries) Dept. of Physics, Philipps-University Marburg, Germany
2002.01 - 2002.12	Visiting Researcher, Workgroup Micro-Optics (Prof. H. Zappe) Institute of Microsystem Technology University of Freiburg, Germany
2000.09 - 2001.07	German language course Tongji University, Shanghai, China
1995.04 - 2000.08	Researcher and Lecturer, Workgroup Optical Engineering Dept. of Electronic Science and Technology Harbin Institute of Technology, China
1992.09 - 1995.03	M. Eng., Workgroup Optical Engineering Harbin Institute of Technology, Harbin, China
1988.09 - 1992.07	B. Eng., Dept. of Optical Engineering Zhejiang University, China